LBL-8280
SAC-16
UC-70

SWEDISH-AMERICAN COOPERATIVE PROGRAM ON RADIOACTIVE WASTE STORAGE IN MINED CAVERNS IN CRYSTALLINE ROCK

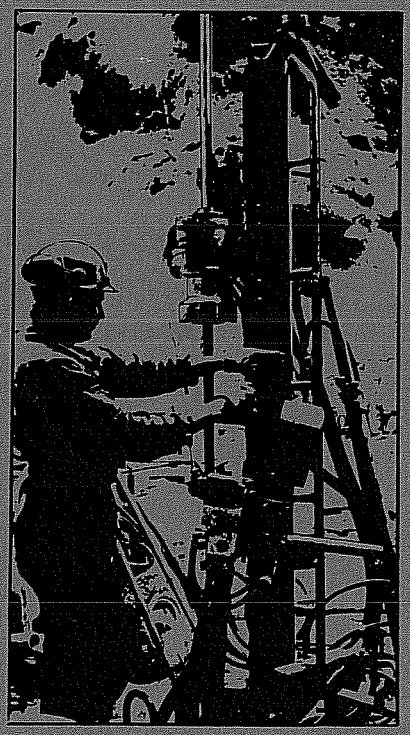

Technical Information Report No. 16

PRELIMINARY REPORT ON GEOPHYSICAL AND MECHANICAL BOREHOLE MEASUREMENTS AT STRIPA

P. Nelson, B. Paulsson, R. Rachiele, and L. Andersson
Lawrence Berkeley Laboratory
University of California, Berkeley
Berkeley, CA 94720

T. Schrauf and W. Hustrulid
TerraTek
Salt Lake City, UT 84108

O. Duran and K. A. Magnusson
Swedish Geological Survey
753-22 Uppsala, Sweden

May 1979

A Joint Project of

Swedish Nuclear Fuel Supply Co.
Fack 10240 Stockholm, Sweden

Operated for the Swedish
Nuclear Power Utility Industry

Lawrence Berkeley Laboratory
Earth Sciences Division
University of California
Berkeley, California 94720, USA

Operated for the U.S. Department of
Energy under Contract W-7405-ENG-48

This report was prepared as an account of work sponsored by the United States Government and/or the Swedish Nuclear Fuel Supply Company. Neither the United States nor the U.S. Department of Energy, nor the Swedish Nuclear Fuel Supply Company, nor any of their employees, nor any of their contractors, subcontractors, or their employees, makes any warranty, express or implied or assumes any legal liability or responsibility for the accuracy, completeness or usefulness of any information, apparatus, product or process disclosed, or represents that its use would not infringe privately owned rights.

Printed in the United States of America
Available from
National Technical Information Service
U.S. Department of Commerce
5285 Port Royal Road
Springfield, VA 22161
Price Code: A08

PRELIMINARY REPORT ON GEOPHYSICAL AND MECHANICAL BOREHOLE MEASUREMENTS AT STRIPA

P. Nelson, B. Paulsson, R. Rachiele, and L. Andersson
Lawrence Berkeley Laboratory
University of California, Berkeley
Berkeley, CA 94720

T. Schrauf and W. Hustrulid
Terra Tek
Salt Lake City, UT 84108

O. Duran and K. A. Magnusson
Swedish Geological Survey
753-22 Uppsala, Sweden

PREFACE

This report is one of a series documenting the results of the Swedish-American cooperative research program in which the cooperating scientists explore the geological, geophysical, hydrological, geochemical, and structural effects anticipated from the use of a large crystalline rock mass as a geologic repository for nuclear waste. This program has been sponsored by the Swedish Nuclear Power Utilities through the Swedish Nuclear Fuel Supply Company (SKBF), and the U.S. Department of Energy (DOE) through the Lawrence Berkeley Laboratory (LBL).

The principal investigators are L. B. Nilsson and O. Degerman for SKBF, and N. G. W. Cook, P. A. Witherspoon, and J. E. Gale for LBL. Other participants will appear as authors of the individual reports.

Previous technical reports in this series are listed below.

1. Swedish-American Cooperative Program on Radioactive Waste Storage in Mined Caverns by P. A. Witherspoon and O. Degerman. (LBL-7049, SAC-01).

2. Large Scale Permeability Test of the Granite in the Stripa Mine and Thermal Conductivity Test by Lars Lundstrom and Haken Stille. (LBL-7052, SAC-02).

3. The Mechanical Properties of the Stripa Granite by Graham Swan. (LBL-7074, SAC-03).

4. Stress Measurements in the Stripa Granite by Hans Carlsson. (LBL-7078, SAC-04).

5. Borehole Drilling and Related Activities at the Stripa Mine by P. J. Kurfurst, T. Hugo-Persson, and G. Rudolph. (LBL-7080, SAC-05).

6. A Pilot Heater Test in the Stripa Granite by Hans Carlsson. (LBL-7086, SAC-06).

7. An Analysis of Measured Values for the State of Stress in the Earth's Crust by Dennis B. Jamison and Neville G. W. Cook. (LBL-7071, SAC-07).

8. Mining Methods Used in the Underground Tunnels and Test Rooms at Stripa by B. Andersson and P. A. Halen. (LBL-7081, SAC-08).

9. Theoretical Temperature Fields for the Stripa Heater Project by T. Chan, Neville G. W. Cook, and C. F. Tsang. (LBL-7082, SAC-09).

10. Mechanical and Thermal Design Considerations for Radioactive Waste Repositories in Hard Rock. Part I: An Appraisal of Hard Rock for Potential Underground Repositories of Radioactive Wastes by Neville G. W. Cook; Part II: In Situ Heating Experiments in Hard Rock: Their Objectives and Design by Neville G. W. Cook and P. A. Witherspoon. (LBL-7073, SAC-10).

11. Full-Scale and Time-Scale Heating Experiments at Stripa: Preliminary Results by Neville G.W. Cook and Michael Hood. (LBL-7072, SAC-11).

12. Geochemistry and Isotope Hydrology of Groundwaters in the Stripa Granite: Results and Preliminary Interpretation by P. Fritz, J.F. Barker, and J.E. Gale. (LBL-8285, SAC-12).

13. Electrical Heaters for Thermo-mechanical Tests at the Stripa Mine by R. H. Burleigh et al. (LBL-7063, SAC-13).

14. Data Acquisition, Handling, and Display for the Heater Experiments at Stripa by Maurice B. McEvoy (LBL-7062, SAC-14).

15. An Approach to the Fracture Hydrology at Stripa: Preliminary Results by J. E. Gale and P. A. Witherspoon. (LBL-7079, SAC-15).

TABLE OF CONTENTS

Page

LIST OF FIGURES vii

LIST OF TABLES x

ABSTRACT 1

1. INTRODUCTION 3

2. GEOPHYSICAL LOGS 13

2.1 Description of Instrumentation 13

2.2 SBH-1 Geophysical Logs 25

2.2.1 Outstanding Features Observed in the Data 32

2.2.2 Detailed Description of the SBH-1 Logs 34

2.3 Time-Scale Borehole Logs 47

2.4 Full-Scale Borehole Logs 60

2.5 Neutron Monitoring of Water Content in Rock. 71

3. MECHANICAL MODULUS MEASUREMENTS WITH THE CSM CELL 77

3.1 Construction and Testing of the CSM Cell 77

3.1.1 Introduction. 77

3.1.2 Laboratory Calibration 78

3.1.3 Laboratory Modulus Measurement 81

3.2 Field Measurements with the CSM Cell 83

3.3 CSM Results 86

3.4 Goodman Jack Tests 88

3.4.1 Calibration 91

3.4.2 Downhole Testing 91

4. ULTRASONIC PROPAGATION MEASUREMENTS 95

4.1 Equipment and Procedures 95

4.2 Repeatability 98

4.3 Preliminary Results 98

Page

5. GEOPHYSICAL LOGS WITH THE SGU LOGGING SYSTEM 105

5.1 Resistivity Measurements 105

5.2 Differential Resistance 108

5.3 Results 110

6. SUMMARY 117

7. ACKNOWLEDGMENTS 121

8. REFERENCES 123

9. APPENDICES 125

A. Potassium, Uranium, and Thorium Content by Spectral Gamma-Ray Analysis 127

B. Calibration of the Neutron-Thermal Neutron Borehole Probe 131

C. Description of Thin Sections from Borehole N1 in Time-Scale Room 143

D. Laboratory Determinations of Porosity and Density 149

E. Laboratory Determinations of Structural Water, Density, and Porosity 151

F. Tabulation of CSM-Cell Determinations of Modulus 153

G. Laboratory Measurements of Density and Ultrasonic Velocity 163

Appendix References 165

LIST OF FIGURES

		Page
1.1	Plan map of surface at Stripa showing outcrop, surface boreholes, and projection of underground experimental areas	4
1.2	Borehole layout in the full-scale drift	6
1.3	Borehole layout in the time-scale drift	7
2.1	Logging unit with 1000 m of armored cable	13
2.2	Block diagram of borehole logging equipment used at Stripa	14
2.3	Geophysical logs in SBH-1, greatly reduced from the 500:1 scale of the original plate	28
2.4	Sonic waveform, core, and TV logs in SBH-1, greatly reduced from the original plate	30
2.5a	Gamma-ray logs along axis of the time-scale drift	48
2.5b	Neutron logs along axis of the time-scale drift	49
2.5c	Caliper logs along axis of the time-scale drift	50
2.5d	Compressional wave arrival times along axis of the time-scale drift	51
2.5e	Gamma-gamma (density) logs along axis of the time-scale drift	52
2.5f	CSM-cell determinations of modulus along axis of the time-scale drift	53
2.5g	Fractures observed in core and major fracture planes along axis of the time-scale drift	54
2.6	Total count gamma log in hole N1 and uranium, thorium, and potassium analyses from spectral gamma-ray laboratory method	56
2.7a	Gamma-ray logs along axis of the full-scale drift	61
2.7b	Neutron logs along axis of the full-scale drift	62
2.7c	Caliper logs along axis of the full-scale drift	63
2.7d	Compressional-wave arrival time logs along axis of the full-scale drift	64

2.7e Gamma-gamma (density) logs along axis of the full-scale drift 65

2.7f Young's modulus from CSM-cell measurements along axis of the full-scale drift 66

2.7g Differential resistance logs along axis of the full-scale drift 67

2.7h Fractures in core, along axis of the full-scale drift 68

2.8 Suite of logs from hole E6 in the full-scale drift 70

2.9 Sectional view through full-scale heater and extensometer drifts with holes N3 and N4 for neutron monitoring 72

2.10 Neutron probe measurements in N1 and N4 at 0.5-m stations with 30-sec counting times 73

3.1 Schematic of the CSM cell system 77

3.2 Calibration run for the CSM cell 79

3.3 Pressure-volume curve for laboratory modulus determination with the CSM cell 82

3.4 Representative CSM measurements at 10.0 m in borehole T9, February 2, 1978 86

3.5 Histograms of CSM-cell determinations of Young's modulus . . 87

3.6 In situ Young's modulus determinations versus fracture density from visual inspection of core 89

3.7 CSM-cell determinations of Young's modulus and fractures observed in core from borehole T6 90

3.8 Pressure-displacement data from the Goodman Jack 92

4.1 Block diagram of cross-hole ultrasonic equipment 96

4.2 Waveforms taken along the reference line using the compressional transducers and shear transducers 99

4.3 Transit times t_p and t_s for the compressional shear waves between M7 and M9 at the heater midplane 102

5.1 Schematic of SGU differential resistance probe with 12-mm-thick insulator between the upper and lower electrodes 109

5.2 Differential resistance log in borehole E7 111

Page

5.3 Laboratory tests of the differential resistance tool in an insulating medium with simulated fissures 112

5.4 Differential resistance signal amplitude against water salinity and width of discontinuities 113

5.5 Resistivity and resistance logs from borehole E6 in full-scale room 114

5.6 Resistivity and resistance logs from borehole E7 in full-scale room 115

B-1 Neutron-tool count rate in sand tank 133

B-2 Neutron probe in center borehole of quartz monzonite calibration block 135

B-3 Neutron tool count rate obtained with various combinations of water and core filling the boreholes in granite test block 136

B-4 Neutron logs in borehole N1, with four combinations of fluid and casing 138

B-5 Effect of hole size on count rate for decentralized neutron tool in water-filled boreholes 139

B-6 Radius of investigation tests in granite block 140

B-7 Neutron logs in holes adjacent to the 406-mm heater hole H9, which is full of water 141

C-1 Fission tracks associated with uranium concentrated between an altered grain of quartz and surrounding plagioclase 147

LIST OF TABLES

		Page
1.1	Geophysical and mechanical measurements in the underground holes at Stripa	10
2.1	Logs acquired with LBL borehole logging system SBH-1, Stripa, January - March 1978	26
2.2	Average water inflow rates in time-scale heater holes, with average gamma-ray activity from borehole log	55
4.1	Repeatability checks at reference positions in boreholes M6 and M9	99
4.2	Measured transit times between stations in boreholes M6 and M8	100
4.3	Sampling of Young's modulus (GPa) determinations in the laboratory and in situ on Stripa granite	103
B-1	Geometrical specifications of the granitic calibration block	135

ABSTRACT

Four different systems of borehole instrumentation have been employed thus far at an experimental site at Stripa, Sweden where a series of hydrological and thermo-mechanical experiments are being conducted to examine the suitability of granitic rock for the storage of radioactive waste materials. A suite of seven logs--neutron, gamma-gamma, resistivity, gamma ray, sonic, caliper, and temperature--operated in a borehole of 380-m depth located eleven zones where the rock permeability is expected to be enhanced due to the presence of open fractures. The sonic waveform record proved especially useful in this regard. Borehole measurements were also acquired in a large number of boreholes from 5- to 14-m length located in experimental drifts some 340-m underground. Here several physical properties, including the porosity, density, sonic velocity, and borehole rugosity, are generally quite uniform, with the exception of a few local chloritic zones and a few minor fractures. However, in situ determinations of the mechanical modulus with the CSM cell indicate substantial variability, with some apparent fracture control. Uranium and thorium concentrations are quite high in the Stripa granite, with local fluctuations associated with mineralogical changes as revealed by the gamma-ray log. A differential resistance probe appears promising as a sensitive detector of fine fracturing. A cross-hole ultrasonic system indicates variations of a few percent in compressional- and shear-wave velocities, reflecting the presence of fractures and changes in fracture characteristics as the rock is heated in a simulated storage test. The geophysical and mechanical data are being compared with the results from core and television logging, with hydrological test data on static pressure and injection permeability, and with displacements induced by thermal loading.

1. INTRODUCTION

The evaluation of potential sites for radioactive waste repositories will place new and stringent requirements on the tools and techniques used in borehole measurements. Of interest are the mechanical, hydrological, and geochemical parameters which will affect the design and the long-term integrity of a repository. In some cases, design criteria will impose unusual requirements in terms of sensitivity of detection. For example, in hard rock the extent and character of fracturing is of prime importance in the assessment of the hydrological regime. Hence borehole probes that can define those characteristics of fractures which determine the permeability to fluid flow will be of great assistance in the site evaluation stage. As a second example, the nature of a repository makes it desirable that as few holes as possible be drilled into the area around a proposed site. Since it will be desirable to extract as much meaningful data as possible from a small number of boreholes, cross-hole techniques will be needed so that larger volumes of rock can be sampled. Many other examples from the operation and monitoring modes of a repository can also be cited in which borehole investigations of various types will be needed.

A diverse technology for borehole measurements has been developed over the years for a wide variety of applications, resulting in an extensive literature. For rock engineering, Van Schalkwyk (1976) concisely summarizes available mechanical and geophysical techniques. For hydrological applications, Keys and McCary (1971) describe at length the fundamentals of the geophysical well-logging methods, many of which were used at Stripa. As suggested above, it is the end use of a repository site which requires new refinements in borehole technology. Additionally, there have been far fewer investigations in hard rock than in sedimentary rock, so the base

of experience is less broad.

An experimental site at Stripa, Sweden has been dedicated to tests for characterizing the thermal-mechanical response of granite to heaters simulating the heat load of radioactive waste cannisters, and to the development of methods for characterizing the hydrological regime in low-permeability rock. Witherspoon and Degerman (1978) discuss the nature and purposes of the project; the results of other investigations at the site are discussed in reports listed in the preface to this report. To prepare the site for the various investigations, about 160 boreholes were drilled, including two cored from the surface to approximately 370-m slant depth. Most boreholes range from 5 to 30 m in length, and were collared in the underground test area, 340 m below surface.

Figure 1.1 is a plan map of the site. The two surface holes, SBH-1

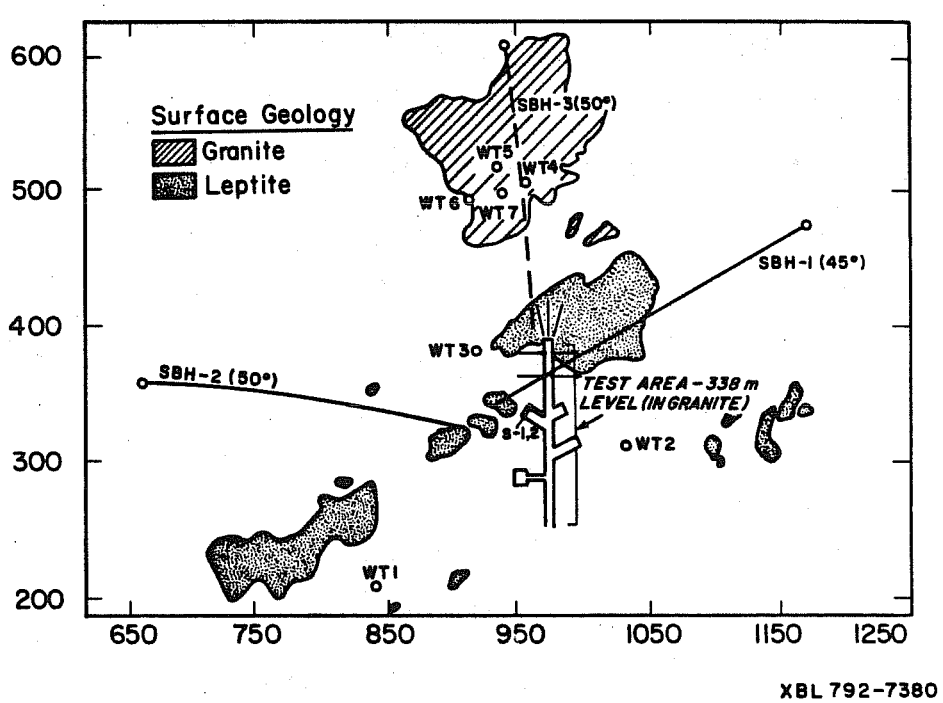

Fig. 1.1 Plan map of surface at Stripa showing outcrop, surface boreholes, and projection of underground experimental areas. Mine coordinates are given in meters.

and SBH-2, alternately penetrate granite and leptite (a high-grade metamorphic rock) before bottoming in granite at an elevation above the underground test areas. The underground areas are indicated by dashed lines on the grid between 300 and 400, and from 950 to 1000. Of interest in this report are the time-scale and full-scale drifts, where several heater experiments are underway to determine the thermal, strain, and stress fields induced by thermal loading from electrical heaters. Figures 1.2 and 1.3 are plan maps showing the heater and instrumentation borehole locations in these two drifts, where most of the underground borehole measurements discussed in this report were carried out. Kurfurst, Hugo-Persson, and Rudolph (1978) discuss the drilling and coring procedures and also tabulate the borehole survey results. The high density of boreholes in the underground drifts affords an unusual opportunity to examine the spatial variation of physical properties of a volume of rock of about 10-m linear dimension.

The borehole measurement program at Stripa is directed toward three distinct goals which correspond to the sequential steps of a drilling program in the investigation, construction, and operation of a repository site:

1) to acquire geological and geophysical information pertinent to the site selection phase, with particular regard to data relevant to the hydrological investigations, such as fracture location, fracture character, and rock porosity.
2) to acquire mechanical, geophysical, and geological information relevant to the design of a repository.
3) to monitor changes in the physical and chemical characteristics of rock as its temperature increases from heat generated by radioactive waste (or as simulated by electrical heaters).

At Stripa the first goal was primarily pursued by logging the surface hole SBH-1, while the measurements in the underground test volumes were directed

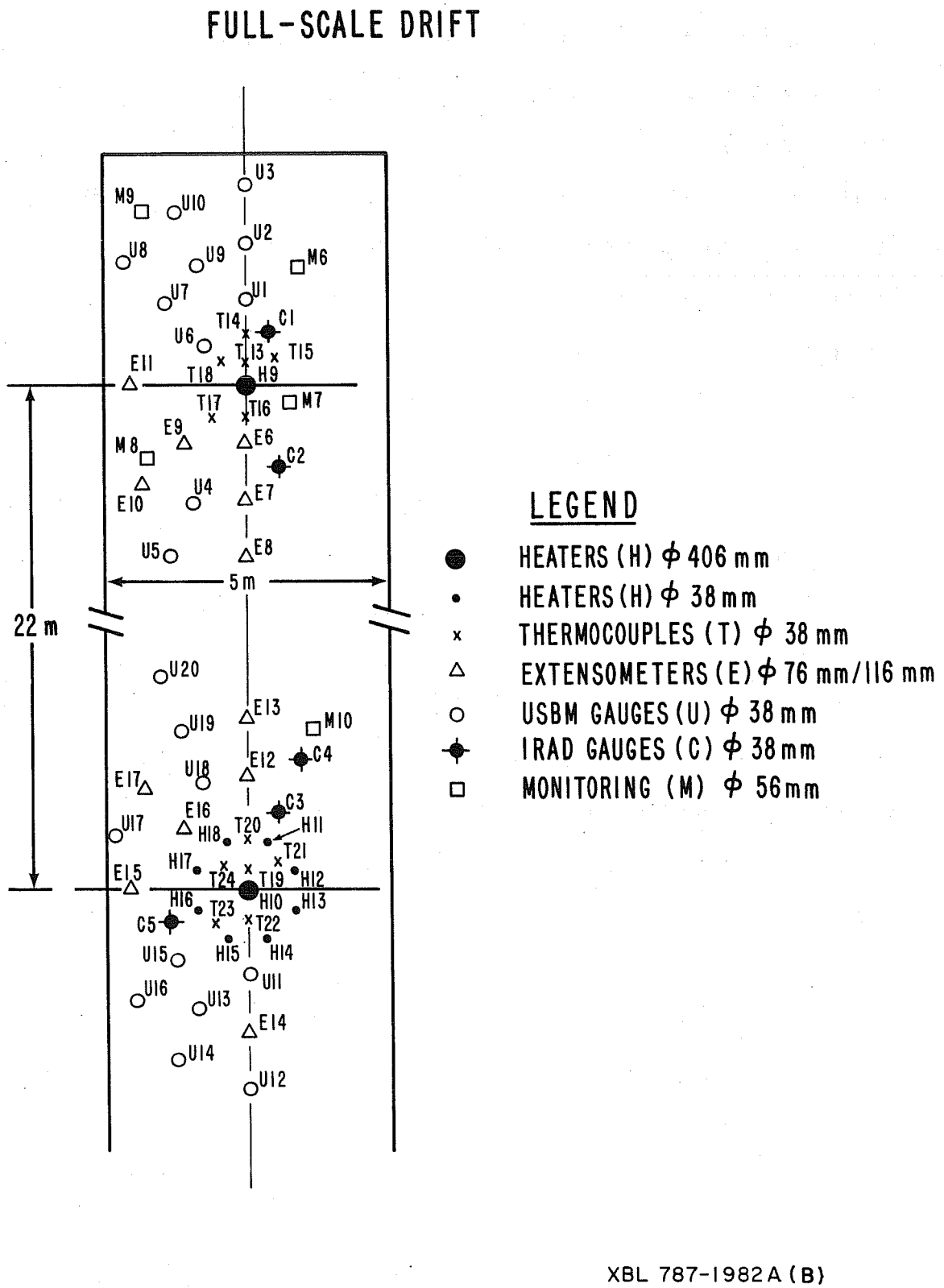

Fig. 1.2 Borehole layout in the full-scale drift (from Kurfurst, Hugo-Persson, and Rudolph 1978).

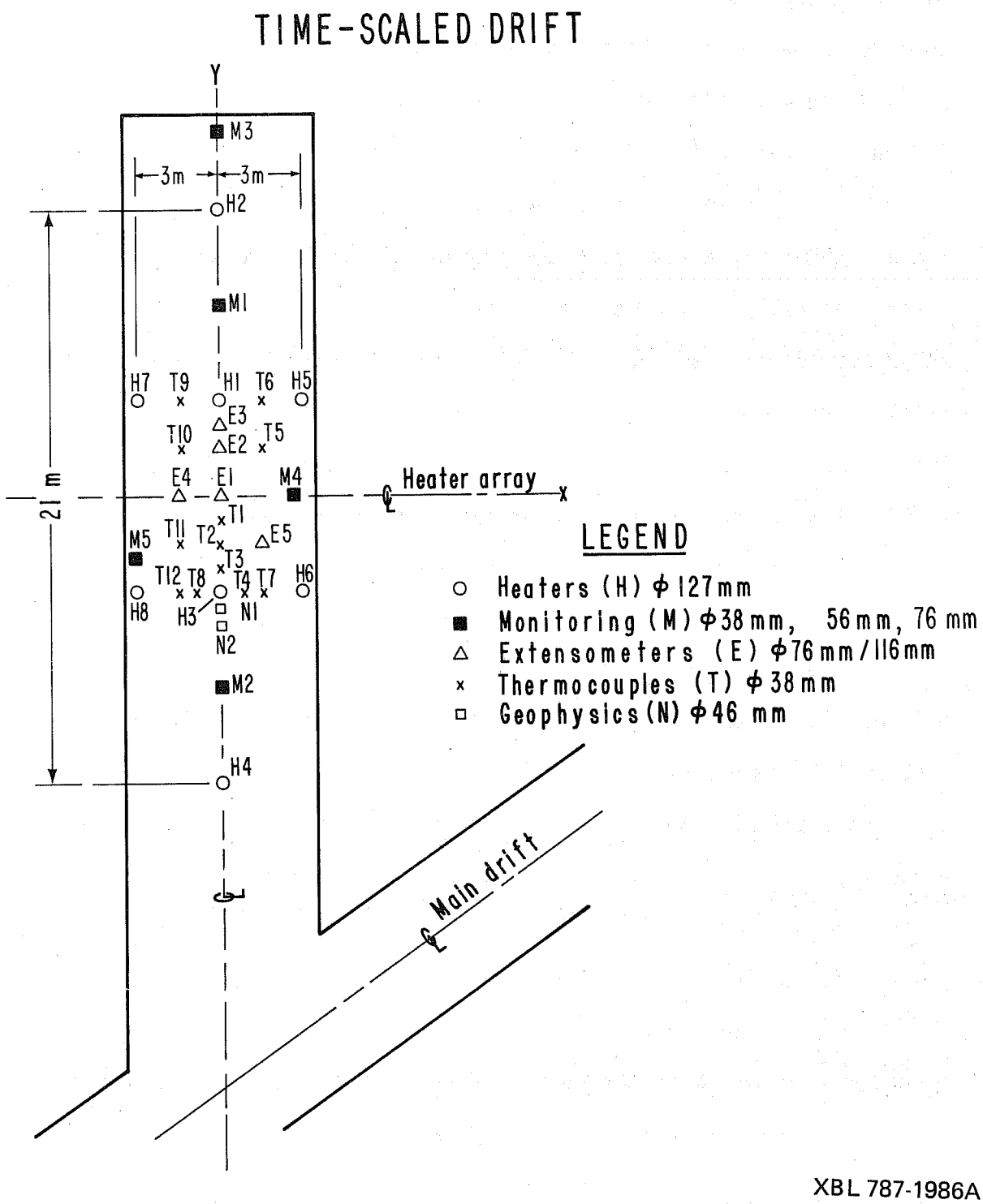

Fig. 1.3 Borehole layout in the time-scale drift (from Kurfurst, Hugo-Persson, and Rudolph 1978).

at the second and third objectives. In practice there is considerable overlap in methodology among the three objectives.

This report describes four sets of borehole measurements made at the Stripa site during 1978. The various techniques represent applications of available, state-of-the-art instrumentation to assess mechanical moduli, gamma-ray activity, water content, borehole rugosity, and fracturing, as well as effects due to the heating of the rock. Most of the measurements were made between January and March 1978, after most of the drilling was completed and before the commencement of hydrological testing from the surface or the installation of the instrumentation for the heater tests. Some measurements are continuing in special monitor boreholes during the heater tests, and others will be repeated after cessation of the heat tests.

This report is preliminary in that many of the measurements are either only partially complete or dependent upon the completion of the heater test and, in some cases, only partial analysis is available. Sufficient data are available, however, to be of possible use in planning similar measurements for other repository investigation projects.

In order of presentation, the four measurement systems are:

- A continuous logging unit equipped with natural gamma, neutron, gamma-gamma, temperature, electrical resistivity, caliper, and sonic probes. The basic unit was acquired by the Lawrence Berkeley Laboratory in October 1977 and shipped to Stripa to commence measurements in January 1978. It was used to acquire logs in the time-scale, full-scale, and ventilation drifts, and also in SBH-1, as shown in Table 1.1. The unit has remained at Stripa for periodic neutron measurements during the heater tests.
- Two mechanical systems for the measurement of mechanical moduli

in boreholes were applied in the underground areas by Terra Tek of Salt Lake City, Utah. Measurements were taken during January-March 1978 in the boreholes indicated in Table 1.1. One of these systems, the Colorado School of Mines (CSM) cell, remains at Stripa and it is planned to repeat some of the modulus determinations after cessation of the heater tests. The CSM cell was operated only in the 38-mm-diameter boreholes.

- Ultrasonic equipment from Terra Tek of Salt Lake City and from the University of Saskatchawan was tested at Stripa for the detection of fractures using compressional- and shear-wave propagation, both in a single borehole and between boreholes. The Terra Tek system was retained at Stripa for periodic measurements during the heater tests. These systems were operated mainly in the 56-mm boreholes designated by an M prefix.

- The borehole logging equipment from the Swedish Geological Survey (SGU) was used in March 1978 in the underground areas, as indicated in Table 1.1. The SGU system emphasizes electrical techniques for the detection of fractures.

Table 1.1. Geophysical and mechanical measurements in the underground holes at Stripa.

											FULL-SCALE DRIFT							
C1					d		m	r	q									
C2							m		q		T23				m			
C3							m				T24				m			
C4							m				U1	g	n	d	m	r	q	
C5							m				U2	g	n	d	m	r	q	
E6	s	c	g	n	d			r	q		U3	g	n	d	m	r	q	
E7	s	c	g	n	d			r	q		U4				m	r	q	
E8	s	c	g	n	d			r	q		U5				m	r	q	
E9	s	c	g	n	d				q		U6				m	r	q	
E10	s	c	g	n	d				q		U7				m	r	q	
E11	s	c	g	n	d				q		U8				m	r	q	
E12	s		g		d			r	q		U9				m	r	q	
E13	s		g		d			r	q		U10				m	r	q	
E14	s		g		d			r	q		U11	g	n	d	m	r	q	
E15	s										U12	g	n	d	m	r	q	
E16	s										U13				m			
E17	s										U14				m			
H9	s										U15				m			
H10	s										U16				m			
M6			g	n	d	u		r	q		U17				m			
M7			g	n	d	u		r	q	h	U18				m			
M8			g	n	d	u		r	q	h	U19				m			
M9			g	n	d	u		r	q	h	U20				m			
M10											H11				m			
T13			g	n	d		m	r	q		H12				m			
T14			g	n	d		m	r	q		H13				m			
T15			g	n	d		m		q		H14				m			
T16			g	n	d		m	r	q		H15				m			
T17							m		q		H16				m			
T18							m		q		H17				m			
T19			g	n	d		m		q		H18				m			
T20			g	n	d		m	r	q									
T21							m											
T22			g	n	d		m	r	q									

Note: LBL Logging system: sonic (s), caliper (c), gamma (g), neutron (n) gamma-gamma (d)
Cross-hole ultrasonic system: (u); CSM cell measurements of modulus: (m)
SGU logging system: resistivity (r), resistance (q), gamma (h)

Table 1.1 (continued)

TIME-SCALE DRIFT

E1	s	c	g	n	d		r	q								
E2	s	c	g	n	d		r	q		N1	g	n	d			
E3	s	c	g	n	d		r	q		N2	g	n	d			
E4	s	c	g	n	d		r	q		T1	g	n	d	m	q	
E5	s	c	g	n	d			q		T2	g	n	d	m	q	
H1	s	c	g	n	d			q		T3	g	n	d	m	q	
H2	s	c	g	n	d			q		T4	g	n	d	m	q	
H3	s	c	g	n	d			q		T5	g	n	d	m		
H4	s	c	g	n	d			q	h	T6	g	n	d	m		
H5	s	c	g	n	d					T7	g	n	d	m		
H6	s	c	g	n						T8	g	n	d	m		
H7	s	c	g	n	d					T9	g	n	d	m		
H8	s	c	g	n	d					T10	g	n	d	m		
M1	s	c	g	n	d		r	q		T11	g	n	d	m		
M2	s	c	g	n	d	u	r	q		T12	g	n	d	m		
M3																
M4	s	c	g	n	d	u	r	q	h							
M5	s	c	g	n	d	u	r	q	h							

VENTILATION DRIFT

R1			
R2			
R3	g	n	d
R4	g	n	d
R5	g	n	d
R6			
R7			
R8		n	d
R9		n	d
R10		n	d
S1		n	d
S2	g	n	d
HG3	g	n	d
HG4	g	n	d

EXTENSOMETER DRIFT

N3	g	n
N4	g	n

2. GEOPHYSICAL LOGS WITH THE LBL LOGGING SYSTEM

2.1 Description of Instrumentation

The borehole logging program at Stripa required a system that could log the 380-m surface holes and also be used to log the 10- to 30-m boreholes in the underground drifts. It was also required that a variety of tools be operated from the same unit and that the electronics and recording systems be fairly flexible. Because of scheduling, a short delivery time was desired. Fortunately, several units are available commercially to satisfy the needs of the coal and uranium exploration industry. The unit selected for Stripa was the Mt. Sopris 3000NB logger manufactured by the Mt. Sopris Instrument Co. of Delta, Colorado (Fig. 2.1).

The logging unit includes an electric winch with a variable speed controller, about 1000 m of armored, four-conductor cable, an encoder which

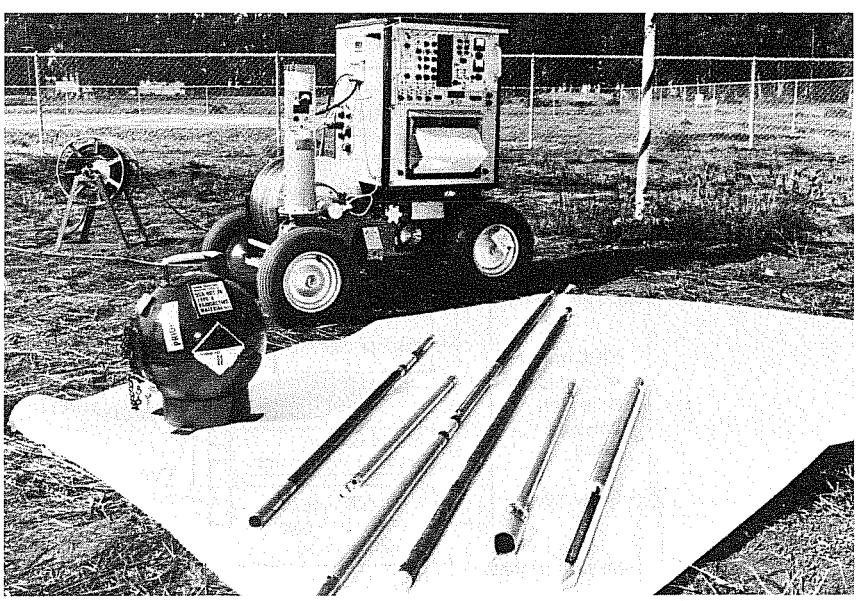

XBB 7711-11183

Fig. 2.1 Logging unit with 1000 m of armored cable. In foreground, from left to right, are storage container for the neutron source, and the neutron, temperature, gamma-gamma, gamma, spinner, and caliper probes. Reel in background contains power cable.

provides pulses proportional to the motion of the cable, housing for nuclear instrumentation module (NIM) electronics, and a four-pen Texas Instruments chart recorder with bi-directional drive. The block diagram of Fig. 2.2 shows the components of the overall system. The total weight of the unit with the cable is about 225 kg. For shipping, the system can be readily broken down into two components: the electronics and chart recorder cabinet, and the frame holding the winch. Overall dimensions of the assembled logger are 67 cm wide by 92 cm high by 97 cm long. Four pneumatic tires were added to the unit (Fig. 2.1), so that two men were able to maneuver it in the underground drifts.

A Gearhart-Owen 1-inch cable head for 4HO cable was specified for the system. All tools mate to it either directly or with an adapter, with

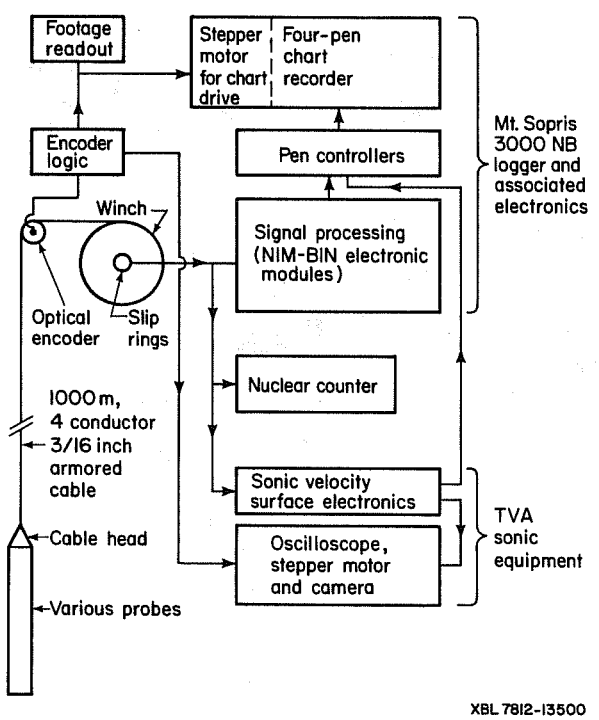

Fig. 2.2 Block diagram of borehole logging equipment used at Stripa.

the exception of the sonic logging unit from the Tennessee Valley Authority (TVA) for which the cable had to be reheaded before it could be used.

Figure 2.2 indicates two other pieces of equipment which were used with the logger. A Canberra model 1775 nuclear counter was used in conjunction with the pulse-type tools, and is particularly necessary with the neutron monitoring. The sonic equipment contracted from the TVA consisted of the surface panel, borehole sonde, oscilloscope, stepper motor, and camera. Except for the nuclear counter and the TVA sonic equipment, all other electronic instrumentation was packaged in nuclear instrumentation modules (NIMs) with plugs compatible with the Mt. Sopris wiring system. The modules used are:

- A Mt. Sopris ratemeter used for the gamma, gamma-gamma, neutron-thermal neutron, temperature, and spinner logs. This module was modified to count negative pulses produced by the temperature and spinner tools. A zero suppress for the recorder was also added.
- A Mt. Sopris caliper module was used for the Mt. Sopris caliper tool, with the output to the recorder modified to expand the range and permit zero suppression.
- Mt. Sopris self-potential and resistivity-resistance modules were used with the combination gamma ray/electrical tool, but these measurements were unsuccessful due to the high resistivity of the granite.
- An expander-offset module fabricated at LBL was used to amplify the dc output of either the ratemeter or caliper modules by a factor of 2, 5, or 10 and, with appropriate zero suppress, to record the result on a second chart recorder pen. With this module, side-by-side dual records were made of most logs. The low-sensitivity record was always on scale and gave a continuous calibrated record. The high sensitivity record was used

for detail and could be brought back on scale with the offset when necessary.

- A power supply fabricated at LBL supplied the high-voltage dc power required by the neutron and gamma-gamma probes.

- A current transmitter and a dual-channel receiver fabricated at LBL formed the basis of a four-electrode resistivity system. Problems developed with the transmitter, however, as described in item F, below.

After some experimentation, all logs were recorded at a depth scale of 50:1, or 1/2 m of borehole per cm of paper. An exception to this is the film record of the sonic waveforms recorded with the TVA sonic equipment, which was run at a scale of 75:1 due to a mismatch between the pulse rate supplied by the encoder and the counting logic in the stepper motor for the oscilloscope camera. Logging speed was 2.5 m/min.

Descriptions of the probes and their calibration status at the time of the logging operation follow:

A. Gamma. The outside diameter of the Mt. Sopris gamma-ray probe is 33 mm, and its length is 2.07 m. The NaI detector is 12 mm in diameter and 38 mm in length. Power is supplied from the supply incorporated in the chassis, and pulses from the probe are detected and counted by the Mt. Sopris ratemeter.

Logs were acquired at a scale of 50 counts per sec (cps) per cm with the backup log at a scale of 25 cps per cm. The averaging time was 4 sec at a logging speed of 2.5 m/min. At these counting rates the compensation circuitry in the ratemeter was not required and was not used. During the use of the probe at Stripa, repeat logs run in three boreholes showed that the counting rate had dropped about 8 to 12 percent in a three-week period. The cause for this drop was not established nor were the logs corrected

for the shift. No other provisions were made for referencing the tool during the logging operations.

The International Atomic Energy Agency (1976) suggests that calibration of a total-count gamma-ray probe be based on a new unit called the unit of radioelement concentration, abbreviated "ur," and defined in terms of the instrument response to one part per million of uranium in equilibrium with its daughter products. An empirical relation between the observed count rate and radioelement concentration which appears applicable to our case is:

$$N(\text{counts per second}) = k\left[1.5\ K(\%)+U(\text{ppm})+0.47\ Th(\text{ppm})\right].$$

Using the data from the upper 4 m in borehole N1, as given in Appendix A and Fig. 2.6 (page 56), the average values are K = 4.29 percent, U = 42.7 ppm, Th = 31.6 ppm, and N = 205 cps. The resulting sensitivity factor for this particular probe is then k = 3.3 cps/ur.

B. Neutron. The neutron probe was purchased from Comprobe, Inc. of Fort Worth, Texas. The outside diameter is 32 mm and its length is 1.5 m. A 1.4-Ci Am-Be source in a stainless-steel source sub-threads onto a spacer at the bottom of the probe. A 7-inch spacer separates the source from the He-3 detector. Above the detector the probe contains the photomultiplier tube and the pulse amplification electronics.

Pulses from the neutron probe were received by either the Mt. Sopris ratemeter or the Canberra Model 1775 nuclear counter (see Fig. 2.2). Power was supplied by the 150-V NIM supply module.

Calibration of the neutron probe was carried out at LBL with a specially constructed granite block. The procedures and results are described in Appendix B. The most pertinent result was the sensitivity of the neutron

probe: as the water content increases 1 volume percent, the count rate decreases by 85 cps (see Fig B-3, page 136). It is also apparent from Fig. B-3 that the count rate at 1 percent water content is around 1800 cps.

In operation underground the probe is referenced by inserting it into a 200-liter water barrel. This referencing operation defines the long-term stability as well as linking the periodic measurements carried out in the vicinity of the heaters (see Section 2.5 on neutron monitoring of water content changes, page 71).

For operation in vertical boreholes, the tool was pressed against the borewall with a piece of spring steel fastened to the probe. If the tool is not decentralized then the count rate varies with the position of the probe in the borehole. The tool was also decentralized during the calibration described in Appendix B.

The procedures for handling and storing the radioactive sources, both the 1.4-Ci neutron source and the 16-mCi gamma source, were developed in cooperation with Statens Stralskyddsinstitut in Stockholm. When not in use the neutron source was removed from the probe and stored in a 38-cm-diameter spherical container furnished by the supplier. Similarly, the section of the gamma-gamma probe containing the gamma source was unthreaded from the probe and placed in a lead shield furnished by the supplier. The shielded sources were stored in a small cavity excavated in a nearby drift. They were locked behind a steel door marked with the appropriate warning signs at the mouth of the opening. Radiation dosimetry badges are worn by personnel operating the equipment and are exchanged monthly and metered at the Statens Stralskyddsinstitut.

C. Caliper. The Mt. Sopris three-arm mechanical caliper probe is 51-mm o.d. and 1.20-m long. Unfortunately, the tool diameter precluded its use

in boreholes smaller than 76 mm. The movement of the three linked arms is sensed as a voltage change on a linear potentiometer, converted to a frequency, then transmitted to the surface module. A set of long (29.9-cm) arms supplied with the probe were too long and soft, providing only limited sensitivity in the boreholes at Stripa--so a second set of arms (6.35 cm) was ordered especially for use in the 76-mm holes. The short arms, equipped with tungsten carbide tips, afforded a great improvement in sensitivity. The force at the tips acting against the borewall was not measured, but it was quite difficult to close the arms by hand; moreover, the arms were stiff enough that the probe could operate accurately in a horizontal 76-mm borehole without centralizers.

The surface electronics module was modified to permit recording on an unusually sensitive scale. The longer arms were too long and too soft to give useful data in the 127-mm heater holes, so the following comments pertain to the 76-mm holes only. Logs were acquired on two scales, 2 mm of diameter per cm of chart and 0.4 mm per cm. The probe was calibrated with a brass tube machined with 1.27-mm diametral steps ranging from 76.2 to 81.3 mm. The calibration tube was used to set the chart scale before logging and again as a check after logging. The resolution of the potentiometer limited the sensitivity to about 0.2 mm of diametral change. Sensitivity to vertical aperture has not been established but is limited by the radius of curvature of the arm tips. Hysteresis, that is, the ability to track the diameter as the arms are closing or opening, is about 0.3 mm.

D. Gamma-Gamma Probe. A gamma-gamma borehole probe for the measurement of rock density was acquired from Comprobe, Inc. of Ft. Worth, Texas. The probe is designed to detect thin beds in sedimentary sequences and is referred to as a "high resolution" density probe. It is 31-mm o.d.

and 2.50-m long. The source, 16 mCi of Americium-241, is located near the bottom of the probe close to the outside edge. A single gamma-ray detector is located immediately above the source with its peak response such that the effective source-detector spacing is 57 mm. In operation it is decentralized against the borewall with a motorized decentralizer arm.

Unfortunately, there was no time to calibrate the probe before shipment to Sweden and no density calibration was available from the manufacturer. However, a few crude measurements confirmed the expected behavior for a density probe: a straight-line decrease of the logarithm of the count rate when plotted against density.

Another quick check on tool performance was accomplished in a sand tank. The tank consisted of a 3.0-inch-o.d. aluminum cylinder which simulated the borewall, and an outer 35-inch-i.d. cylinder of steel. Sand filled the annular space between the aluminum and steel; a very thin 0.5-mm steel sheet was placed horizontally within the sand, configured so it fit snugly around the aluminum "borehole." The count rate was recorded at fixed locations. The rate adjacent to the sand was approximately 450 cps, dropping to a minimum of 310 cps opposite the thin horizontal steel sheet. The half-width of the minimum was about 4 cm. When the probe was pulled past the sheet in a continuous logging mode, the location and size of the minimum depended on the pull rate and the averaging time of the electronic circuitry. This test simply showed that the spatial resolution of the tool was quite good when the target was a very good absorber.

E. Sonic Velocity and Waveform. The TVA sonic velocity equipment consisted of an S.I.E. 70-mm camera, a digital camera drive, a Hewlett-Packard 1206B oscilloscope, surface electronics, and a borehole probe containing a magnetostrictive acoustic source, receiver, and borehole electronics.

The borehole probe and surface electronics were manufactured by Simplec, Inc. of Dallas, Texas with modifications by the TVA. The probe is approximately 1.4-m long and 60 mm in diameter. The source-receiver distance is 0.30 m.

The equipment was operated from the LBL logging unit as indicated in Fig. 2.2. The transit time of the first compressional wave arrival was taken from the analog output of the surface electronics and recorded on the chart recorder on two pens at scales of 5 and 10 μsec per cm. Due to variations in the gain and discriminator settings, the uncertainty in the absolute value of transit time measurement was about 3 μsec or 6 percent in velocity. Waveforms were recorded both in variable density format and as individual waveforms. The variable density films were run at scales of 20 μsec/cm and 50 μsec/cm on the oscilloscope and at a 75:1 depth scale. Individual waveforms were recorded every 0.5 m of borehole in the underground holes. In each of the underground holes three logging runs were made: first with the variable density at 20 μsec/cm and a transit time log, second with the variable density at 50 μsec/cm and another transit time log, and third with the individual traces. In SBH-1 only the first type of run was made, with one interval repeated as a quality check.

The 60-mm probe diameter precluded logging in any holes except the 76-mm, 127-mm, and larger heater holes. See Table 1.1 for a record of the holes that were logged.

F. Electrical Resistivity. An electrical resistivity measurement system was designed and built at LBL for use at Stripa. The system consists of a transmitter and a receiver, each housed in a NIM, and two electrode bridles with heads compatible with the cable head on the logger.

The transmitter was designed to switch regulated current through a

resistive load at frequencies ranging from 0.1 to 1000 Hz. It consists of timing signal circuitry with a reference output, a current source and metering, and four power transistors in a bridge configuration. Current output is limited by the dc power supplied to the unit and the size of the resistive load.

The receiver is a dual-channel unit with switchable gain and synchronous detection requiring a reference signal from the transmitter. The output is a logarithmic voltage used to drive the chart recorder. The controls on the front panel are gain, 50/60-Hz notch filter, averaging time, low-pass filter frequency, output offset, and span.

Both electrode bridles are 20-m long with lead electrodes at the bottom and 16 m from the bottom. One bridle has potential electrodes 2 m and 4 m from the bottom electrode, the other at 0.5 m and 1 m from the bottom. They were designed to be used with the dual-channel receiver so that a suite of four "normal" or pole-pole resistivity arrays could be acquired in two logging runs.

In practice the current-regulating circuitry in the transmitter proved inadequate. Consequently the transmitter current was not held constant as the load (electrode) resistance varied. The net effect was to accentuate the low-resistivity zones, but no quantitative information could be retrieved because the current information was lost. The resulting "pseudo-resistivity" log is still valid for qualitative examination and is presented in (Fig. 2.3, page 28)* for comparison with the other logs.

G. Temperature. Temperature was measured in the continuous logging mode

---

*Figures 2.3 and 2.4 are representative, reduced versions of Plates 1 and 2, which are not included in this report, to reduce printing costs.

with a thermistor probe acquired from Well Reconnaissance of Dallas, Texas. The pulse output of the probe was detected by the Mt. Sopris ratemeter after the circuitry was modified to accept negative pulses. Calibration of the the sensor was done with a calibration unit supplied by the manufacturer and the Canberra ratemeter. The nonlinear response of the thermistor was compensated by relating the temperature to the pulse rate with a quadratic fit. Since the temperature range encountered while logging was less than 4°C, the nonlinear effects were small. Because only changes in the temperature gradient were sought, absolute accuracy was not established.

H. Spinner. A three-blade spinner tool was acquired from Well Reconnaissance of Dallas, Texas. The rotation of the spinner in the fluid is converted to electronic pulses by a Hall-effect device sensing the rotation of a magnet on the shaft. The pulse output of the probe was detected by the Mt. Sopris ratemeter and recorded on the chart using a gain of 10 on the expander module. A test in borehole SBH-1 indicated a sensitivity of about 2.5 m/min per one pulse per sec, a rate too low for application at Stripa.

Depth accuracy. The depth of a tool is measured by an optoelectronic encoder on a perforated wheel which turns as the cable moves past. The measure point of an individual tool is preset by the operator with thumbwheel switches. In SBH-1 the overall accuracy of the system was checked by comparing log anomalies with geological features noted on the core log. This has the advantage of incorporating offsets due to preset errors, integration time constants, logging speeds, and all mechanical and electronic errors, but has the disadvantage of relying completely on the driller's tally.

The logs were checked in SBH-1 between 208 m and 339 m against nine geological features, such as greenstone occurrences and pegmatite dikes. Depths of individual features on the neutron, caliper, and P-wave velocity

logs were within 0.5 m of the core log features. The gamma log depth is 0.5 m too low due to adoption of the SP electrode as the measure point; hence 0.5 m was subtracted from the original depths. The gamma-gamma depth setting was 1 m too high; that is, all the original logged depths required the addition of 1 m. These corrections have been incorporated into the detailed analysis and the final composited logs of Fig. 2.3, page 28, so they will be of concern only when referring to the original logs. After correction, the depth accuracy is regarded as better than ± 0.5 m. Hence in the discussion anomalies are referred to the nearest 0.5 m.

Operation sequence. The LBL logging unit arrived at Stripa in early January and was immediately set up on SBH-1 to run the TVA sonic waveform tool. Because the TVA tool was on contract, and scheduling was tight, the procedure was to run all the sonic logs first, both on the surface and underground. After running the SBH-1 sonic log, the equipment was moved to SBH-2. The sonic waveform log was run from 359 m to 122 m in SBH-2. The log was not satisfactory, so the waveform film record was destroyed and the chart record (P-wave transit time) was retained. Upon inspection, this log proved to be of such poor quality that it has not been analyzed or described. A second run was begun at 359 m, but the tool stuck fast at 356 m and could not be freed by pulling on the armored cable. The drilling rig was still on the site, so a fishing head was machined by Hagby-Bruk and retrieval operations began. Tool recovery consumed two days time and required lifting the jammed tool the entire length of the hole with the drill string. Although the tool suffered no damage, logging operations were terminated due to the possibility of getting stuck again. No other logging was attempted on SBH-2 with the other (smaller diameter) tools because of apprehension over tool loss and because of time and manpower limitations.

The equipment was then moved underground for five weeks to log the boreholes in the time-scale and full-scale heater experiment drifts. In mid-February the unit was moved back to the surface and the remainder of the SBH-1 measurements were completed. No problems were encountered with the probes hanging up or sticking in SBH-1. In early March the unit was returned underground, where a few more logs were acquired in the full-scale drift and logging in the ventilation drift commenced. (Ventilation-drift logs are not discussed in this report.) In June periodic neutron measurements in the N-holes commenced.

During the measurement operation a variety of electronic malfunctions occurred which were repaired by the operators or technicians from associated projects (with the exception of the electrical resistivity unit, as discussed above). Mechanical problems were rare and of little consequence.

Copies of all logs were retained in the files at Stripa for future reference and to ensure against loss during shipment to LBL. At LBL the logs were digitized at a rate of one point per mm of chart paper, equivalent to one point per 5 cm of borehole. Digitization was carried out on a Tektronix 4956 digitizer using a Tektronix 4051 as a controller. Subsequently the data were transmitted via telephone link to the LBL central computing facility to be stored on disc file. Software development was required for the communication link between the 4051 and the central computer and also for the file storage and retrieval system. For display, data were recalled from file storage to the 4051 system and plotted on a Tektronix 4662 digital X-Y Plotter. Having the logs in digital form made it possible to readily change scale, perform simple arithmetic operations, and make plots as desired.

2.2 SBH-1 Geophysical Logs

Table 2.1 lists the logs originally acquired in surface borehole SBH-1,

Table 2.1. Logs acquired with LBL borehole logging system SBH-1, Stripa, January - March 1978

Log type	Depth interval(m)	Date	Operator
P-wave transit time[1]	310-384	Jan 10 78	PN, DS, BP[6]
Acoustic Waveform (film)[2]	310-384	Jan 10 78	PN, DS, BP
P-wave transit time	70-384	Jan 10 78	PN, DS, BP
Acoustic Waveform (film)	70-384	Jan 10 78	PN, DS, BP
Gamma Ray[3]	2-380	Feb 17 78	PN, DS, BP
Temperature[3]	2-380	Feb 20 78	PN, BP, LA
Resistivity[4]	81-380	Feb 21 78	PN, LA
Gamma-gamma (density)[3]	10-380	Feb 22 78	BP, LA
Temperature	5-380	Feb 23 78	BP, LA
Caliper[5]	0-380	Feb 23 78	BP, LA
Neutron[3]	2-380	Mar 2 78	BP, LA

(1) P-wave transit times are relative only, not absolute, due to the uncertainty in gain and discriminator settings. Chart is scaled in microseconds per cm of chart.

(2) Acoustic waveforms recorded on film at a 75:1 depth scale. All other logs recorded on paper chart at 50:1 scale.

(3) Scales of the radiation tools are given in counts per second per cm of chart paper, pending final tool calibration.

(4) The resistivity logs are not quantitatively valid (hence no scale) due to transmitter malfunction.

(5) The caliper calibration is absolute. Chart is scaled in mm of hole diameter per cm of chart paper.

(6) PN-P. Nelson, BP-B. Paulsson, LA-L. Andersson, all LBL; DS-D. Scott from Tennessee Valley Authority (TVA), Knoxville, Tenn.

together with the depth interval, date of acquisition, and other comments relevant to the original records. The detailed and summary descriptions which follow are keyed to Figs. 2.3 and 2.4. Figure 2.3 is a reduction of a composite which was done at a 500:1 scale of all the logs originally recorded on chart paper, along with auxiliary data from the core logging and television logging. All data and comments are presented as a function of slant depth in the borehole, which is less than vertical depth due to the dip of the hole. In the comment column are given the major subdivisions based upon interpretation of the geophysical logs, as well as selected comments on the more important features. Also included is a key indicating those zones considered likely to be most permeable. Selection of these zones is discussed in the detailed description below.

Figure 2.4 contains replicas of the film records of the acoustic waveforms. The waveform record requires explanation. These records were made by greatly amplifying the sonic wave trace and intensity, modulating the z-axis of the oscilloscope so that a bright spot appears at the negative-going portion of the waveform and no trace appears at the positive-going portions. By stepping the camera which records the oscilloscope image while the probe is moving upward in the borehole, a high-density record of the zero-crossing behavior of the waveforms is obtained. In Fig. 2.4 time increases to the right with about 30 μsec between the first few dark bands, or negative-going portions of the wavetrain. Also recorded in Fig. 2.4 are the indications of fractures as noted by the core and television logging of SBH-1.

The following paragraphs summarize the outstanding features observed in the data. Following this summary, specific features in the logs are

SBH-1 BOREHOLE LOGS

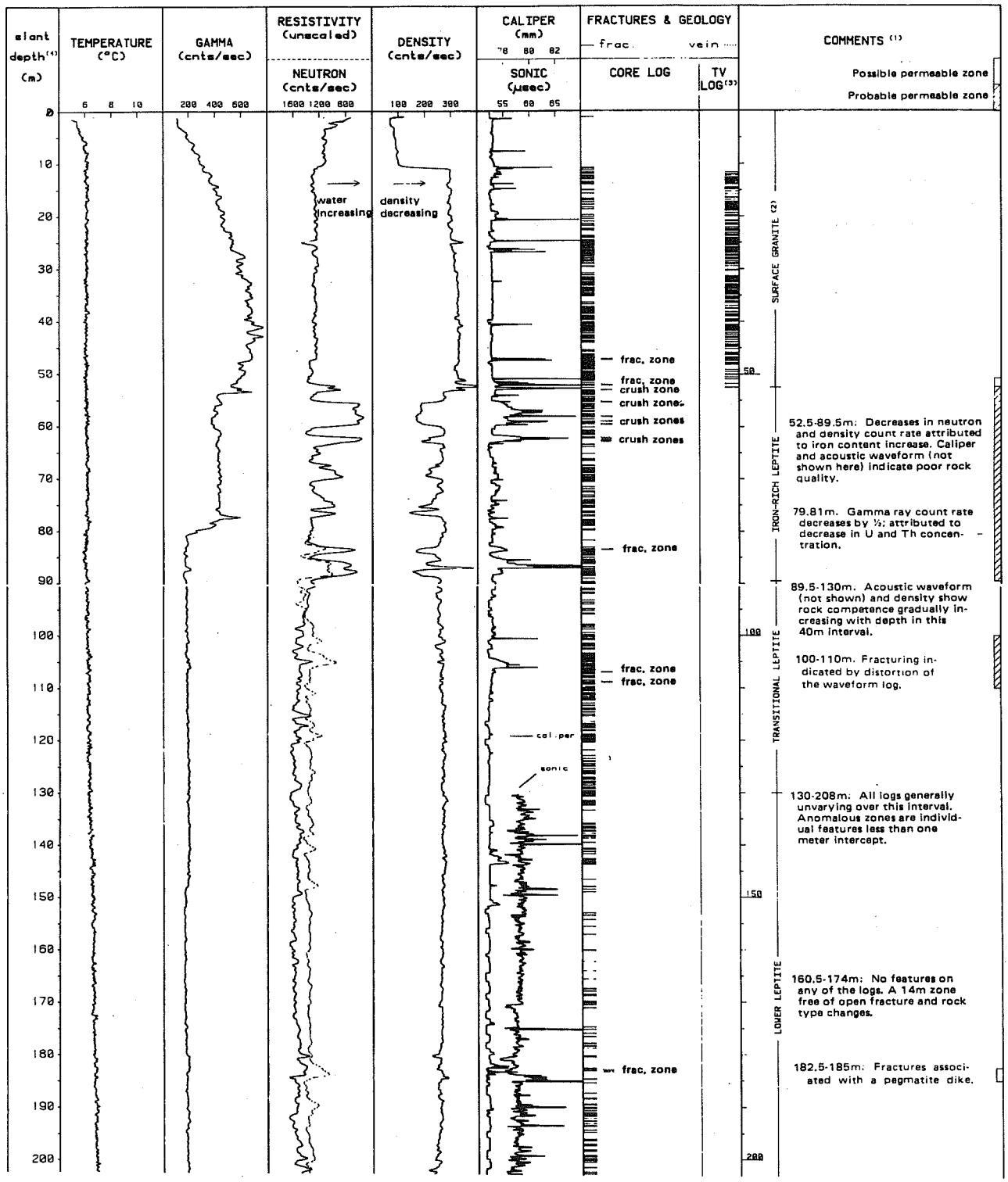

Fig. 2.3 Geophysical logs in SBH-1, greatly reduced from the 500:1 scale of the original plate.

SBH-1 BOREHOLE LOGS (Continued)

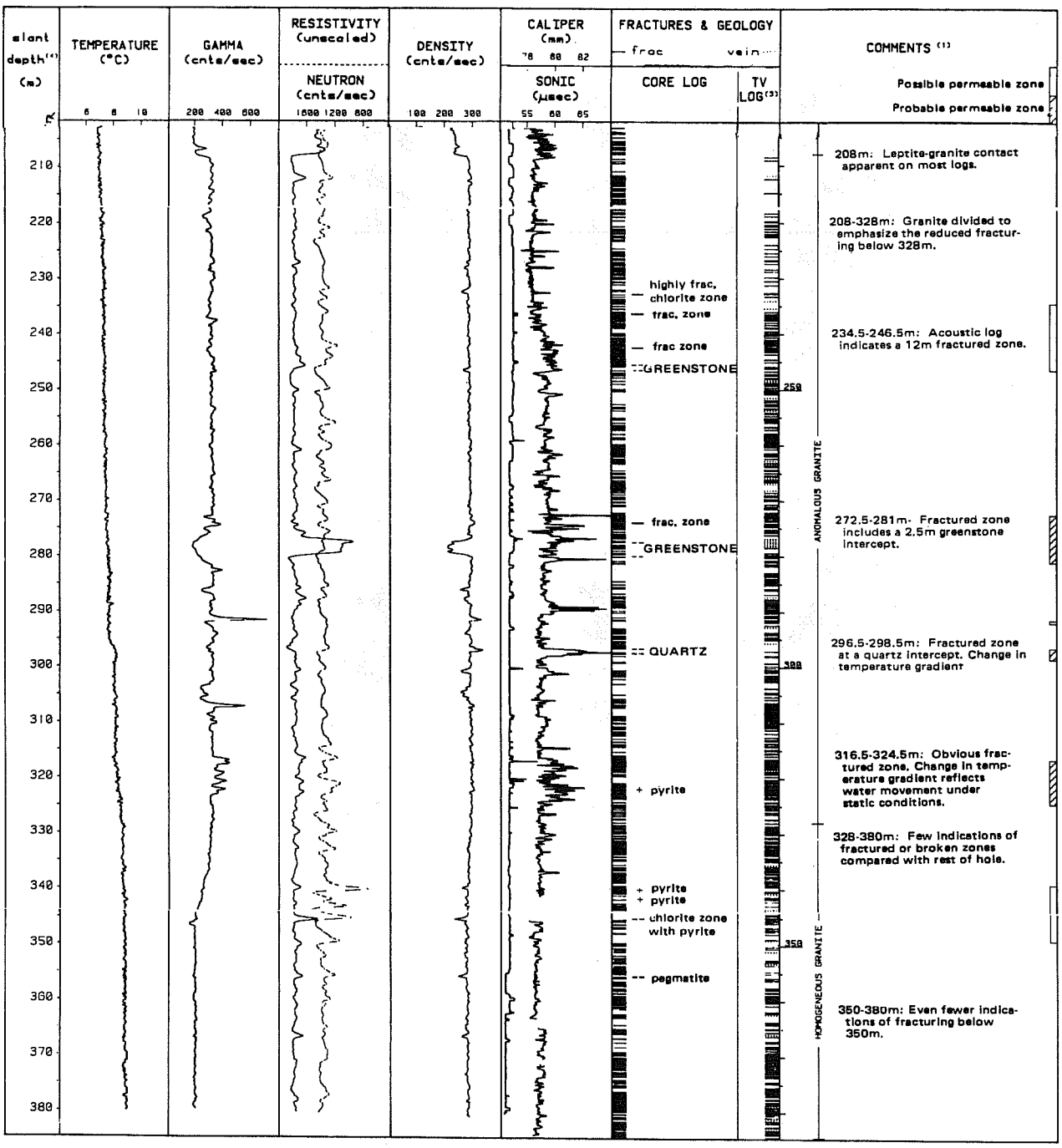

(1) Descriptive comments are excerpted from the accompanying report. See report for details.

(2) The names attached to the depth intervals in the comments column are based upon the logs and are not of geological origin.

(3) No television logging in the leptite interval, 52.5 – 208m.

(4) Depth given is slant depth, as measured along the borehole. The true depth is given approximately by: true depth = 0.707 × slant depth.

Plate 1 Geophysical, geological, fracture and television logs from surface hole SBH-1, Stripa, Sweden

Logged by P.Nelson, L.Andersson, B.Paulsson Feb.-Mar., 1978

Compiled by R.Rachiele Commentary by P.Nelson

Vertical scale 500:1

Lawrence Berkeley Laboratory, Berkeley, Ca.

XBL 7811-12284

SBH-1 : SONIC WAVEFORM, CORE LOG and TV LOG

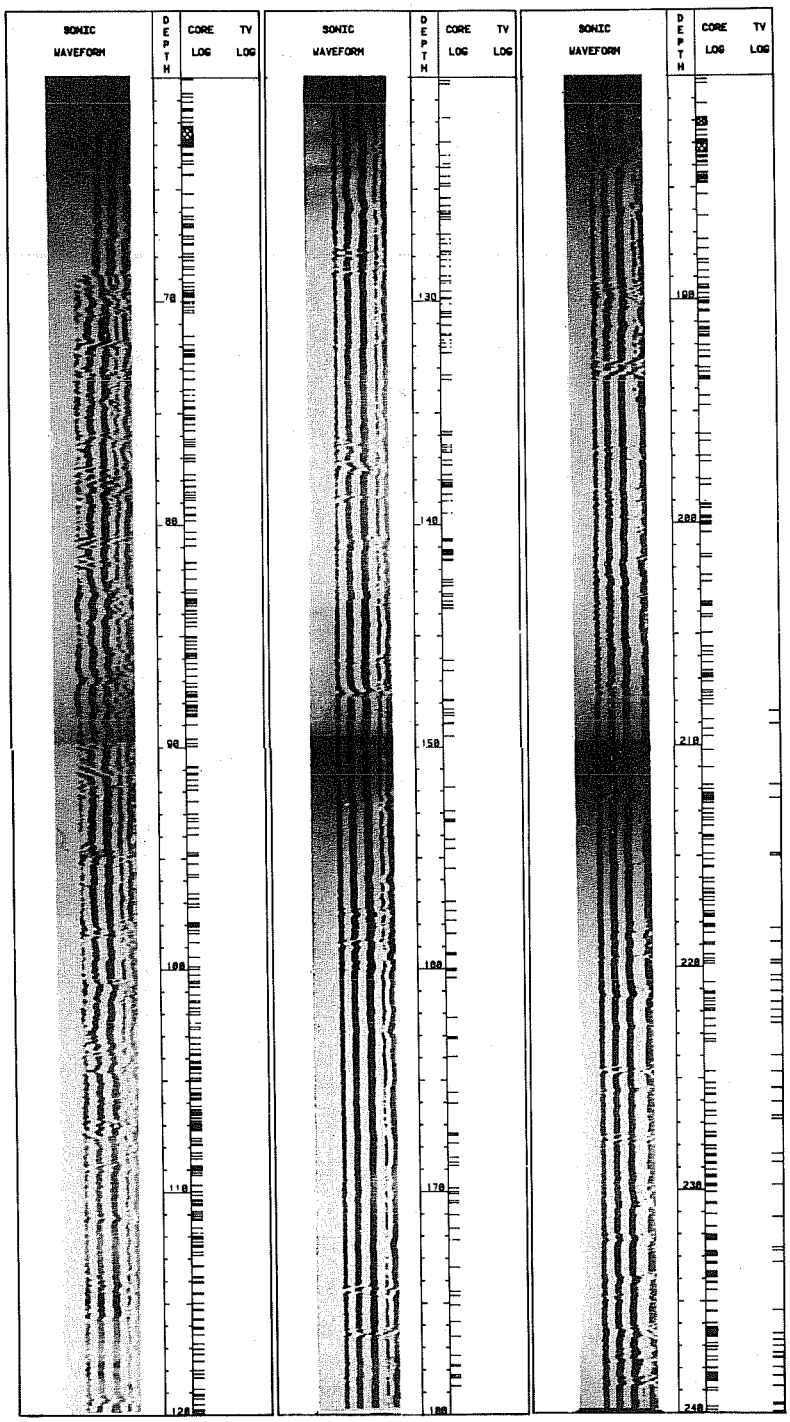

Fig. 2.4 Sonic waveform, core, and TV logs in SBH-1, greatly reduced from the original plate.

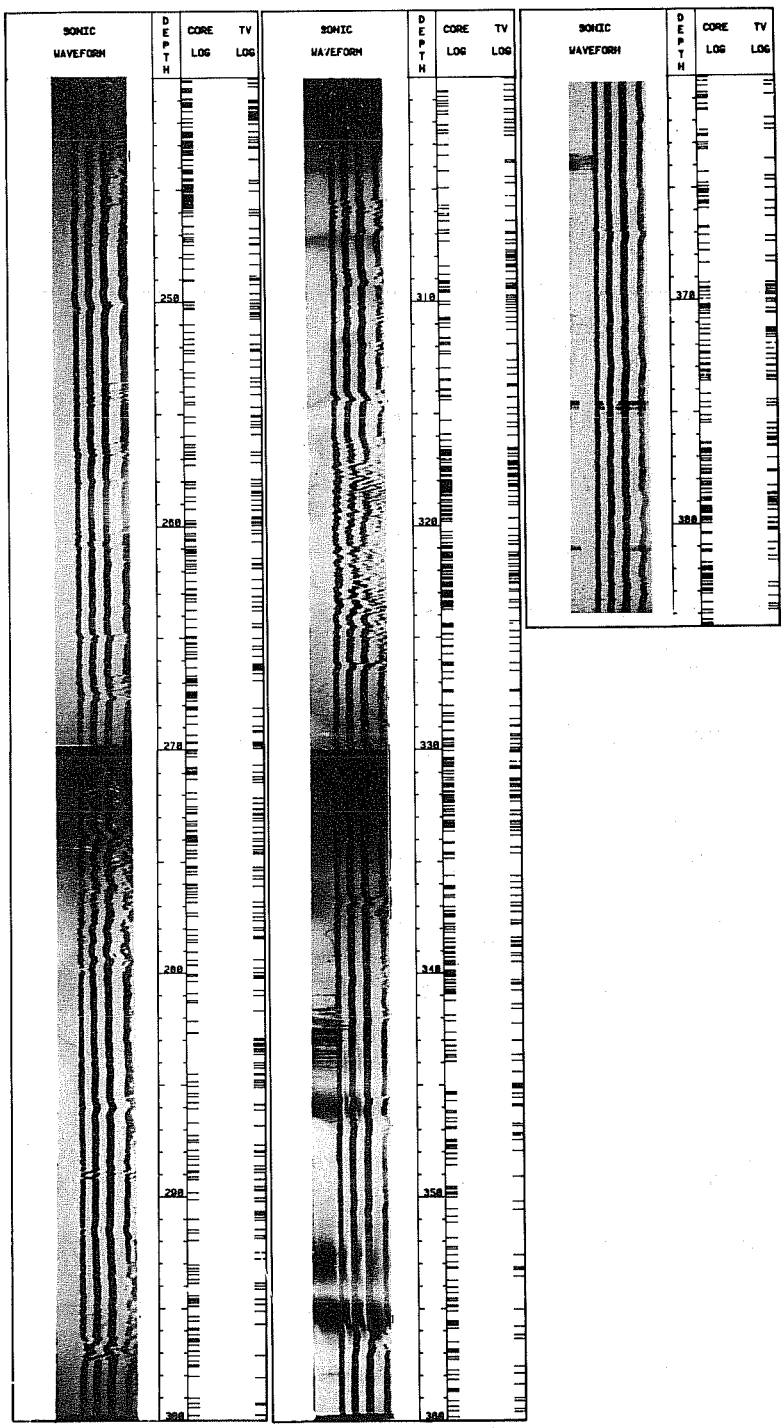

Plate 2
Lawrence Berkeley Laboratory

XBB 780-14171

Fig. 2.4 (continued)

discussed as a function of depth in the hole. Both discussions refer to Figs. 2.3 and 2.4.

2.2.1 Outstanding Features Observed in the Data

The physical contrasts between the leptite and the granite stand out clearly on all the logs. The more important contrasts are:

- The leptite is a denser rock than the granite.
- The leptite has a different natural gamma count rate than the adjacent granite.
- The leptite generally has a lower acoustic velocity than the granite, and the leptite velocity is generally more erratic, reflecting more fracturing. (However, at greater depth one cannot distinguish the granite from the leptite just by looking at the acoustic waveform log).

When viewed in their entirety the SBH-1 logs subdivide as follows:

A. Surface Granite, 0 to 52 m. Since there are no acoustic data for this zone, it is difficult to comment on the degree of fracturing. The gamma-gamma log does suggest that fracturing is not as severe as it is in the leptite in the 52- to 130-m interval. The caliper shows discrete openings of 2 to 10 mm, generally of a few centimeters vertical extent. The water content (neutron log) is uniform with depth so we can infer that the granite is not significantly altered by weathering. But the gamma-ray counts increase with depth, interpreted to be due to the leaching of uranium by groundwater percolation rather than to a change in potassium content.

B. Iron-Rich Leptite, 52 to 90 m. The large gamma-gamma and neutron excursions (about one-third of the interval) are interpreted as high iron content, possibly a relic banded iron formation. The acoustic waveform

shows the entire interval is fractured, more so than anywhere else in the hole. Likewise, the caliper shows that the borehole wall is rougher than any other interval in the hole, but most of the roughness is only several millimeters in diameter. The iron-rich intervals seem to be more broken than the other intervals.

C. Transitional Leptite, 90 to 130 m. This is a transitional zone between the fractured "iron formation" leptite above and the competent rock below. The acoustic, gamma-gamma, caliper, and core logs all show fracturing and roughness decreasing with depth in this interval.

D. Lower Leptite, 130 to 208 m. Overall, this is a rather monotonous interval, with generally unvarying logs throughout. Anomalous zones occur as individual features (refer to detailed description, page 40), generally of less than 1-m intercept.

E. Anomalous Granite, 208 to 328 m. The division between the "anomalous" and "homogeneous" granite is based primarily on the acoustic waveform log with support from the gamma-gamma and gamma-ray logs. At 328 m there is a noticeable decrease in the frequency of observable features, and the granite below 328 m is remarkably free of anomalous features on any of the logs. Note that the core log is not consistent with this division, in that the frequency of observed fractures in core does not decrease below 328 m. Also, the term "anomalous granite" is a bit misleading because this rock has the same log characteristics as the "lower leptite" above it except for a shift in average values.

F. Homogeneous Granite, 328 to 380 m. (See comments above, on anomalous granite.) This interval has remarkably few indications of fracturing, especially when compared to the rest of the hole. Several anomalous peaks in the neutron and gamma-gamma logs were interpreted as mafic inclusions.

2.2.2 Detailed Description of the SBH-1 Logs

The detailed description of the SBH-1 logs of Fig. 2.3 follows. For convenience the description is divided into three major intervals: granite from 0 to 52.5 m, leptite from 52.5 to 208 m, and granite from 208 to 380 m. Depths are given either singly, in which case the logs reveal a discrete anomaly whose vertical extent is no greater than the vertical resolution of the tool, or as an interval, in which case the features are continuous or gradational over a finite length usually on the order of 1 to 10 m.

Intervals that appear to be of special hydrological or geological interest are flagged:

- The double @ (@@) designates the zones in the 52.5- to 208-m interval judged as most likely to be highly permeable.
- The single @ designates the second priority zone in the 52.5- to 208-m interval, in terms of locating permeable zones.
- Overall, the granitic section 208 to 380 m has three zones which stand out as the best candidates for hydrological testing. These three are indicated with a double asterisk (**).
- Two other lower-priority zones, at 234.5 to 246.5 m and at 292.0 m, are indicated with a single asterisk (*).
- Anomalies and zones flagged with a superscript, have coincident increases in both the density and the water content, but no associated change in the natural gamma log. One such anomaly is coincident with a pegmatite intercept and another lies 1 m below a pegmatite intercept--the others have no such associated intercept. It is very doubtful that the density increase is caused by pegmatite. It is more likely that the anomalies are due to an increase in the mafic mineral content, possibly with some additional pyrite

such as occurs at 340.0 m and 345.5 m. It seems likely that small fragments of greenstone were assimilated into the granite, as suggested by similar log responses at the identifiable greenstone intercept at 277.5 to 280.0 m and at 246 m. (A similar association of density and water increases with a fine-grained mafic increase occurs in borehole N1 in the underground drilling.)

Fracturing is associated with more than half of these anomalies. If they are indeed due to mafic remnants assimilated by the granite, then the spatial extent of the fracturing cannot be great and the associated fractures will not be important hydrologically. An obvious exception to this statement is the zone 272.5 to 281 m, which stands out as one of the two most fractured zones in the granite in SBH-1.

A. Granite 0 to 52.5 m

Depth (m)

11.0 Gamma-gamma counts increase from 100 cps in the steel casing to 300 cps in the granite. Neutron counts decrease 12 percent. The caliper blips at 1.3 m and 7.4 m are assumed to be joints. The caliper shows that much of the borehole in the rock is actually smoother than the inside of the casing.

0 to 40.0

Gamma-ray counts gradually increase with depth from 100 cps at 2 m to 650 cps at 40 m. Possibly the uranium has been redistributed by ground-water circulation.

@24.5 Density decrease. Water increase (?). Caliper shows a 1-cm-diameter opening. Probably the best candidate for permeable fracture in the 0- to 50-m interval.

10.6, 20.5, 24.6

26.0 to 26.8

40.5, 47.0, 47.3

Caliper openings greater than 2 mm occur at these depths, indicating fractures. Acoustic velocity not available.

@50.8, 51.5, 52.2

52.5 to 53.0

Caliper openings. Density decrease. Some of the density decrease is due to hole enlargement, but the density anomalies are so large that these zones must be fractured.

B. Leptite 52.5 to 208.0 m

@@52.5 to 89.5

(55.0 to 60.0,
62.0 to 63.5,
67.0 to 70.0,
73.0 to 75.5,
76.0 to 77.0,
82.5 to 84.5
85.5 to 88.5)

Zone with interpreted iron-rich intercepts. This 37-m zone is characterized by numerous caliper openings of 1 to 10 m, large decreases in the gamma-gamma count rate indicative of high density, and large decreases in the neutron count rate. These anomalies are interpreted as iron formations in the leptite, or at least a high iron content, for the following reasons:

- the densities are quite high, exceeding 3 gm/cc according to a crude calibration of the gamma-gamma tool;

- one of the high-density zones (76 to 77 m) correlates with the iron occurrence observed in the core;
- the neutron response is consistent with high iron content, as discussed in the next paragraph.

The neutron excursions must be controlled by the iron content, for several reasons: (1) The neutron log tracks the gamma-gamma log very well, but in the opposite sense than if porosity were the controlling factor. (2) The decrease in the neutron count rate (∿500 cps) is of the same order as that observed when steel casing was inserted into boreholes N1 and N2 underground. (3) Iron is a good absorber of thermal neutrons, with an absorption cross section about fifteen times greater than that of silicon. (4) The neutron tool ordinarily responds quite differently to water than to air. In the 52.5- to 89.5-m zone, the tool operated similarly in both the air-filled and the water-filled boreholes.

Because of this dominance of the neutron log by the iron content, the neutron log cannot be used to examine the water content in this zone.

Although the caliper openings coincide with the gamma-gamma and the neutron anomalies, the anomalies cannot be borehole effects because the gamma-gamma counts would increase, not decrease, with increased diameter, and because the observed changes in the neutron count rate are much too great to be caused by hole size changes of only a few millimeters. The caliper log does show, then, that the iron-rich intervals are more friable than other intervals elsewhere in the leptite. There is a good chance that they are also more permeable.

The core log description (not shown in this report) shows a number of features labeled "crush zones," rock with the appearance of a breccia which has been sealed, rather than a collection of rubble. These features

correlate well with the caliper openings in the interval 52 to 63 m and with the neutron and gamma-gamma excursions. Hence the "healed breccia" intervals occur in and contribute to the reduced rock competence of the mafic zones.

The depths of the seven high density zones are given above, in the left column in parentheses.

The acoustic waveform log begins at the water level (70 m). It shows the 70- to 90-m interval to be fractured much more than is the granite below 208 m or the leptite below 130 m. As a result of the poor rock quality, the P-wave transit time (velocity) log is useless over this interval because the gain was not increased to compensate for the reduced signal level. The result is loss of the first break and numerous spikes due to "cycle skipping." This condition continues to 130 m. Note that the acoustic waveform log on Fig. 2.4 is usable even though the P-wave arrival in Fig. 2.3 is not.

Core box #12 (82.4 to 89.6 m) was inspected visually after initial inspection of the logs. The leptite consists of bands of very fine-grained, light-gray rock alternating with bands of a mottled green color. The mottled green zones are a highly contorted mix of pistachio green and dark green, visually similar to skarn mineralogy. The mottled green zones are about one meter thick. They match perfectly with the low count-rate anomalies of the neutron log, with no depth offset required. The mottled green zones appear less competent and are more broken along fracture planes, confirming the caliper result mentioned above. Several quartz veins, as well as quartz fragments 1 to 3 mm in diameter, occur in the mottled green zones.

87.5 Gamma-ray peak. No associated anomalies on the other logs.

79.0 to 81.0

Gamma-ray counts decrease from ∿ 200 cps below 80 m, probably due to change in the uranium decay series elements at this depth or possibly a change in rock composition reflected in the potassium level. No changes on the other logs.

89.5 to 130.0

The acoustic waveform log shows extensive fractured rock in this interval, gradually decreasing with depth. Below 130 m the fractures appear as discrete events in an otherwise quiet record. Above 130 m they emerge from a choppy, erratic record.

The gamma-gamma log confirms the acoustic waveform. It has none of the high-density zones recorded above 90 m. Instead it shows low-amplitude fluctuations which become progressively less erratic with depth. The rock becomes increasingly competent and uniform approaching 130 m, and does not change much below that depth.

90.0 to 92.0

Bottom two meters of the highly fractured and broken interval discussed previously.

94.5 to 95.5

Fracture on waveform log.

98.0 Neutron log shows water decrease at 98.5 m, attributed to the granite noted in the core at 98 m.

101.5 to 102.5

Water increase on neutron log. Density increase on gamma-gamma log.

104.5 to 106.0

Caliper openings of ∿ 1.5 mm. Water increases on the neutron log

peaks at 105 m. Coincident density increases on gamma-gamma log.

@@100.0 to 110.0

The waveform log shows more distortion over this 10-m interval than over the 8-m interval above it or any other interval of comparable length below it, until the 274-m interval.

111.5 Waveform log shows fracture. No other anomalies.

115.0 and 117.0

Neutron log peaks at these two depths, showing water increase.

119.0 Waveform log shows fracture.

106.0 to 120.0

Core over the 106- to 120-m slant-depth interval was examined visually after initial inspection of the logs . There was no apparent explanation for the acoustic waveform distortion over the 100-to 110-m interval. Nor were there any observable features correlatable with the neutron peaks at 115 m and 117 m.

128.5 to 129.5

Waveform log indicates about four fractures. Slight water increase on neutron log.

137.0 to 139.0

Fractures on waveform and P-wave logs; several appear to be of high angle. No other anomalies.

140.0 Single fracture on waveform and P-wave logs. No other anomalies.

140.5 to 143.5

Slight borehole roughness (∿1 mm) on caliper.

148.5 Waveform and P-wave anomaly. Probably a fracture, but could just be lower velocity material. The gamma log has a step-like decrease of

10 to 15 percent, with a reduced count rate below 150 m.

158.5 and 160.0

Two events on the waveform and P-wave logs. No other anomaly.

160.5 to 174.0

Absolutely quiet interval. No features on any of the logs. Could be useful test zone, if a long zone which is free of fractures is desired. The core log also shows remarkably few fractures (∿13) in this zone.

175.0 and 177.0

Two fractures on waveform and P-wave logs.

180.0 Water increase, density increase, P-wave velocity increase. Not a fracture--this must be a compositional change.

@182.5 to 185.0

Pegmatite dike. From 183.5 to 185.0 m, a 1.5-m zone of lower velocity, including two fractures. The fracture at 184.5 m has an associated density decrease. Caliper opening of 2 to 4 mm at 182.5 m. Because of the density drop at 184.5 m this interval is likely to be permeable, at least with respect to other fractures in the leptite below 130 m. Note the absence of any gamma-ray features.

193.0 to 194.0

Waveform log shows fractured zone. No other anomalies.

202.0 Water increase and density increase.

203.5 to 208.0

Erratic waveform and P-wave velocity logs at bottom 4.5 m of the leptite. Does not appear to be fracturing.

208.0 The leptite-granite contact appears dramatically on all logs except caliper. Going downward from leptite into granite we see an increase in neutron counts of 25 percent (reduced water), an increased seismic velocity

with less velocity variation, a 50 percent gamma-ray activity increase, and a density decrease on the gamma-gamma log.

212.0 Slight water increase, small density anomaly.

220.5, 221.5, 225.0,
228.0, 232.5

Single fracture anomalies on P-wave and waveform logs. Anomalies at 228.0 m and 232.5 m have associated density increases. No other response on other logs. No obvious associations with the core fracture log.

*234.5 to 246.5(1)

A 12-m interval of decreased velocity (P-wave delay of ∿4 μsec) and more erratic waveform. Includes a density and a water increase at 246 m which correlates with a 1-m-wide greenstone intercept. The 12-m interval includes a 5-m interval of high fracture density observed on the core log from 241 to 246 m.

251.0 Single fracture on waveform and P-wave logs.

**272.5 to 281.0(1)

An 8.5-m interval of decreased velocity (P-wave delays of ∿8 sec) and more erratic waveform. This interval stands out more than the 234.5- to 246.5-m interval. A greenstone intercept at 277.5 to 280.0 m correlates quite well with marked water and density increases and a slight (<1 mm) increase in hole diameter. Gamma-ray activity decreased 50 percent in part of this interval. This zone is an obvious hydrological test zone.

286.0(1) Density increase. Slight water increase. Gamma-ray decrease. No waveform anomaly.

287.5 to 290.0

Waveform shows two fractures between 288.0 m and 290.0 m. Slight

density and water increases at the top of this interval. An 8-cm quartz intercept occurs at 288.6 m.

*292.0 P-wave event associated with density decrease and pronounced gamma-ray peak.

**296.5 to 298.5

Very marked decrease in velocity (∿6 to 7 μsec/ft) at quartz occurrence. Density decrease. Fracture at upper edge of quartz (∿297.0 m). The temperature gradient changed at this depth on the first temperature log, but did not repeat on the second. Even so, this zone is a candidate for hydrological testing.

300.5(1) Density increase. Slight water increase. Waveform log shows fracture at 301.5 m. Quartz occurrence indicated at 300.6 m on core log.

306.0 to 307.0

Waveform distortion indicates four fractures, P-wave delay of 2 to 3 sec/ft. Gamma-ray peak at 307 m.

314.5 Waveform distortion has a symmetrical pattern, suggesting horizontal fracture. P-wave delay of 6 μsec. No other associated anomalies.

**316.5 to 324.5

Fracture zone on waveform log. P-wave delays of 1 to 9 μsec. Gamma-ray peak increases of ∿30 percent. Water content increases. A few very small caliper blips of 1 to 2 mm diameter change, and of several centimeters vertical extent. This zone coincides with an increase in fracture density over the same interval, as recognized on the core logs. (However other zones of similar fracture density on the core logs do not coincide with waveform disturbances similar to this one). With the coincident water and gamma activity increases, it is likely that a change in rock composition occurs here. A change in temperature gradient occurs at this depth, repeated

nicely on a second temperature log--making this zone a prime candidate for hydrological testing.

Core boxes 59, 60, and 61 (315.3 to 328.4 m) were visually inspected after initial inspection of the logs. The interval is visually impressive because of the large number of fractures beginning at 316.6 m and ending at 324.6 m, with a 1-m unfractured zone at 319.9 to 320.9 m. (These depths correspond with the interval noted above, with only a 0.1-m discrepancy.) The fractures are reliably recorded in the core logs but the visual examination emphasizes the fracture intensity. Inspection with a hand lens revealed no apparent textural or mineralogical change associated with the fractured zone.

326.5 Fracture on waveform log. P-wave delay of 4 μsec. No other anomalies.

330.0 to 334.0

Very modest waveform disturbance over a 4-m zone. Of minor significance.

337.0 Fracture on waveform log. P-wave delay of 4 μsec.

343.0 to 345.0

The P-wave log is invalid due to noise on the early part of waveform. The waveform log shows no fracturing in this interval. When logging, we repeated this interval several times, but were unable to diagnose the cause of the noise. The caliper is smooth, so borehole roughness does not appear to have been the problem.

338.0 to 346.0

Gamma-ray count drops from an average value of 300 cps above this transition zone to 200 cps below it, indicating a 50 percent decrease in the uranium content at these depths. The gamma-gamma (density) log count rate decreases very slightly, a change probably contributed by the natural

background and not a true density change.

*339.0 to 349.0

Four prominent resistivity peaks occur in this zone, along with three associated neutron peaks and two associated zones of shear-wave distortion. These zones do not appear to be especially fractured but the resistivity log does indicate a high interconnected porosity. The zones are listed separately below. Because of their close proximity to one another, this interval should be considered as a hydrological test zone.

340.0(1) A 25-cm pegmatite dike shows up as a resistivity decrease, a density increase, and a water increase. No fracturing indicated. The core log indicates a 20-cm pegmatite dike at 339 m, and pyrite concentration at 340.0 m and 340.3 m.

343.0 Resistivity decrease, some shear-wave distortion on waveform log.

345.5(1) Density increase, resistivity decrease, water increase, and waveform anomaly. Core log indicates pyrite concentration and a 10-cm chlorite zone.

349.5 Resistivity decrease and water (neutron) increase.

350.0 to 380.0

Waveform log is cleaner in the interval 350 to 380 m than in the interval 328 to 350 m, where shear arrivals are occasionally distorted. The granite appears even more homogeneous (unfractured) below 350 m.

355.5 to 357.0(1)

Density and water increase at 355.5 m. Correlates with a 15-cm-wide pegmatite intercept on core log. Waveform record shows fractured interval extending to 357.0 m.

366.5(1) Density increase. Water increase. Fracture on waveform record

appears 0.5 to 1.0 m below these peaks. No P-wave delay.

377.5[1] Small density increase, slight water increase.

SBH-1 Summary

A few final comments on the performance of individual probes are now in order. The natural gamma log shows the major contacts clearly, but there are also shifts in total count rate at other locations, such as the transition from the "non-anomalous" to the "anomalous" granite. In addition to identifying what are probably petrological transitions, the gamma log also contains a number of spike increases. West and Laughlin (1976) have discussed similar occurrences in a Precambrian sequence in New Mexico, where spectral gamma logging showed that the more mobile uranium caused peaks at open or sealed fractures, whereas a felsic inclusion in a schist produced peaks in potassium, uranium, and thorium. Lacking the added information available with spectral logging, we have used gamma peaks to interpret fractures only when other logs also indicated the existence of fracturing. We recognize that spectral logging in repository investigations will be advantageous for geological and structural clues as well as for documenting the distribution of the natural radiogenic elements.

The sonic logs have been the most useful in picking fracture locations. The waveform record is especially worthwhile, although the compressional-wave travel time log is a shorthand representation which is adequate over much of the log.

As is usually the case in log interpretation, the quality of the analysis improves as more types of data are available, especially in areas where the problems are new and a standard methodology has not yet emerged. For example, the neutron excursions could not be interpreted as simple porosity increases where the gamma-gamma log indicated a density increase. In locating

the fractures, the very small shifts in the temperature profile are quite significant, especially in the absence of lithologic changes which could have changed the thermal conductivity coefficient. Because different probes measure different physical properties, an interpretation often can be either excluded or firmed up when correlative data are available. In simple terms--the more logs, the better.

2.3 Time-Scale Borehole Logs

Almost all boreholes in the time-scale drift were logged with the LBL borehole probes, as indicated in Table 1.1, but only a representative portion of the logs will be discussed here. The vertical section down the central longitudinal axis of the time-scale room is the most complete, and for that reason the following discussion concentrates on the data shown in Fig. 2.5a-g.

The gamma-ray profile of Fig. 2.5a has a number of anomalous features at various locations in the profile, the most outstanding being the transition from a lower (200 cps) count rate in the center of the room to higher count rates in the front in borehole H4 and at the rear of the drift in H2 and M1. Particularly striking is the high count level in H2, where the count rate is enhanced seven-fold at the peak at +3.5 m. Water inflow into the heater holes, recorded since the commencement of the heater experiments in the time-scale drift, reached a quasi-steady state after a month of heating. The average water inflow rates in liters per day for July through October are shown in Table 2.2, for comparison with the natural gamma logs. The higher gamma-ray counting rates occur where the water influx is greatest, apparently due to the very high activity of radon and its daughter products. Fritz, Barker, and Gale (in preparation) report

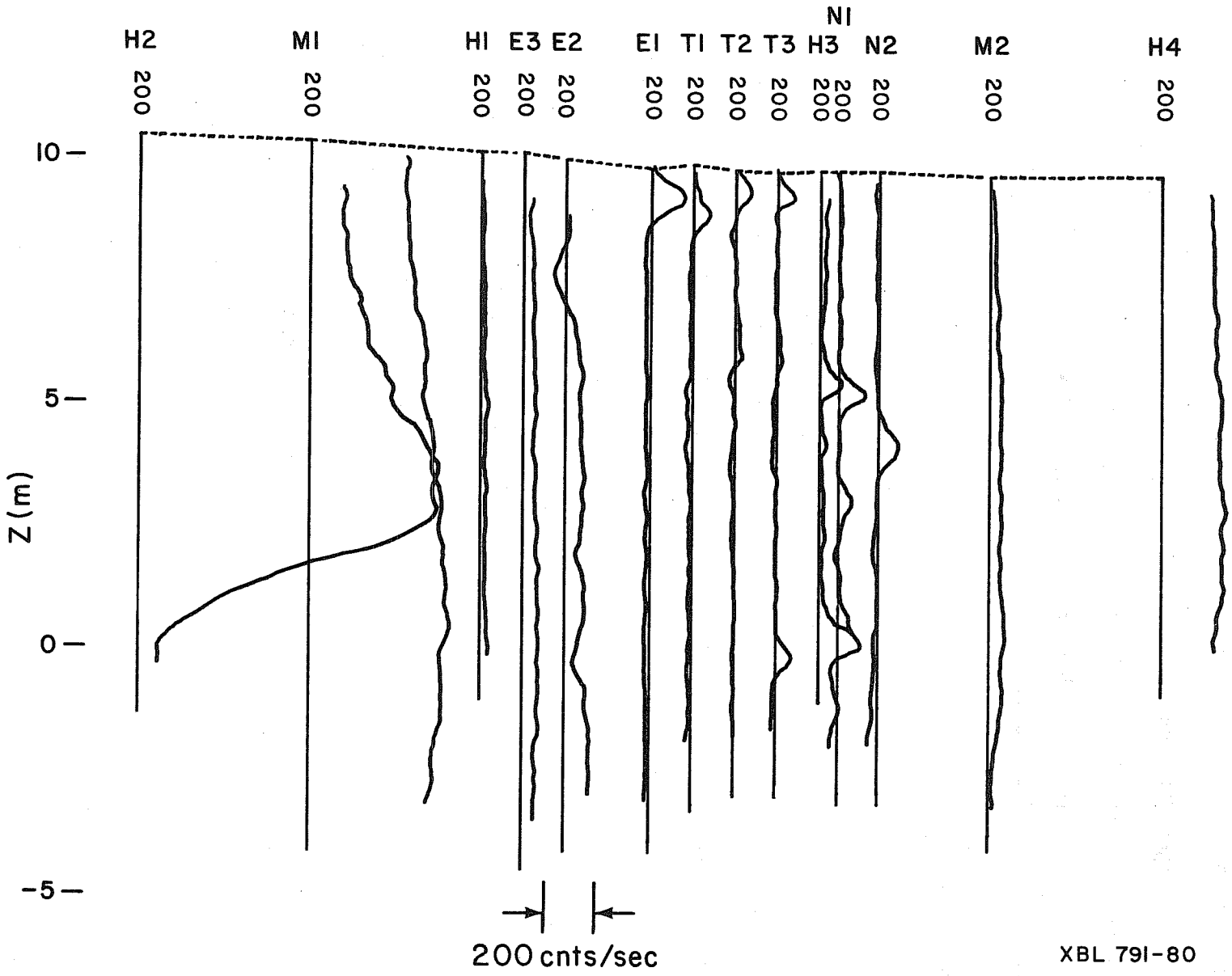

Fig. 2.5a Gamma-ray logs along axis of the time-scale drift.

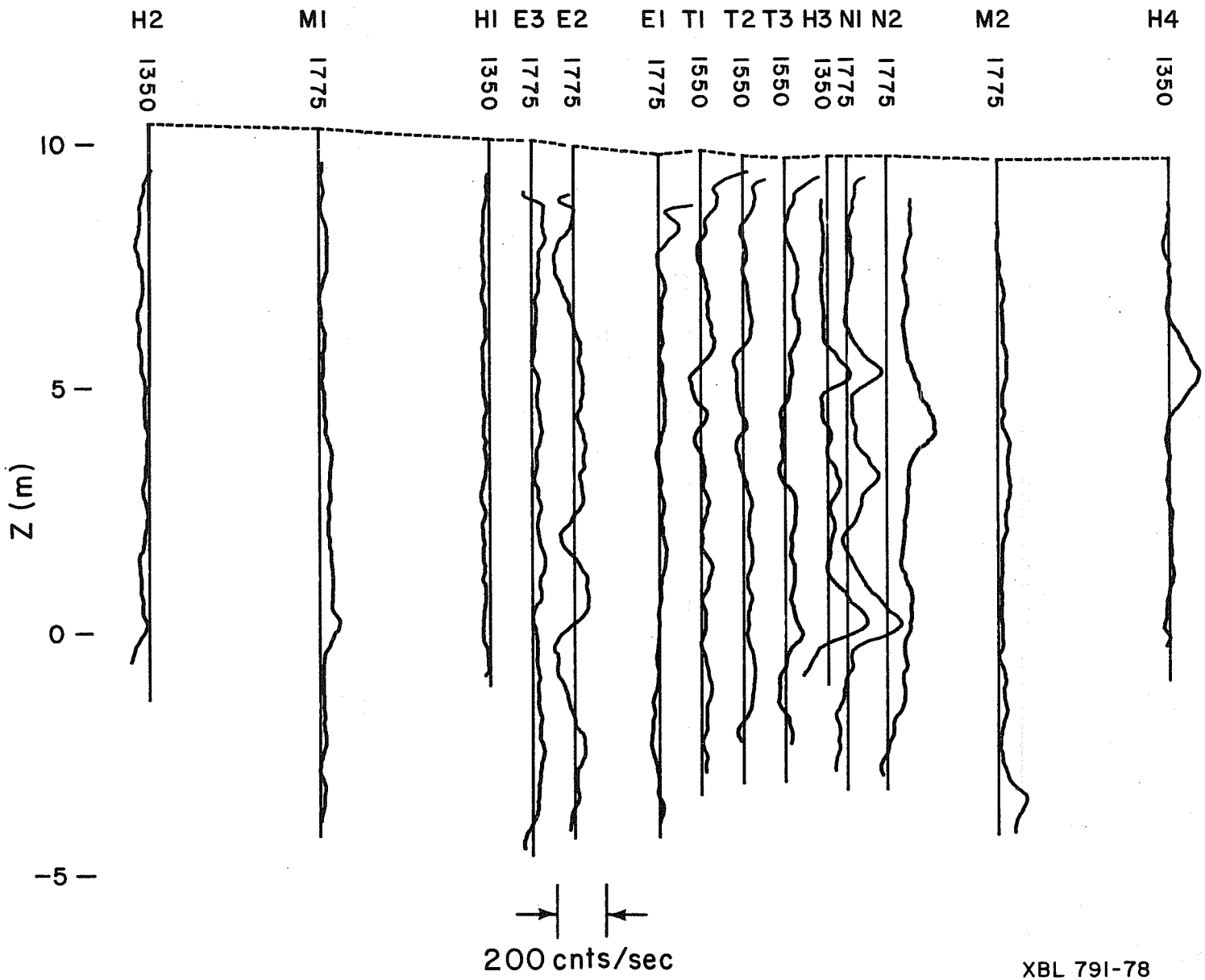

Fig. 2.5b Neutron logs along axis of the time-scale drift.

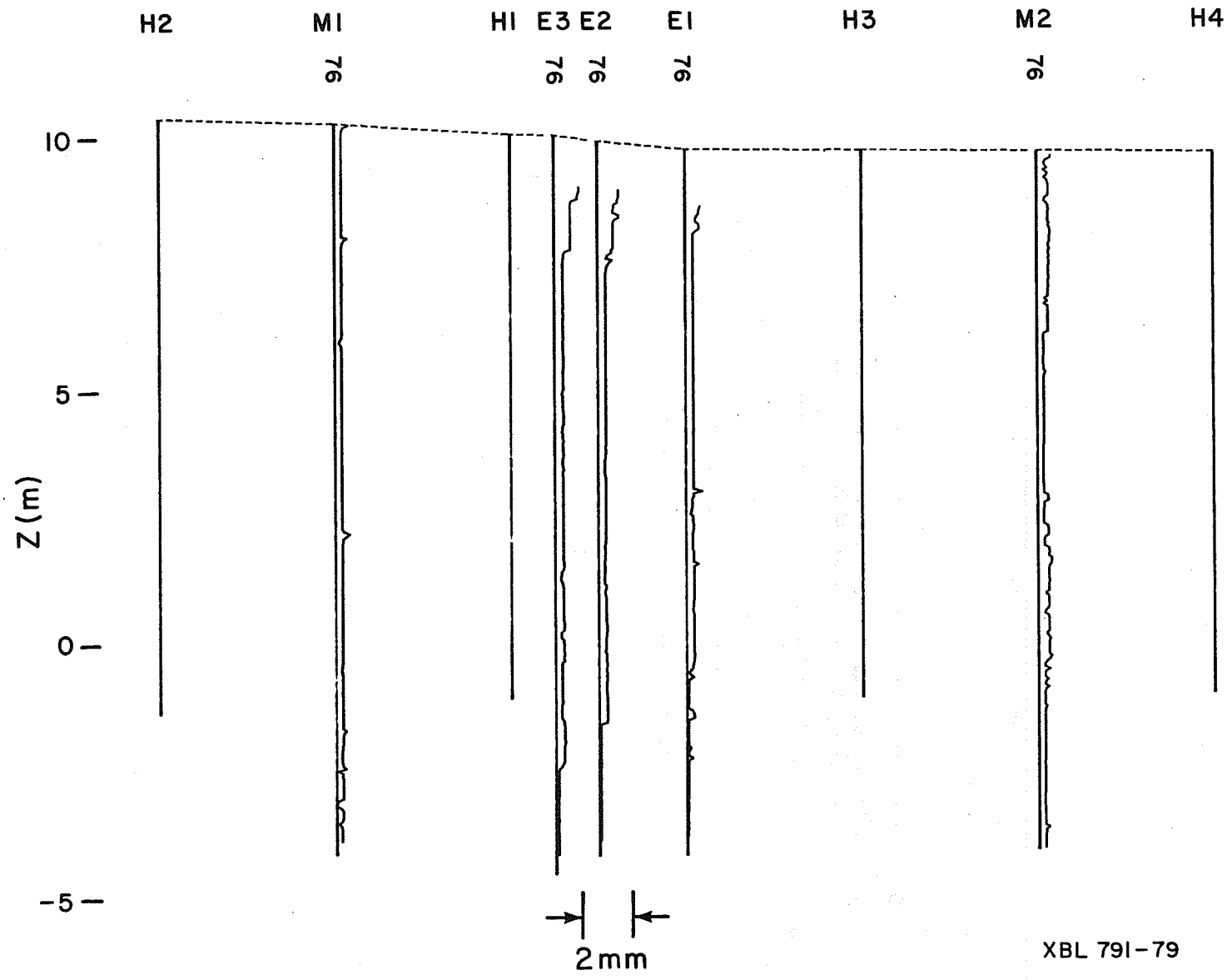

Fig. 2.5c Caliper logs along axis of the time-scale drift. Hole diameter increases to the right.

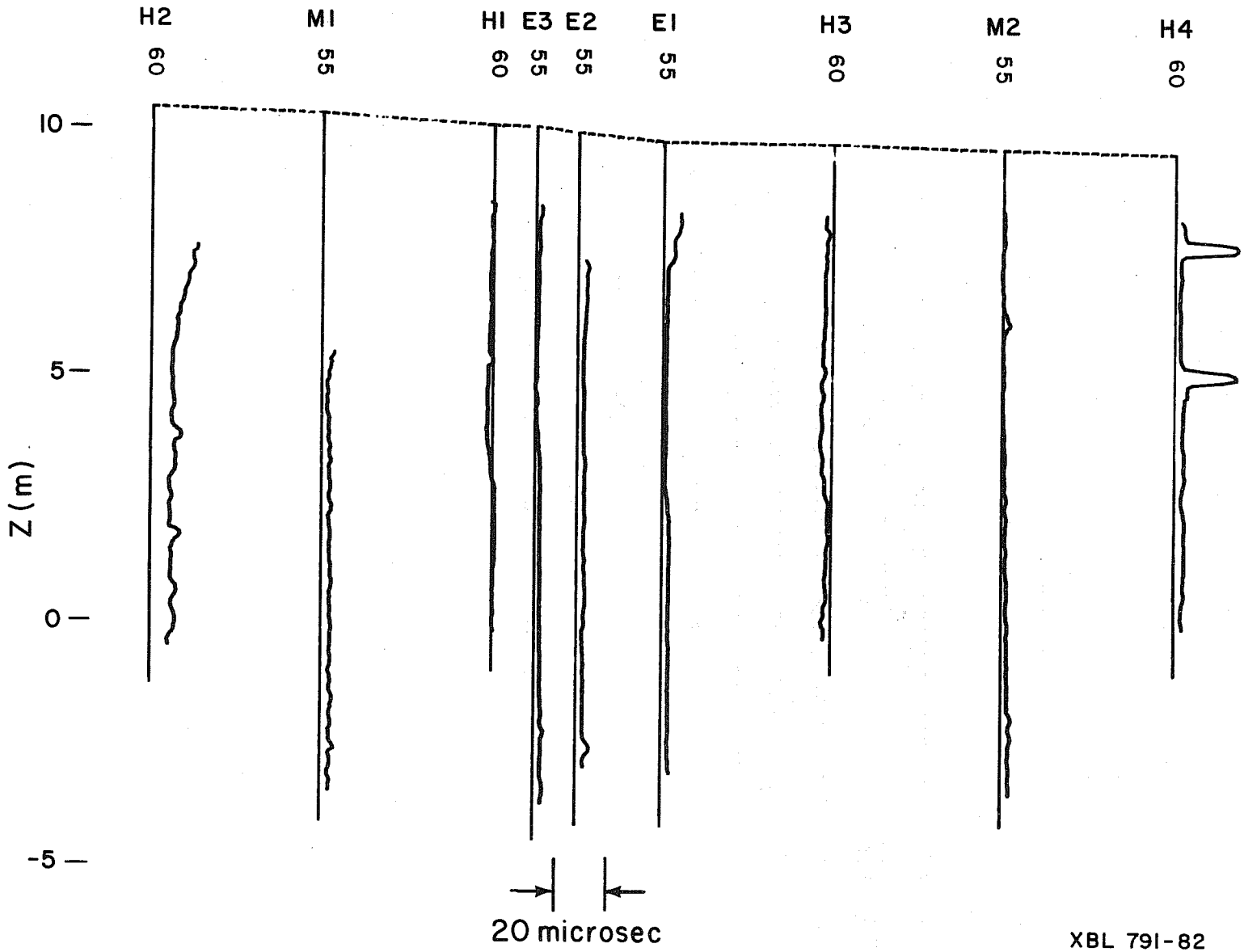

Fig. 2.5d Compressional wave arrival times, increasing to the right, along axis of the time-scale drift. Velocity increases to the left.

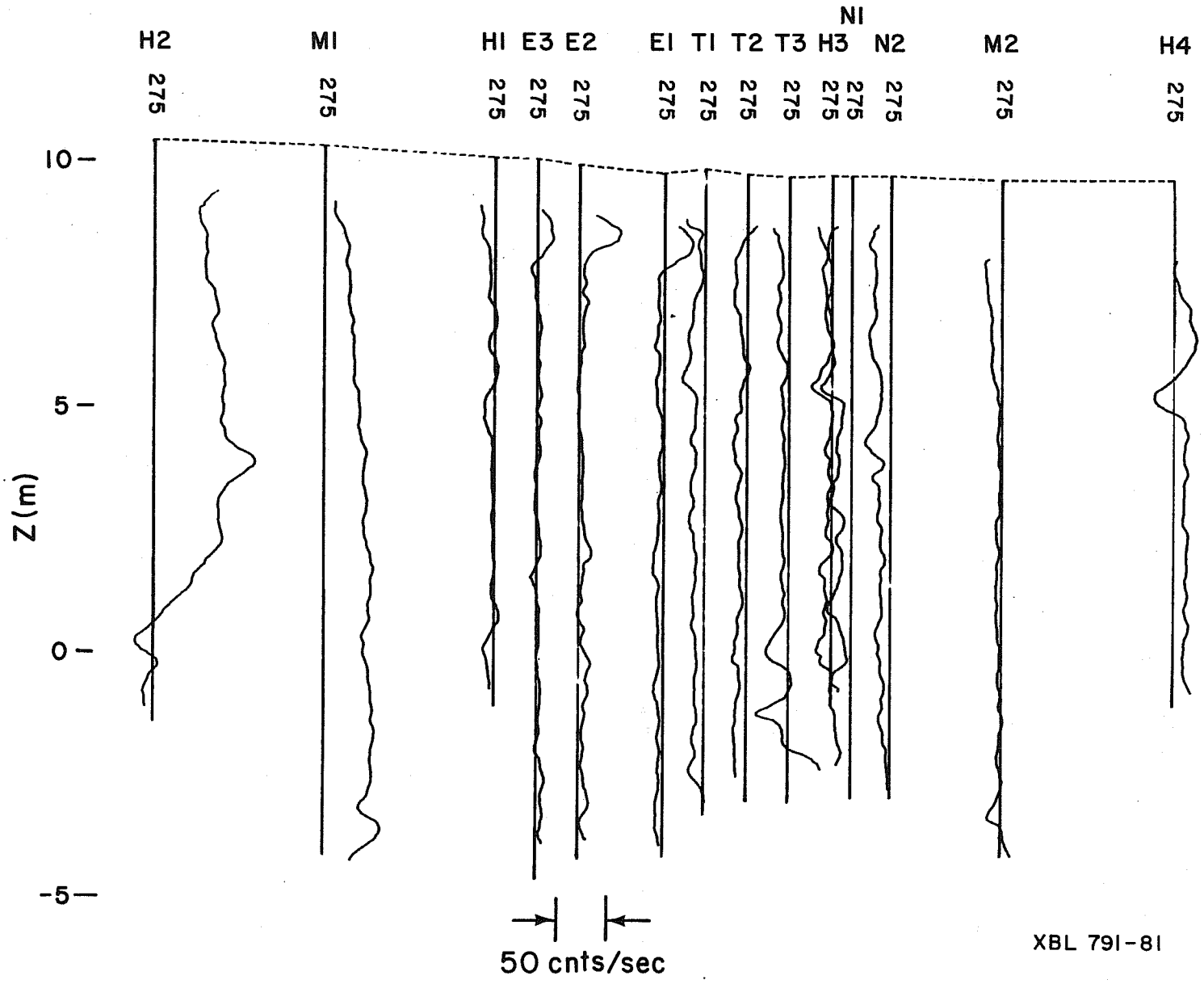

Fig. 2.5e Gamma-gamma (density) logs along axis of the time-scale drift. Count rate increases to the right.

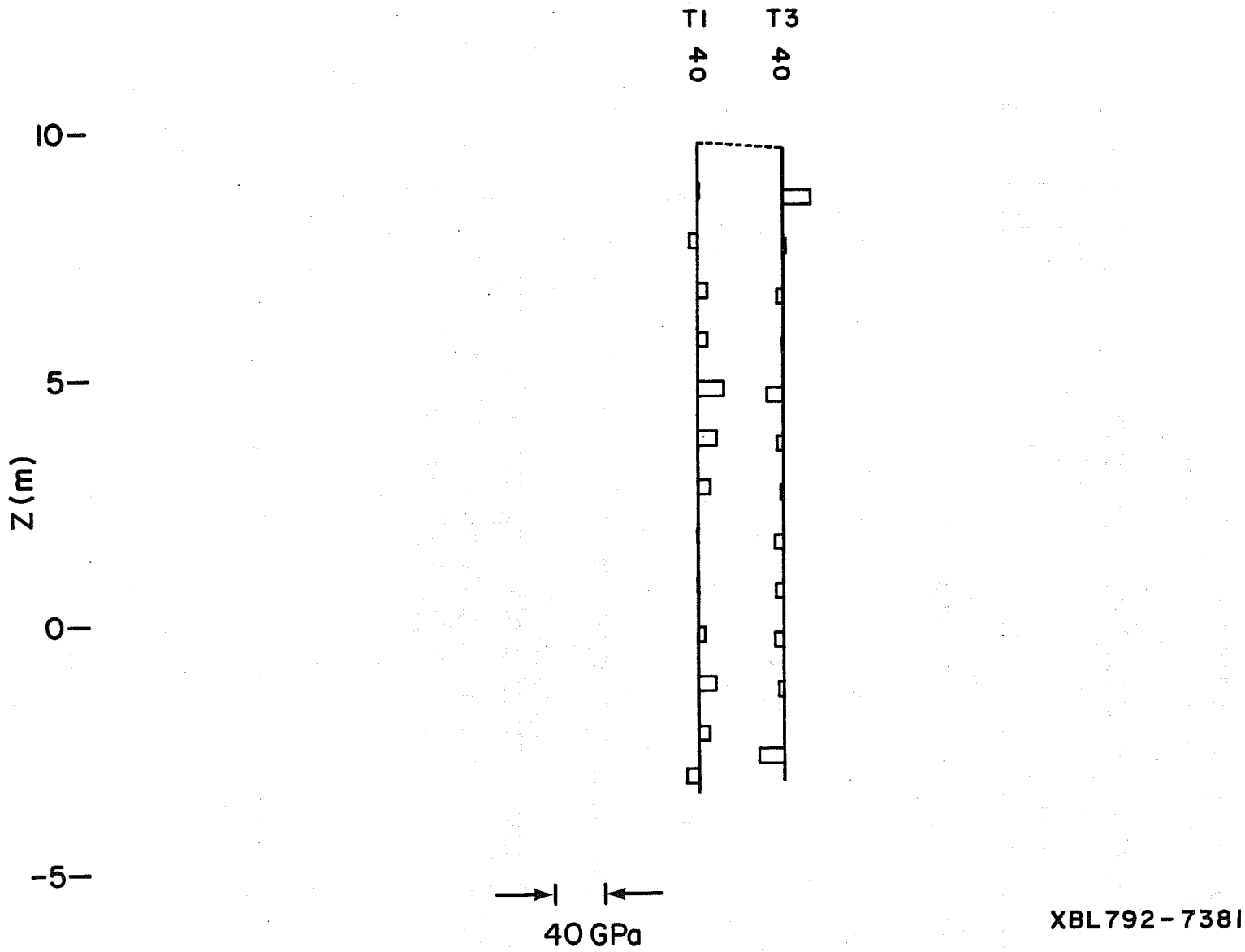

Fig. 2.5f CSM-cell determinations of modulus along axis of the time-scale drift.

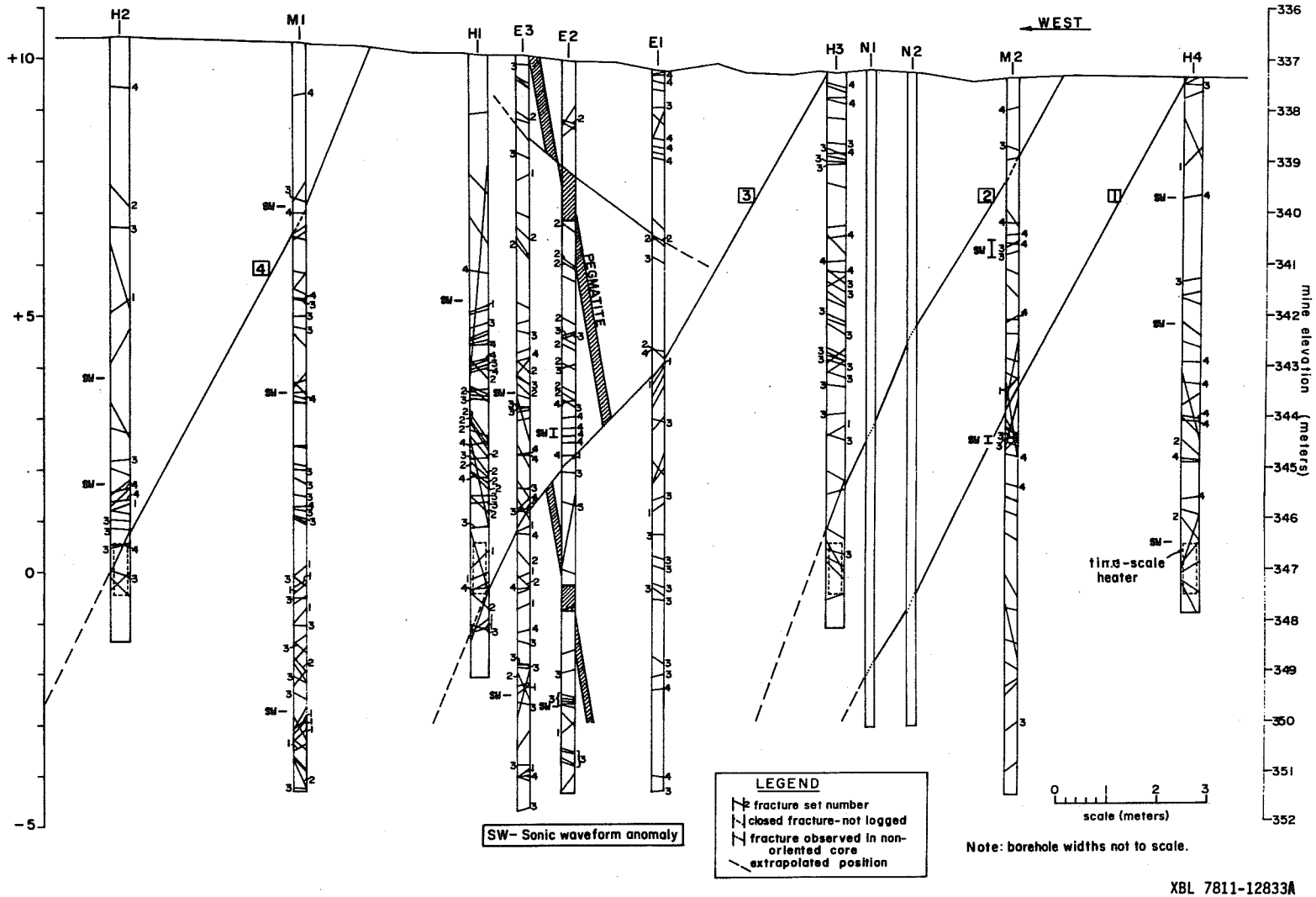

Fig. 2.5g Fractures observed in core and major fracture planes along axis of the time-scale drift, from Thorpe (in press). Locations of sonic waveform anomalies are also shown. Integers 1 through 4 refer to fracture sets as discussed by Thorpe.

Table 2.2 Average water inflow rates in time-scale heater holes, with average gamma-ray activity from borehole log.

Heater hole	Average water inflow (liters/day)	Average gamma-ray activity (cps)
H2	8.0	1200 (max)
H4	2.0	440 (±20)
H7	1.1	310 (±10)
H1	0.6	220 (±10)
H5	0.4	300 (max)
H6	0.2	225 (±20)
H3	0.2	210 (±10)
H8	0.1	200 (±10)

activity levels of 1 to 2 μCi/liter in water samples taken from M3 at the extreme rear of the time-scale drift.

Also apparent in Fig. 2.5a are three small zones where peaks in the gamma-ray logs correlate across two or more adjacent boreholes. These zones occur in the top 1.5 m of boreholes E1, T1, T2, and T3; in the 4- to 6-m interval of H3, N1, and N2; and at the heater midplane (0 m) in T3, H3, and N1. The long dimension of the zone is no less than 2 to 3 m. Results of the spectral gamma-ray analysis for the N1 core (Fig. 2.6) suggest that these local anomalies are due to enhanced uranium and thorium concentrations. The thin occurrences of anomalous uranium and thorium produce anomalies which are broadened by the detector characteristics, the time averaging, and the movement of the probe during logging. The peak in the

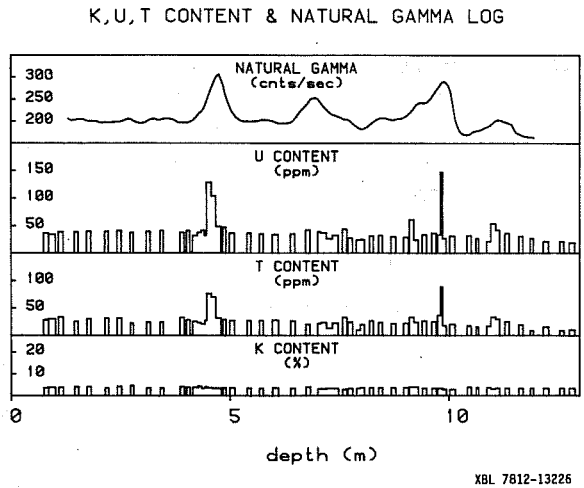

Fig. 2.6 Total count gamma log in hole N1 and uranium, thorium, and potassium analyses from spectral gamma-ray laboratory method.

gamma log at 3.3 m does not show up in the spectral analysis. Presumably it was a very narrow feature in the core, which was missed in the laboratory sampling. Petrographical examination (Appendix C) indicates that appreciable amounts of uranium and thorium are associated with chlorite mineralization.

Another notable feature revealed by the spectral gamma-ray analysis is the high uranium and thorium concentration of the Stripa granite, typically 40 ppm uranium and 30 ppm thorium (Appendix A). These values are much greater than the concentrations of 3 ppm uranium and 9 ppm thorium usually encountered in a granitic terrain (Clark 1966).

Neutron logs for the same vertical section are shown in Fig. 2.5b. So that water content increases to the right, the logs are plotted with count rate increasing to the left. A 200-cps decrease corresponds to a water content increase of about 2.6 volume percent. Note also that borehole diameter affects the baseline count rate of the neutron logs, with the 38-mm-diameter (T) holes averaging close to 1550 cps, while the 76-mm (E)

holes average about 1775 cps. This dependence of the neutron probe response on the borehole diameter is discussed further in Appendix B. Fortunately, the spatial mixing of the various borehole sizes assures us that we have not overlooked any geological trends that might be reflected in the water content of the rock. In other words, Fig. 2.5b does show that the background water content does not vary significantly (certainly less than ± 0.5 volume percent if local peaks are excluded) along the profile. The laboratory core analysis (Appendix E) indicates a total water content of 2.4 ± 0.5 volume percent, including both the pore water and the structural water.

The conspicuous peaks in holes N1 and N2 indicate higher water content in the same zones that show the higher gamma-ray count rates. Water content also increases at the top of the logs in boreholes T1, T2, and T3. Hence it appears that the neutron anomalies are associated with gamma-ray anomalies. In the core samples, these anomalous zones have a dark mafic appearance which thin-section study (Appendix C) reveals is due to an increased chlorite content. Most of the neutron anomaly can be attributed to the water contained in the chlorite. The core analysis of Appendix E confirms this, showing that the structural water content is quite high (4.8 percent) in a sample taken from the interval at the upper neutron peak in N1.

Figure 2.5c displays the caliper logs. These are remarkable for their lack of character, demonstrating the smoothness of the bore. All of the features visible in Fig. 2.5c represent diametral changes of less than 0.5 mm. Caliper logs for the heater holes H1 to H8 were obtained with a long set of arms on the caliper tool which greatly reduced the sensitivity and reliability of the logs, and the logs are not presented here. Only the 76-mm holes were calipered with the short arms which provided logs

with adequate sensitivity to indicate the small openings present.

Figure 2.5d displays the compressional-wave arrival times from the sonic log. Aside from the two conspicuous features in H4, the most remarkable aspect of these logs, like the caliper logs, is the lack of anomalous fluctuations which would be indicative of fracturing. A quick review of the arrival times plotted for SBH-1 (Fig. 2.3) shows that the compressional arrival times are sensitive to fracturing; hence we can infer that the rock in this vertical section of the time-scale room is much less fractured than much of SBH-1. In fact, this holds true for most of the underground sonic logging; we observe very few events in the compressional-wave information. To take full advantage of the sonic logging it is necessary to examine the waveform films and use the shear-wave information incorporated there. The locations of these events in the waveform records are indicated in Fig. 2.5g, plotted alongside the fracture results from the time-scale room prepared by Thorpe (in press).

Figure 2.5e displays the gamma-gamma logs obtained along the longitudinal-axis profile of the time-scale drift. Like the other measurements, the gamma-gamma data have been plotted so that porosity increases to the right--hence density increases to the left, with the scale not indicated because the tool is not yet calibrated. Laboratory data (Appendices D, E, and G) have established the average density of the granite where chlorite concentrations are absent to be 2.63 gm/cc. The offsets in boreholes H2, M1, and H4 are obviously linked to the higher natural gamma count rates in these holes. Empirically, at natural gamma count rates in excess of 250 cps, the gamma-gamma response is contaminated by the natural gamma contribution at a 10 percent rate; that is, for every 100-cps increase in the natural background, the gamma-gamma probe response increases 10 cps. Hence the

gamma-gamma data are erroneous in those boreholes with high gamma-ray activity. However, in most of the boreholes where the gamma activity is about 200 cps, the gamma-gamma logs appear to be uncontaminated. This was confirmed by a check in borehole E11 in the full-scale room, where the gamma-ray tool recorded a peak count rate of 310 cps. With the gamma-ray source removed from the gamma-gamma probe, the log was duplicated with the gamma-gamma probe set at one-tenth the counting rate, attaining a peak rate of 32 cps. Thus, the two anomalies indicating higher density (decreased cps) at z = +5.5 m in boreholes H3 and N1 are valid and, in fact, occur very near gamma-ray peaks.

As discussed earlier, the dark chloritic zones noted in the N1 core, and also identifiable in H3 and H4 from the television logs, correlate well with peaks on the neutron and natural gamma logs. Examination of Fig. 2.5e reveals that these anomalous zones are often associated with decreases in the gamma-gamma count rate.

Other vertical sections have been drawn paralleling the section of Fig. 2.5 to help resolve the three-dimensional structure in the rock. In combination with Fig. 2.5, these gamma, neutron, and gamma-gamma logs show only a few poorly defined features that correlate among two or more boreholes. Boreholes T6, E2, and T10 have slight (1 percent) decreases in water content with coincident slight decreases in the gamma-ray activity in the interval +6 and +9 m. The gamma-ray feature near the floor of the drift in boreholes E1 through T3 shows up in holes E4, T12, and M4 in the parallel sections, and a slight gamma-ray increase at +6 m in borehole T12 is a poor indicator of lateral extension of the feature in hole H3.

However, other profiles are more helpful in defining the horizontal extent of the +6 m feature which appears as a gamma-ray and water-content

increase in boreholes H3, N1, N2, H8, M5, T12, and T8. From these several boreholes it appears that the dimensions of this feature, the most noticeable irregularity in the time-scale experiment area, is about 1 m in the vertical direction, about 2 m in the y (room axis) direction, and at least 3 m in the x direction, with its extent in the -x direction beyond H8 unknown.

Boreholes E4, T5, and T6 as well as H2, H4, H7, and H5 (Table 2.2) show gamma-ray increases over their entire lengths. Such offsets in isolated boreholes are difficult to explain geologically, and are attributed to radiogenic elements in the groundwater. Hence these three holes probably intersect permeable zones, as do the four heater holes.

2.4 Full-Scale Borehole Logs

The suite of logs acquired in the vertical boreholes along the central longitudinal axis of the full-scale drift is shown in Fig. 2.7a-h. In Fig. 2.7a, the gamma-ray feature dipping downwards to the left is caused by the pegmatite dike in the H9 experiment area. Ordinarily a pegmatite dike in granitic country rock would give a gamma-ray increase due to its high potassium content, but here a decrease occurs because the Stripa granite is unusually high in uranium and thorium, with the pegmatite dike containing less of these elements. Except for the dike, the gamma-ray logs are remarkably featureless in the H9 and H10 areas.

The pegmatite also can be seen in the neutron logs of Fig. 2.7b. The neutron logs also have large, obvious offsets in boreholes T14 and T13 adjacent to H9 and T19, and T22 adjacent to H10. At the time of the logging both heater holes were filled with water, dramatically affecting the neutron logs in the immediately adjacent holes. In Appendix B this result is used to help determine the radius of investigation of the probe.

The caliper logs (Fig. 2.7c) in the H9 area show only very small

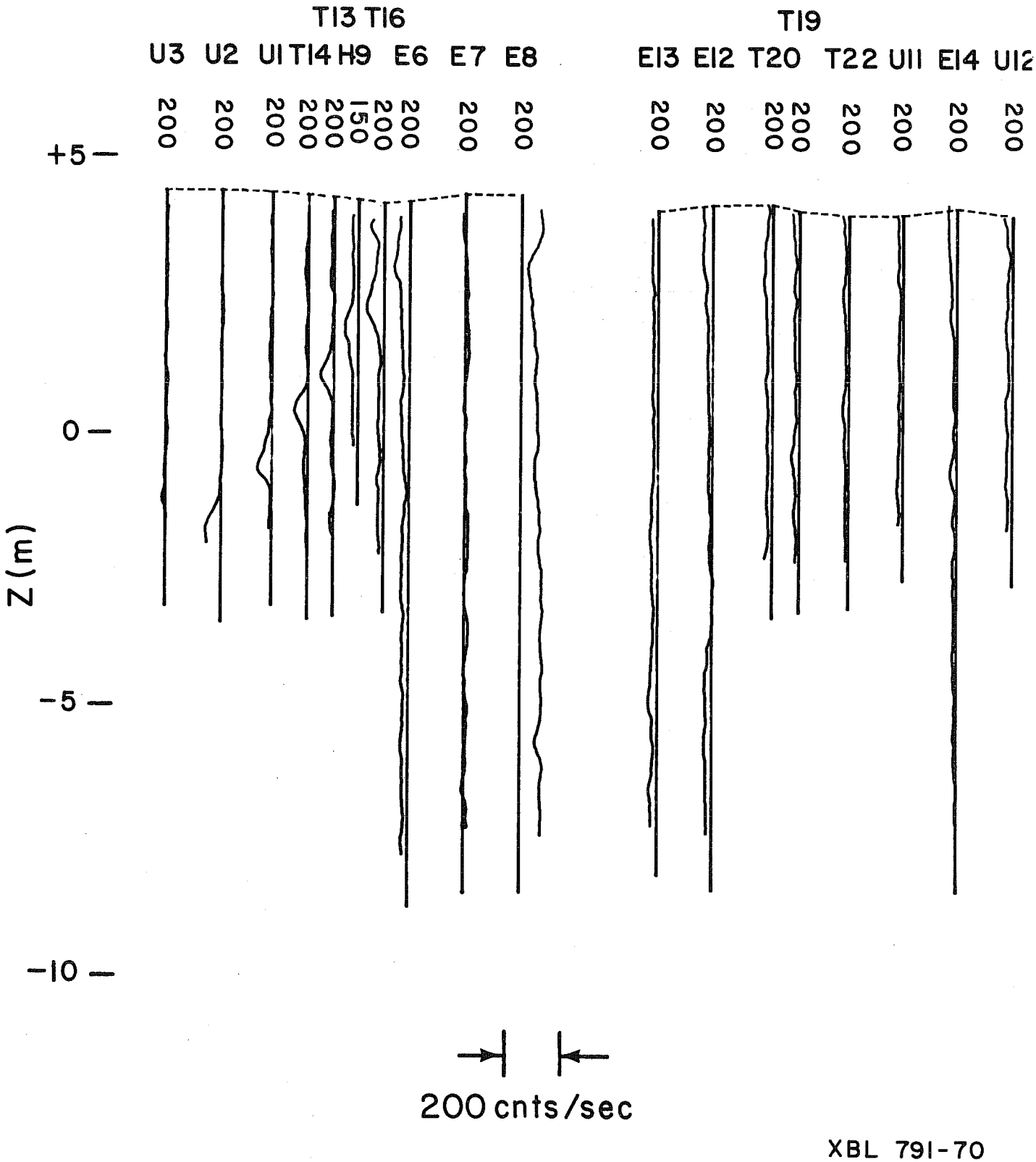

Fig. 2.7a Gamma-ray logs along axis of the full-scale drift. Vertical and horizontal spatial scales are identical except at discontinuity between E8 and E13.

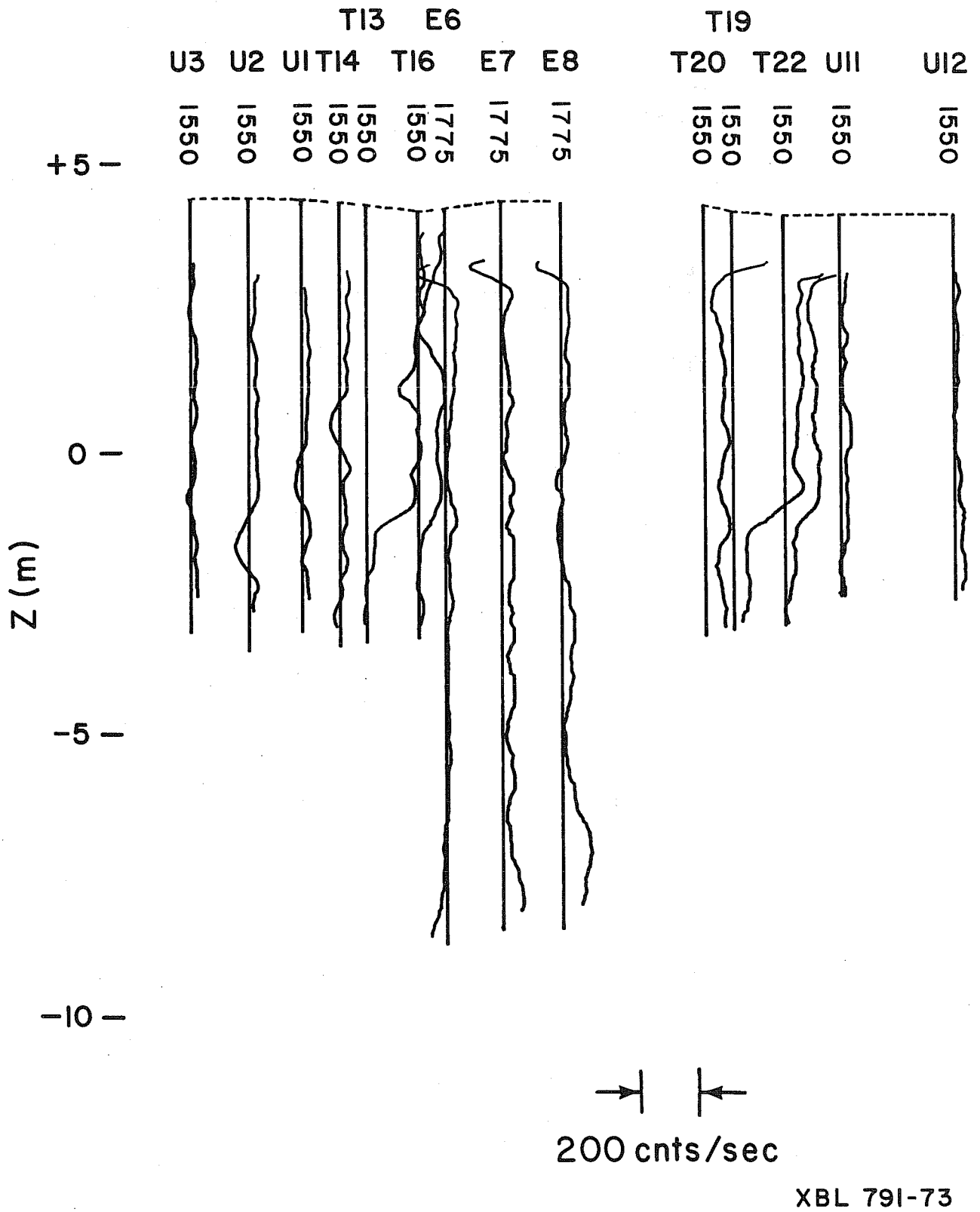

Fig. 2.7b Neutron logs along axis of the full-scale drift. Water content increases to the right.

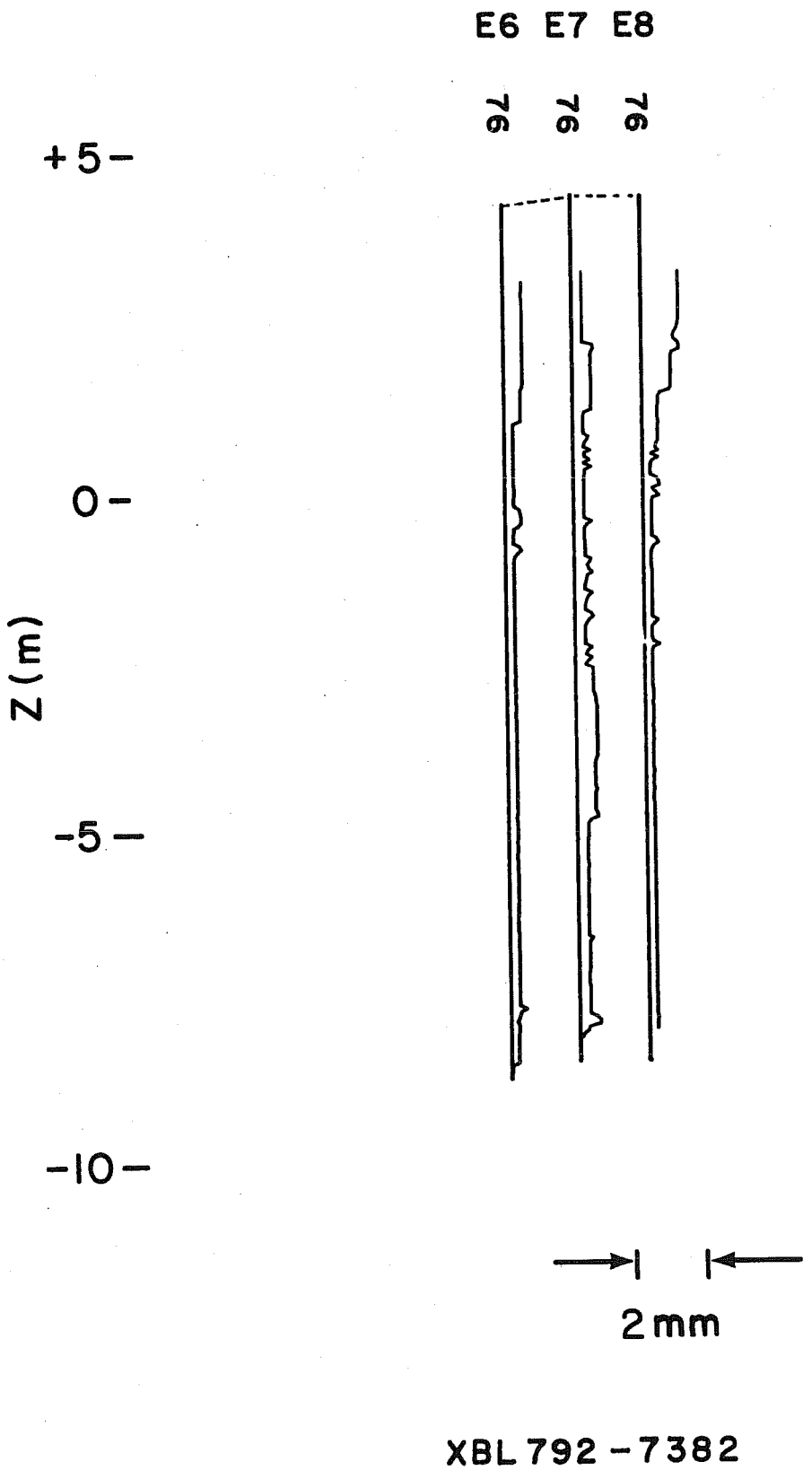

Fig. 2.7c Caliper logs along axis of the full-scale drift.

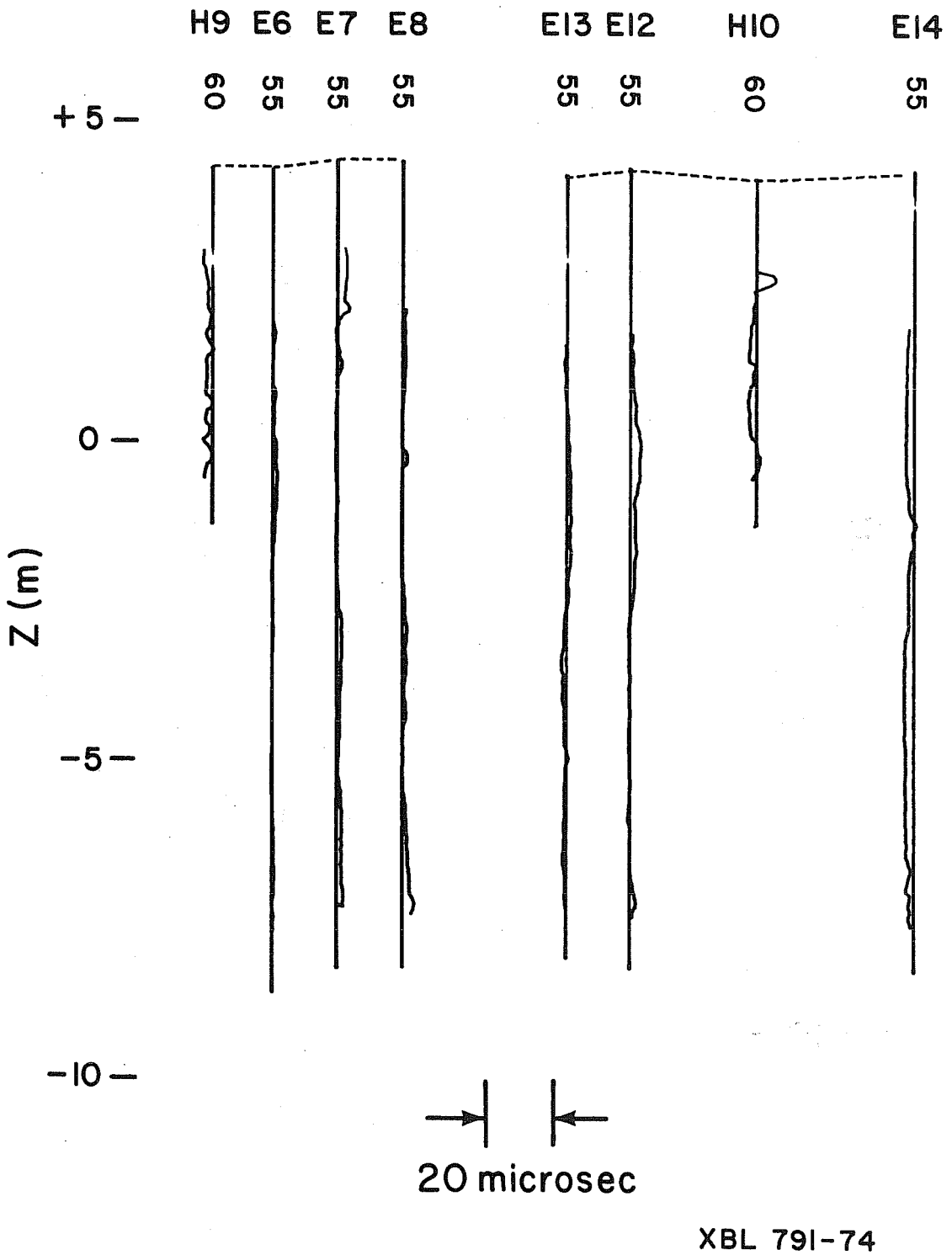

Fig. 2.7d Compressional-wave arrival time logs along axis of the full-scale drift. Baseline value of 55 microseconds is approximate.

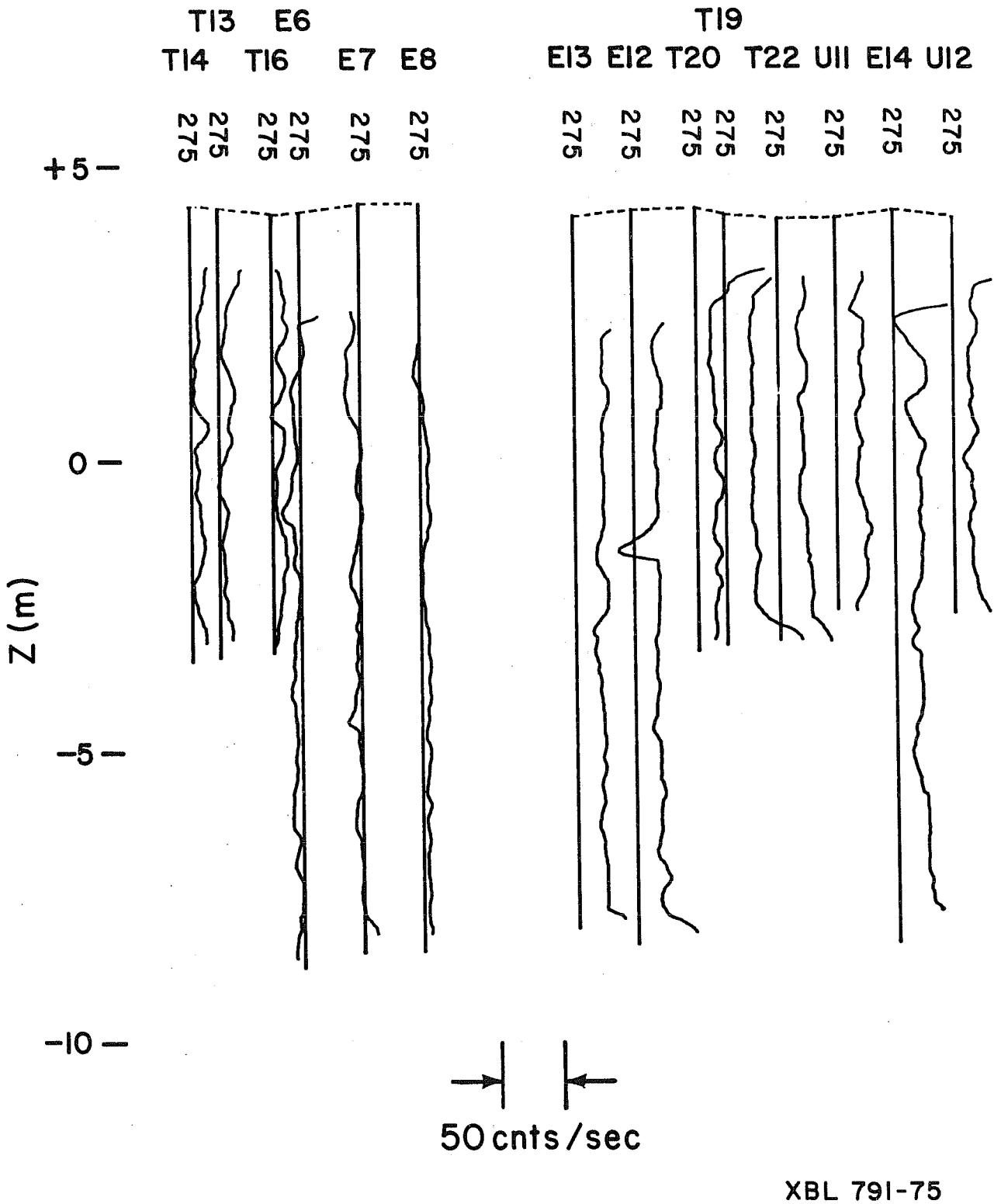

Fig. 2.7e Gamma-gamma (density) logs along axis of the full-scale drift. Density increases to the left.

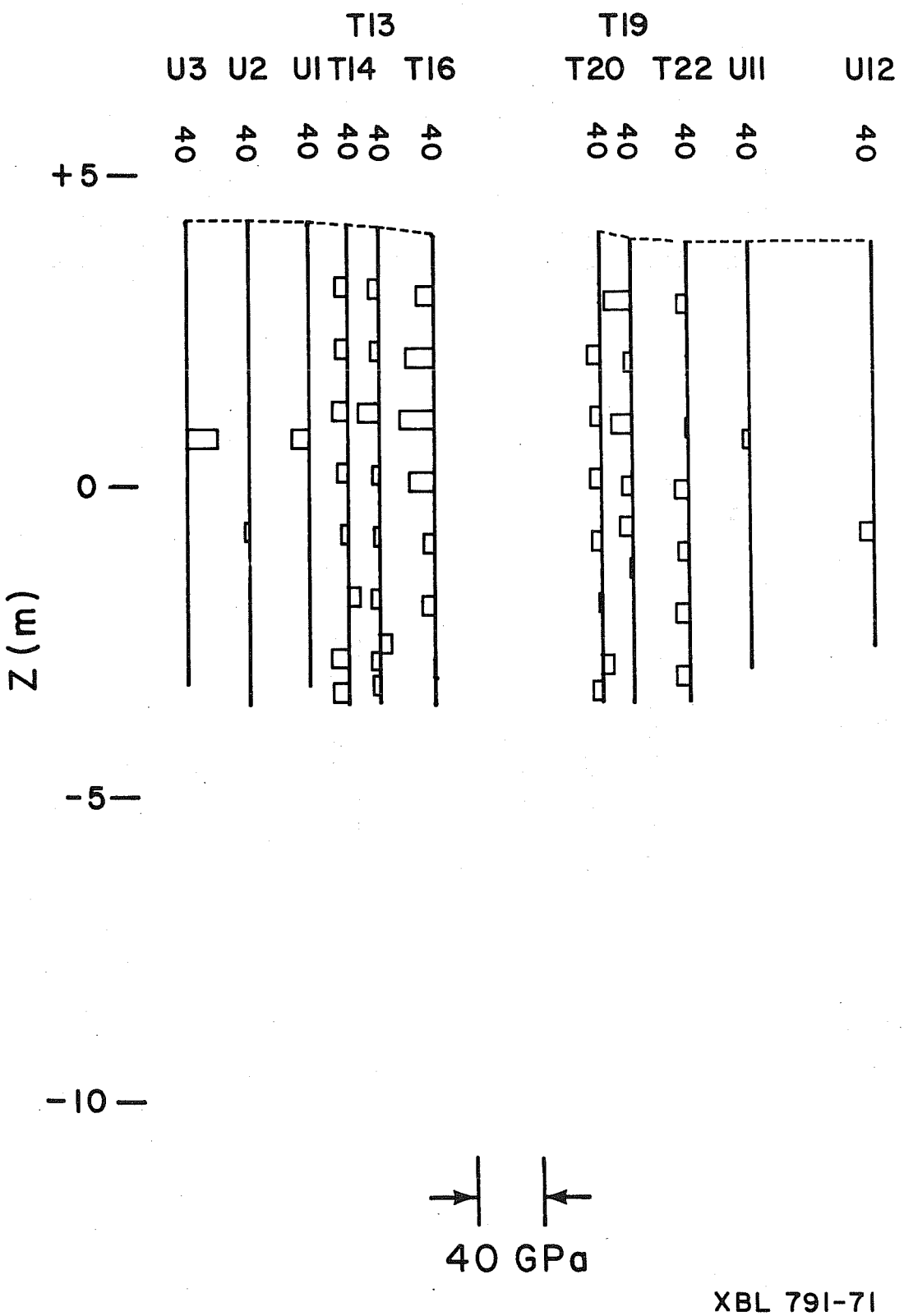

Fig. 2.7f Young's modulus from CSM-cell measurements along axis of the full-scale drift. Values greater than 40 GPa extend to the right.

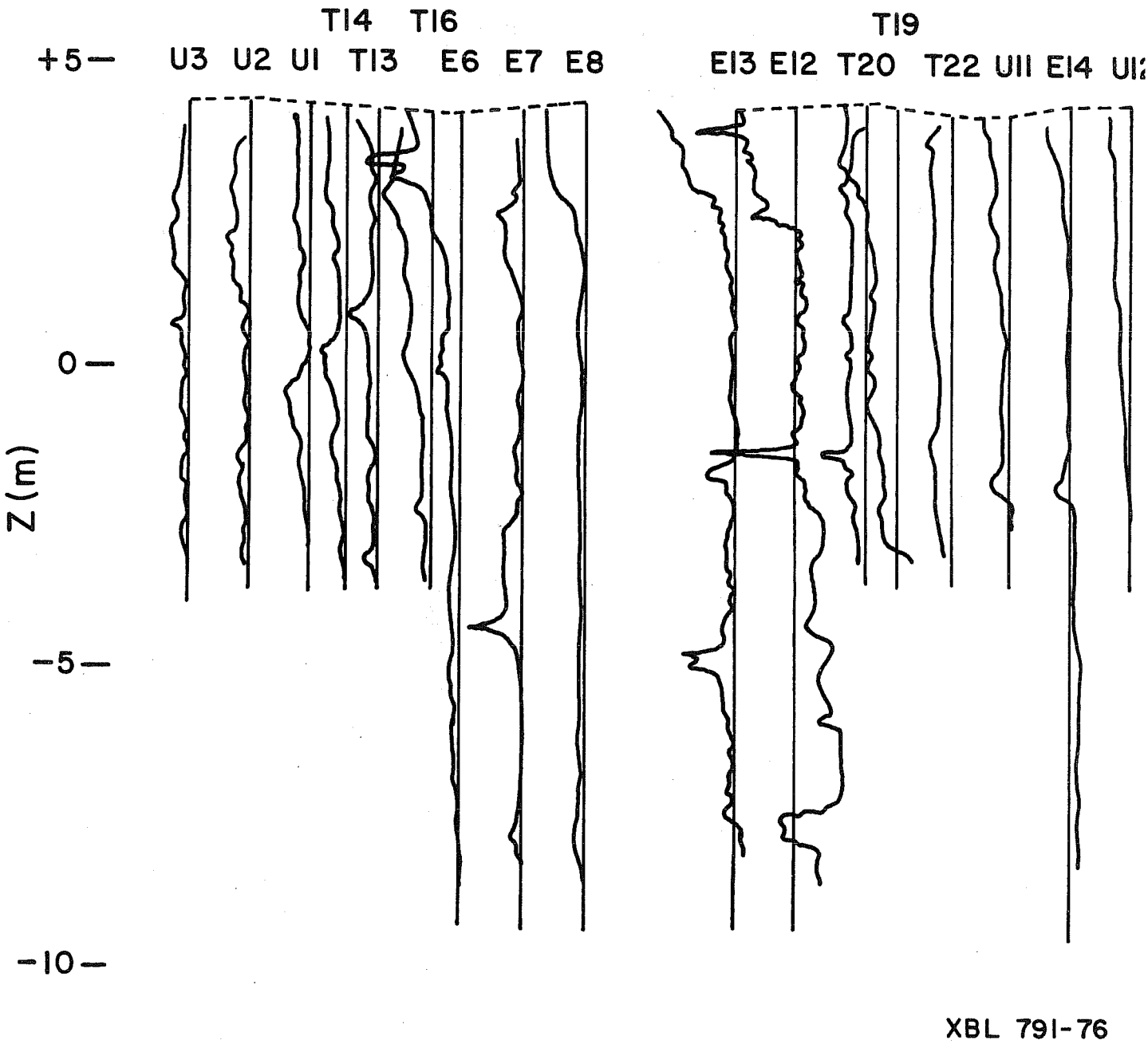

Fig. 2.7g Differential resistance logs along axis of the full-scale drift. Resistance increases to the right.

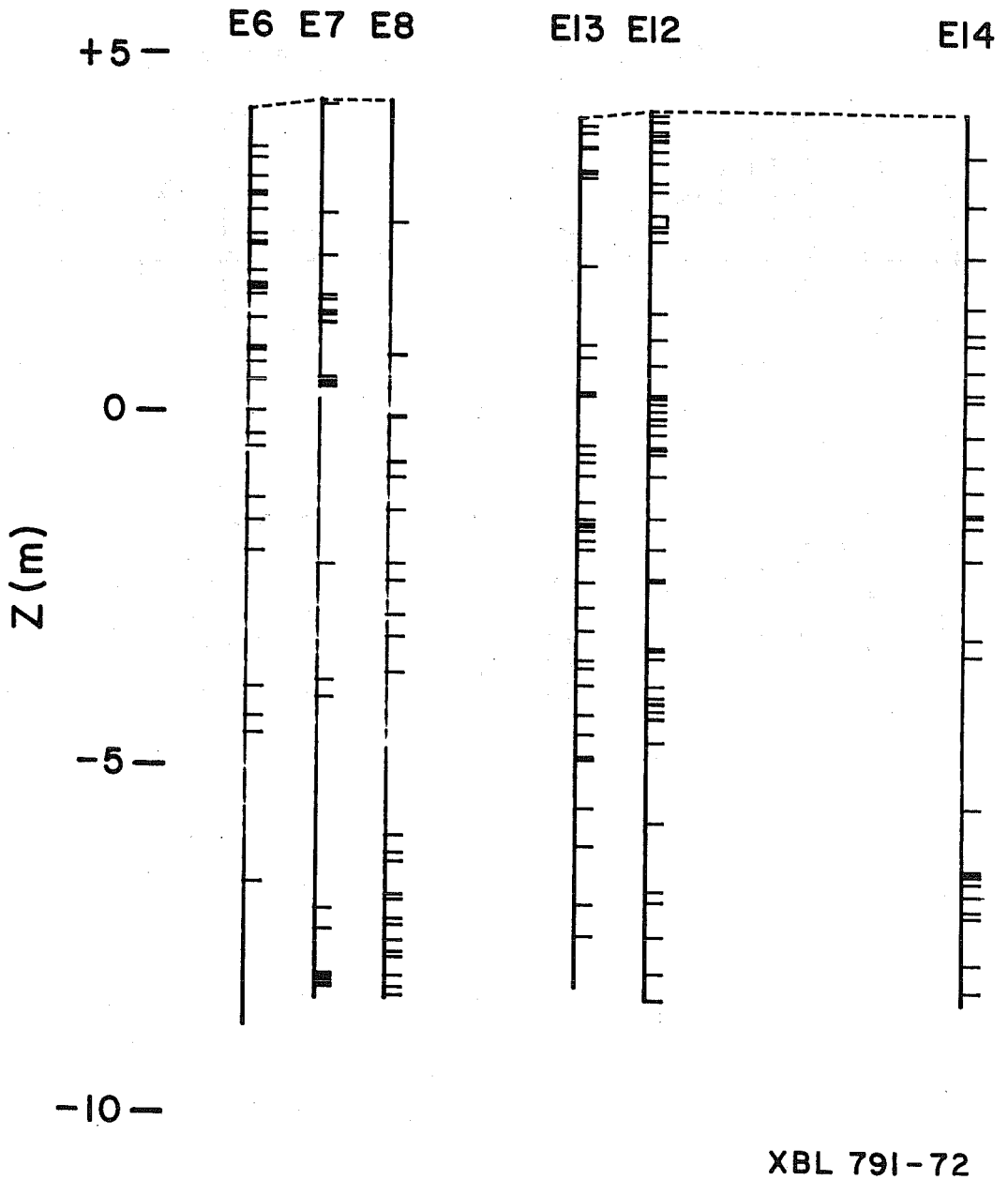

Fig. 2.7h Fractures in core, along axis of the full-scale drift.

deflections of less than 0.5 mm, again demonstrating the extreme smoothness of the bore and the lack of breakage in the borewall. No caliper logs were run in the H10 area.

The compressional-wave arrival time logs (Fig. 2.7d) are as devoid of detail as they were in the time-scale drift. Again it will be necessary to inspect the waveform records to pick out subtle features recorded with this probe. A typical waveform record is shown in Fig. 2.8. In contrast to the SBH-1 waveform records in Fig. 2.4, the underground records show few events and these are often discernible only in the shear-wave portion of the record. Typically, less than five events are present in a 12-m borehole.

The gamma-gamma logs in Fig. 2.7e show numerous small features in the H9 area and two large density-increases in the H10 area. In the time-scale room, such increases are associated with the neutron and natural gamma excursions which were attributed to increased chlorite content. The same explanation probably holds here, except the gamma logs are featureless and the neutron logs unfortunately were not run in E12 and E14. In E12 the core log does note "granite pieces in chlorite, 25-mm thick" at 6.25 m in E12. Neither the core nor the TV logs indicate any features which correlate with the gamma-gamma feature in E14, however. The gamma-gamma logs obtained in holes U1, U2, and U3 are not shown in Fig. 2.7e because they are extremely erratic and appeared to be invalid.

The CSM modulus results in Fig. 2.7f are projected from a baseline value of 30 GPa. On a percentage basis the values shown fluctuate widely, as the scale is 40 GPa per cm. Neither the sonic logs nor the gamma-gamma logs display correlative fluctuations with the CSM measurements.

Figure 2.8 presents a typical suite of logs from E6, representative

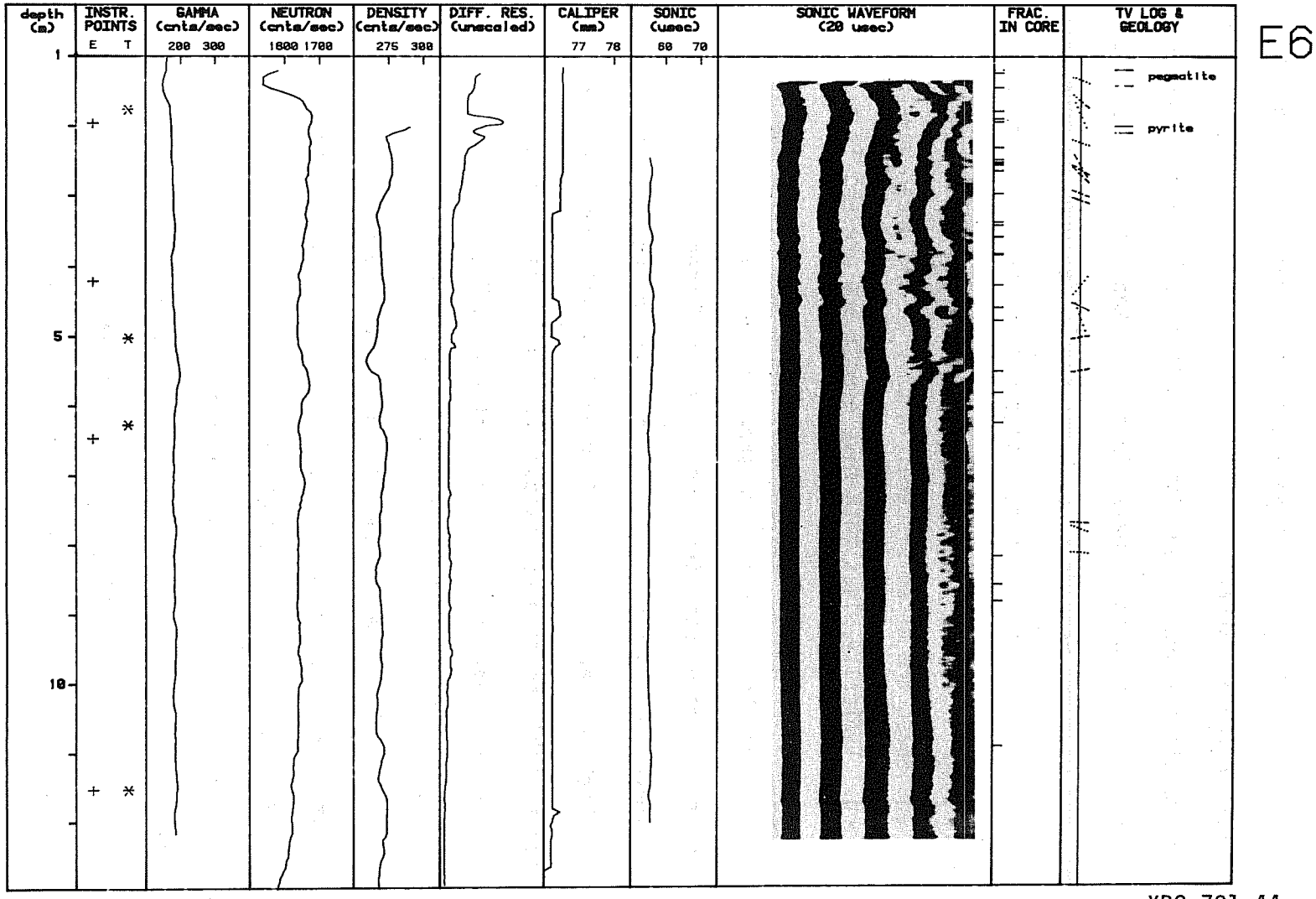

E6

XBC 791-44

Fig. 2.8 Suite of logs from hole E6 in the full-scale drift. Extensometer (E) and thermocouple (T) locations given in left-hand column.

of the data recovered from a single hole underground. Again note the general lack of features, as compared with any 10-m interval in the SBH-1 borehole. Four anomalies are discernable in the shear-wave portion of the waveform log, one of which corresponds with a conductive peak in the differential resistance log. At 5.5 m, the density and neutron logs reflect a small increase in chlorite content. It is again apparent that the rock mass in the volume of the underground heater tests appears generally to be homogeneous and intact in terms of these particular logging probes and their resolution capability. Exceptions to this statement include the chloritic zones, the pegmatite dikes, the high variability in the uranium and thorium concentrations, and a few occasional minor fractures.

2.5 Neutron Monitoring of Water Content in Rock

Neutron probes are now commonplace in well logging for petroleum and hydrological applications. A good description of the physical principles and practical considerations in their use is given by the International Atomic Energy Agency (1970). Neutron logs at Stripa have been discussed in the preceding sections. In this section we review our efforts thus far to detect changes in water content in the rock surrounding the heaters in the full-scale and time-scale experiments. The purpose is to establish the procedures necessary for reliable water determination at low (<2 percent) water contents and then monitor the water content periodically for changes due to heating or drainage. Our efforts thus far have been thwarted by unexpected sensitivity of the probe electronics to temperature. Hence this discussion is limited to some considerations on the method.

Four boreholes of 46-mm diameter were drilled for the neutron probe. Two of these, N1 and N2, are vertical holes located at distances of 0.4 m and 1.2 m from H3 in the time-scale room (see Fig. 1.3). The two others,

N3 and N4, are near-horizontal holes collared in the extensometer drift (see Fig. 2.9). The collar of N4 lies 50 cm below E29. It is 11.04-m long, passing beneath the center of H10 at 9.6-m distance from its collar. Similarly, N3 is collared 50 cm below E20, is 11.22-m total length, and passes beneath the center of H9 at approximately 9.7 m from its collar. Both N3 and N4 pass below the heater holes at an approximate distance of 2.25 m below the heater midplanes. None of the N holes were surveyed because the drilling was consistently within specifications (Kurfurst, Hugo-Persson, and Rudolph 1978) and the large radius of investigation of the neutron probe did not require precise spatial control.

All four holes were cased with steel casing of 44-mm o.d. and 37-mm i.d. As discussed in Appendix B, the casing was somewhat detrimental in both

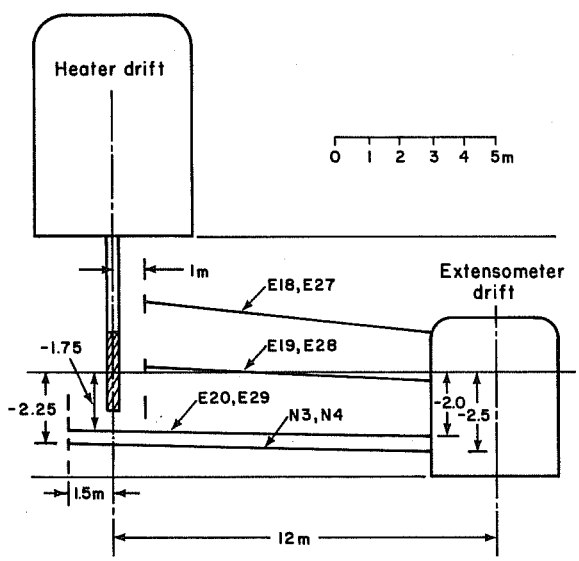

Hole	Diameter(mm)	Length(m)	Angular direction	Inclination
N3	46	11.2	90°	~1°
N4	46	11.0	90°	~1°

Hole N3 in same vertical plane as E18, E19, E20
Hole N4 in same vertical plane as E27, E28, E29

XBL 791-62

Fig. 2.9 Sectional view through full-scale heater and extensometer drifts with holes N3 and N4 for neutron monitoring.

total counts and sensitivity, but safety of operation was the deciding factor in the decision to case the holes. To maintain sensitivity, the sequential measurements are run with water in the casing. Boreholes N3 and N4 slope upwards at a slight ($\sim 1^{o}$) angle, an operational inconvenience, requiring that the casing be bled of air and kept full of water during the measurements. Because the casing decreases the counts and because the N-boreholes are not 76-mm diameter, the granite block calibration discussed in Appendix B does not directly apply here.

Representative results for N1 and N4 from two different dates are plotted in Fig. 2.10 as a function of position in the borehole. To increase the precision over that obtained by continuous measurement, individual readings

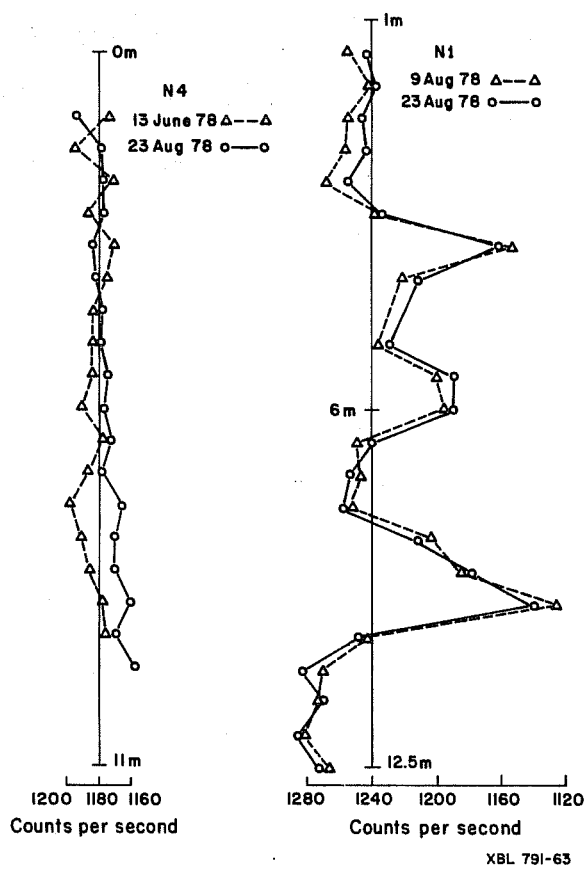

Fig. 2.10 Neutron probe measurements in N1 and N4 at 0.5-m stations with 30-sec counting times.

are acquired every 0.5 m by taking three 10-sec readings on the Canberra ratemeter. The average of the three readings is plotted. The data from N1 can be compared with the continuous logs of Fig. 2.5b, where the same features are present but at reduced sharpness due to the convolution of the anomalies with the response of the moving probe. In contrast to N1, the neutron response in N4 is virtually featureless. (The spread between the data points below 6 m in N4 is likely due to the temperature dependence of the probe, and must be discounted.) The non-anomalous character in N4 is an advantage in performing sequential station measurements, in that failure to position the probe accurately each time in N1 could result in large apparent changes in the response, which would erroneously be considered time-dependent fluctuations. Borehole N3 (not shown) is as free of neutron anomalies as is N4, while N2 is similar to N1 (see Fig. 2.5b).

Consider the precision of the measurement which is by nature statistical. We observe N counts during a time T seconds, at a rate R = N/T. Beers (1962) states that the standard deviation of the total count is

$$\sigma_N = \sqrt{N} \quad .$$

If two variables y and x are linearly related by y = mx + b, then their standard deviations are related by

$$\sigma_y = m\sigma_x \quad .$$

Hence,

$$\begin{aligned} \sigma_R &= \sigma_N/T \\ &= \sqrt{N}/T \\ &= \sqrt{R/T} \quad . \end{aligned}$$

In our case the rate R is 1200 per sec and we count for 30 sec so that

$$\sigma_R = \sqrt{1200/30} = 6.31 \quad .$$

As shown in Appendix B, the neutron-porosity calibration is of the form $\phi = mR + b$. In the granite block,

$$m = \Delta\phi/\Delta R = 1\%/80 = 0.0125 \quad .$$

However, in the cased, smaller diameter N-holes at Stripa the sensitivity is reduced by about two-thirds so the slope m is 0.019. Hence the standard deviation of the porosity estimate is approximately

$$\sigma_\phi = m\sigma_R \cong 0.019 \times 6.3 = 0.12\% \quad .$$

Hence the standard deviation of the system is around 0.1 volume percent.

The most obvious effect of temperature on the water content in rock is the creation of steam in pore spaces where the rock temperature exceeds 100°C and the pressure is relieved through fractures. Here we would expect to see a water decrease comparable to the accessible pore volume of the rock. Below boiling temperatures, the effect of temperature is to decrease the density of water, presumably causing an increase in the neutron count rate. For example, a temperature rise from 10° to 50°C expands the water from a specific volume of 0.9998 to 1.0116 cc/gm, assuming that the water is free to migrate along cracks at relatively constant pressure. This effect is expected to be below the range of our detection capability.

An opposite effect could occur due to thermal expansion of the rock, if water were free to migrate into any newly created pore space. Such a net increase in water would be expected to be near the level of detectability.

3. MECHANICAL MODULUS MEASUREMENTS WITH THE CSM CELL

3.1 Construction and Testing of the CSM Cell

3.1.1 Introduction

The Colorado School of Mines (CSM) cell is a borehole instrument for measuring the in situ elastic modulus of rock. The cell operates by pressurizing a cylindrical membrane against the sides of an EX (38-mm) borehole. Data are produced in the form of a linear pressure-volume curve, from which the stress-strain relationship of the rock can be determined.

The main components of the CSM cell (as shown in Fig. 3.1) are (1) the pressure generator, (2) the pressure transducer and readout, and (3) the borehole cell (or pressurizing membrane).

The pressure generator serves the two-fold purpose of measuring the volume reduction of the fluid system and acting as a pressure source. A thick-walled cylinder tightly fitted with an internal piston, the pressure generator reduces the fluid-system volume while increasing fluid pressure by feeding the internal piston through the cylinder. This piston movement is actuated by turning the rear portion of the generator. Volume displacement of the piston is conveniently determined by recording the number of turns of the pressure generator.

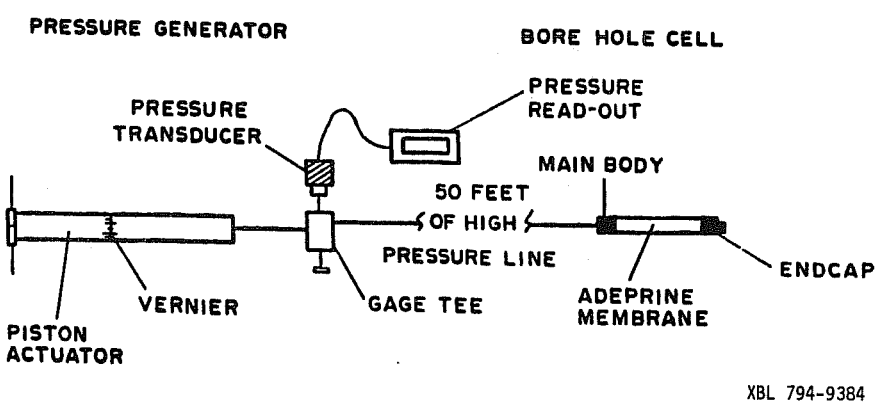

Fig. 3.1 Schematic of the CSM cell system.

The pressure transducer is a strain-gaged membrane which produces an electrical output that is linear with pressure increase. The pressure readout-unit scales this output to indicate the system pressure directly in pounds-per-square-inch on a digital display.

The borehole cell is a cylindrical adiprene membrane mounted on a stainless-steel spindle and held by a threaded endcap. The membrane is 16.51-cm long, with a 3.81-cm o.d. The borehole cell is connected to the remainder of the system by 15.24 m of high-pressure stainless-steel tubing.

3.1.2 Laboratory Calibration

The CSM cell was calibrated using three aluminum cylinders, approximately 18-inches long, with the following diameters:

Cylinder Number	i.d.-mm (inches)	o.d.-mm (inches)
1	37.74 (1.486)	50.67 (1.995)
2	37.74 (1.486)	63.17 (2.487)
3	38.00 (1.496)	75.82 (2.985)

Elastic properties of the calibration cylinders, as determined by axial loading, are as shown (E = elastic modulus, ν = Poisson's ratio).

Cylinder Number	E GPa (psi)	ν
1	68.95 ~~14.5~~ (10.0 x 10^{+6})	0.343
2	70.33 ~~14.8~~ (10.2 x 10^{+6})	0.342
3	69.64 ~~14.5~~ (10.1 x 10^{+6})	0.349

Six calibration runs were conducted by pressuring the CSM cell to about 3000 psi inside the three cylinders. The pressure-volume relationships (slope of pressure-volume curve between 1000 and 3000 psi) measured during

these tests is shown below. Note that, for convenience, volume is recorded as the number of turns of the pressure generator.

Run Number	Cylinder Number	Loading Slope (psi/turn)
1	3	460.7
2	2	462.1
3	1	425.0
4	1	426.1
5	2	459.3
6	3	454.9

Data from Run Number 1 are shown in Fig. 3.2.

The volume change associated with each pressure increase is a result of (1) expansion of the pressurized calibration cylinder, and (2) expansion

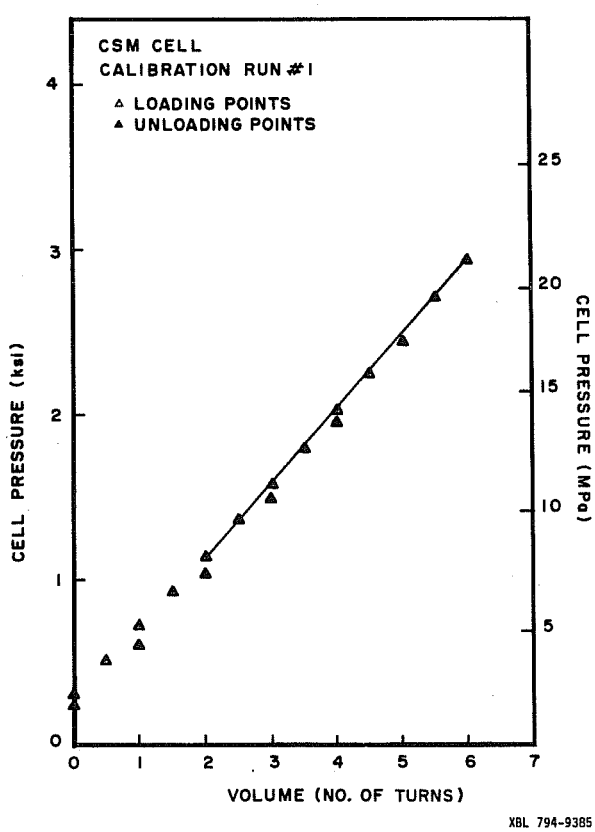

Fig. 3.2 Calibration run for the CSM cell.

of the remainder of the system (fluid lines, transducer membrane, etc.). The elastic properties of the cylinders may be used to determine the expansion of the pressurized cylinder (M_c) by the following formula (Hustrulid and Hustrulid 1972):

$$M_c = \frac{\partial G_c}{\pi L a^2 \dfrac{1 + B_c - 2\nu_c B_c}{1 - B_c}} \quad \text{(psi/turn)}$$

where ∂ = fluid volume (in.^{3}) per turn of pressure generator

L = length of cell membrane

a = inside radius of calibration cylinder

b = outside radius of calibration cylinder

$B_c = (\frac{a}{b})^2$

G_c = shear modulus of calibration cylinder

$G_c = \frac{E_c}{2(1 + \nu)}$

E_c = elastic (Young's) modulus of calibration cylinder

ν_c = Poisson's ratio of calibration cylinder.

The expansion of the remainder of the system may now be computed as:

$$M_s = \frac{M_c M_m}{M_c - M_m} \quad \text{(psi/turn)}$$

where M_s = the pressure increase per turn for the CSM-cell system

M_c = the pressure increase per turn for the calibration cylinder

M_m = the measured pressure increase per turn (loading slope).

Using the measured values of M_m, and the elastic properties of the calibration cylinders to compute M_c and M_s, the following values were determined for the six calibration runs:

Run Number	M_c (psi/turn)	M_s (psi/turn)
1	4968	508
2	4246	518
3	2733	503
4	2733	505
5	4246	515
6	4968	501

$M_s = 508 \pm 7$ psi/turn

The computed values of M_s compare quite favorably for repeated tests of the same cylinder and between tests of different cylinders. This indicates both good instrument repeatability and agreement with theory.

M_s is now used in further testing to determine values of M_c from the measured values M_m. In this sense, M_s is a calibration factor for the CSM cell and a measure of the system stiffness. Since the amount and temperature of fluid in the system affects the value of M_s, recalibration of the CSM cell is required before each series of field tests.

3.1.3 Laboratory Modulus Measurement

After the CSM cell was calibrated, two modulus measurements of the Swedish granite were conducted in the laboratory.

The CSM cell was inserted in a rock core of the granite with a 1.48-inch i.d. and a 5.68-inch o.d. To accommodate hoop tensile stresses in the core, external uniform biaxial loads of 10.3 MPa (first measurement) and 5.5 MPa (second measurement) were imposed. Pressure-volume curves for the two tests are shown in Fig. 3.3. Elastic moduli computed from these data, using a value of 0.226 for Poisson's ratio, were 61 GPa (biaxial pressure = 10.3 MPa) and 48 GPa (biaxial pressure = 5.5 MPa). These values

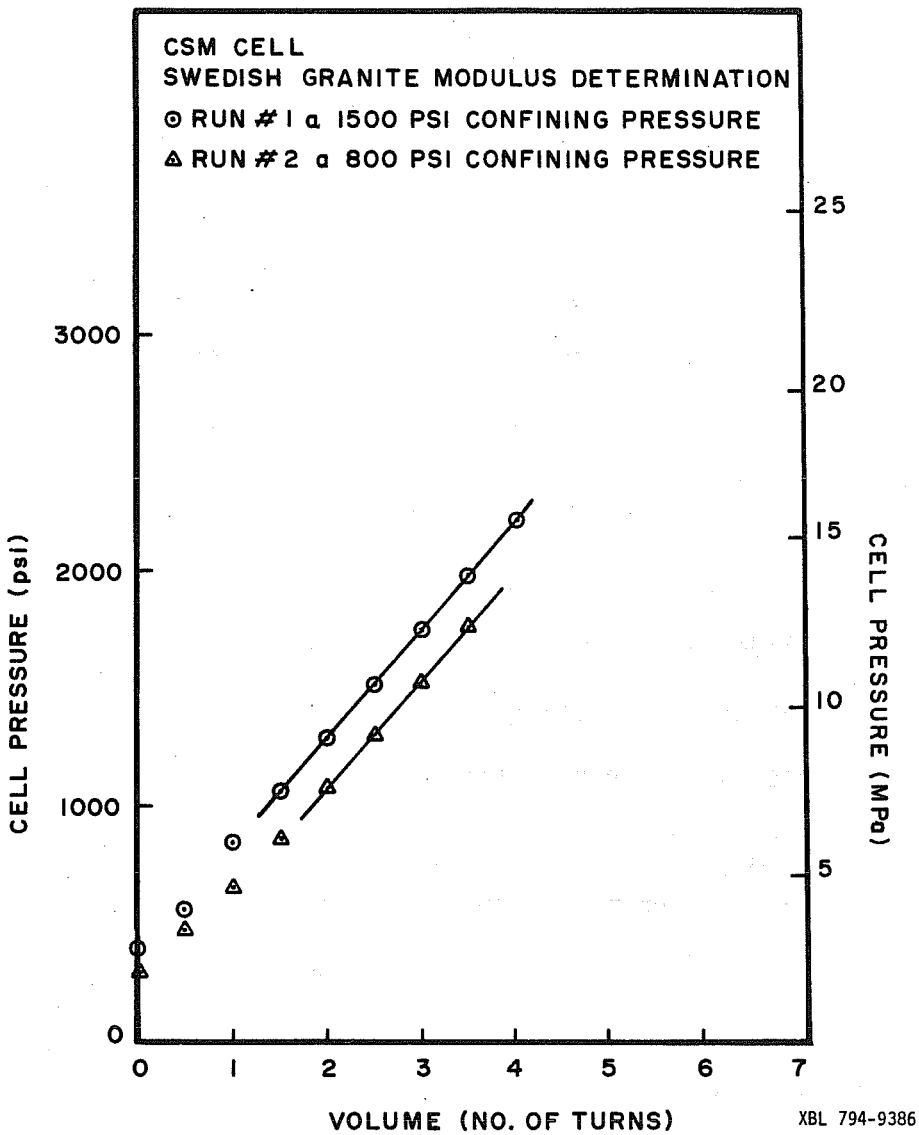

Fig. 3.3 Pressure-volume curve for laboratory modulus determination with the CSM cell.

compare reasonably well to the values of 53 GPa and 54 GPa previously determined during unconfined compression and biaxial loading (Pratt et al. 1977). These two modulus values were computed as follows:

Let

M_m = loading slope of pressure-volume curve (psi/turn)

M_s = previously determined system stiffness (508 psi/turn)

then

$$M_R = \frac{M_s M_m}{M_s - M_m} \text{ (psi/turn)}$$

$$G_R = M_R \frac{\pi L a^2}{\partial} \left[\frac{1 + B_c - 2\nu_c B_c}{1 - B_c}\right] \text{(psi)} = 3.59 \times 10^6 \text{ psi}$$

$$a = 1.48 \text{ in.}$$

$$B_c = \left(\frac{1.48 \text{ in.}}{5.68 \text{ in.}}\right)^2 = 0.068$$

ν_c = 0.226 (from uniaxial loading tests)

L = 6.5 in.

∂ = 0.0218 in.^{3}/turn

and from elastic theory

$$E_R = 2(1 + \nu)\, G_R$$

$$E_R = 2(1 + 0.226)\ 3.59 \times 10^6 \text{ psi} = 8.8 \times 10^6 \text{ psi (at 15,000 psi)}$$

or

$$E_R = 61 \text{ GPa (at 10 MPa).}$$

3.2 Field Measurements with the CSM Cell

CSM cell measurements were conducted in all vertical 38-mm boreholes at Stripa. Thermocouple holes were tested at 1-m intervals; IRAD and USBM gage holes, at instrument location depths. Thirty repeat measurements were made to check instrument performance and accuracy. All tests proceeded from the bottom of the boreholes upward.

Using the CSM cell in the field involves the following tasks: (1) initial assembly, setup, and testing of the system; (2) instrument calibration and borehole measurements, and (3) replacement of membranes and pressure seals (periodic maintenance).

Instrument assembly, setup, and testing requires one to two days for a two-man crew. Assembly is straight-forward, but requires patience and attention to detail if the instrument is to perform properly. The only problem is completely purging the system of air, as even slight amounts affect results. This task is, in general, much easier if the pressuring fluid (50 percent water, 50 percent ethylene glycol) is premixed and left standing a few days before the system is filled. The pressure generator is filled first, and then the line and transducer. The pressuring cell is assembled while submerged, and then connected to the remainder of the system.

Once the system is assembled, the borehole cell is placed inside one of the calibration cylinders and inflated by steps, as is normal for a calibration. We then check the system by examining the slope of the plotted pressure-volume curve. Air bubbles or leaks produce strong nonlinearity in the curve.

The instrument is calibrated before and after each test day. Three calibration runs were performed at Stripa in three aluminum calibration cylinders (2.0-, 2.5-, and 3.0-inch o.d.) each morning, and the results averaged. One to three calibration runs were performed at the end of each day, depending on the indicated agreement with the morning calibration. Slight shifts in the calibration constant occur due to small fluid losses in the seals in the pressure generator. The daily calibration procedure accounts for the consequent systematic changes. The procedure for the calibration measurements is the same as that described below for borehole measurements.

Borehole measurements, which are easy to perform, require one to two persons, depending on the depth of the measurement. Because the modulus

of the Swedish granite is high, its volume change is small compared to that of the instrument, and accurate modulus determination required more sensitive measurement than is necessary for a softer rock. Hence, both the time between measurement points and the number of points were increased. The procedure for borehole measurements is as follows:

1. Cell is lowered to the measurement location.
2. Cell is pressurized to 3000 psi and held for 10 sec.
3. Cell pressure is reduced to about 500 psi and allowed to equilibrate.
4. First pressure reading is taken; pressure generator handle is turned in, one-half turn.
5. After 30 sec, exactly, has elapsed, Step 4 is repeated for second reading. This process is repeated until the cell pressure slightly exceeds 3000 psi. (The 30-sec period between readings is to allow for pressure drop in the system due to heat loss of the compressed fluid. Thirty seconds was chosen as the minimum time required for the system to reach a near steady-state condition.)
6. Cell is depressurized and moved to a new position.

Sample data from a measurement run are shown in Fig. 3.4. The data are converted to modulus in the same manner as described above for the laboratory determination, except the outside radius, b, becomes infinite, making the ratio of a to b equal to zero.

Only two parts of the CSM cell subject to wear require maintenance: the cell membrane and the pressure generator seals. After approximately every 100 measurements, inelastic stretch of the cell membrane could allow cell leakage or prevent the cell from fitting the borehole, or both. The cell must be removed, disassembled, and the membrane replaced. Pressure generator (chevron) seals, which also wear out periodically, can be tightened

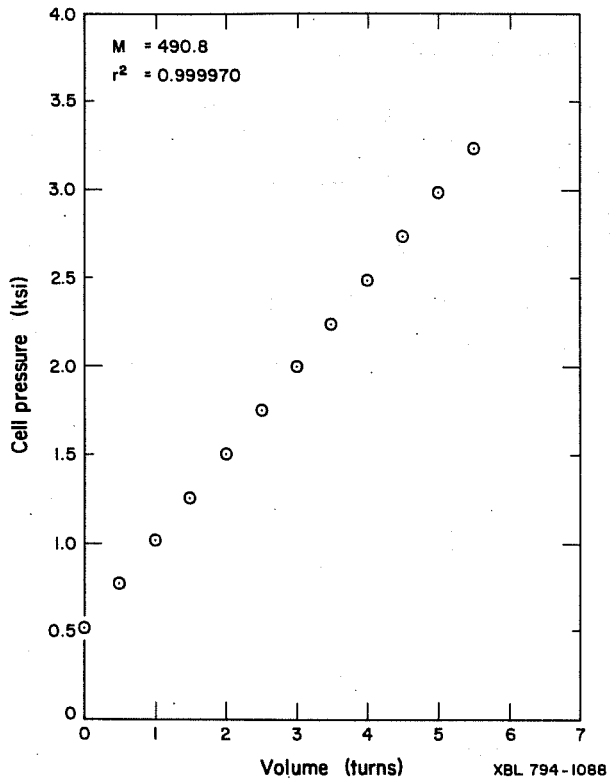

Fig. 3.4 Representative CSM measurements at 10.0 m in borehole T9, February 2, 1978.

to increase their use time. When replacement is necessary, the pressure generator is easily disassembled.

3.3 CSM Results

During early 1978, 269 CSM-cell measurements were performed in the time-scale and full-scale drifts, at an average rate of 9.4 measurements per day. A complete summary of the field measurements is included in Appendix F, and presented as a histogram in Fig. 3.5. Note that the field measurements indicate an average modulus of 36.8 8.6 GPa (5.3 x 10^6 psi) and rarely exceed the laboratory-measured value of 55 GPa (8.0 x 10^6 psi). Thirty repeat measurements were performed, yielding an average absolute difference of 3.7 GPa (0.5 x 10^6 psi) between first and second measurements, with two-thirds of the repeats less than this difference.

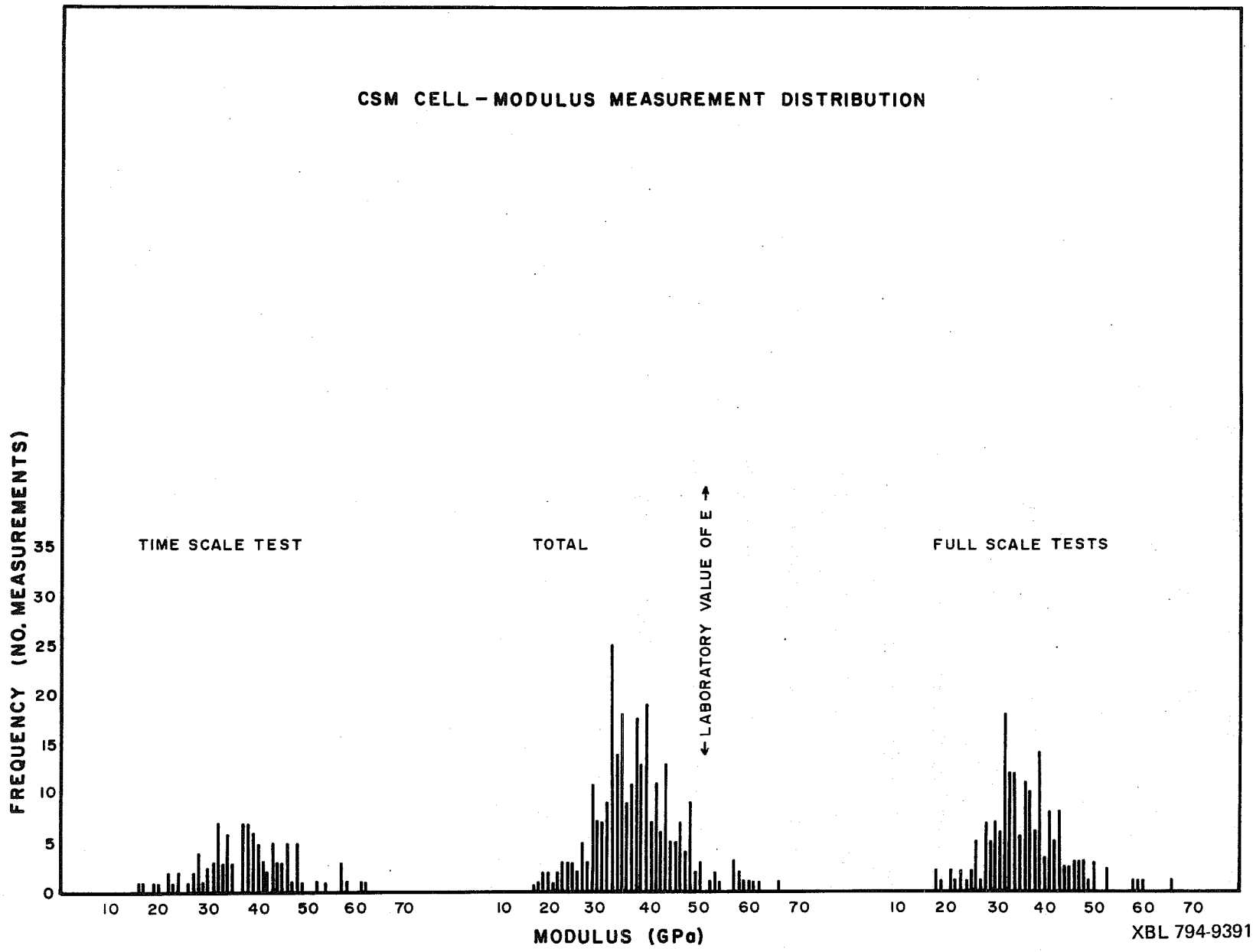

Fig. 3.5 Histograms of CSM-cell determinations of Young's modulus.

The CSM-cell modulus measurements indicate a greater variability in rock properties than is shown by geophysical logging in the same or neighboring holes. This may be partially due to the small volume of rock which influences the CSM-cell measurements. The stress distribution produced by the pressurized cell drops off rapidly with radial distance. At a radial distance of 4 cm from the borehole wall, the radial and tangental stresses produced are 10 percent of those on the borehole wall. This means that each modulus measurement is essentially a point measurement.

The validity of the measurements is supported by several observations. First, the variation of repeat measurements is far less than the indicated data spread. Note that these repeat measurements were performed on different days, with the times between measurements as great as one month. Secondly, although there is no exact correlation between fracture frequency and the measured modulus, the influence of highly fractured areas is apparent. Figure 3.6 displays the average modulus measured as a function of the number of fractures within ±0.5 m of the measurement point. Visual correlation in several holes also appears good, as shown in the comparison of the fracture logs and modulus measurements for hole T6 (Fig. 3.7). Exact correlation with fracture logs is difficult due to the large number of fractures induced by the drilling in the small core of the 38-mm holes and the variability of fracture properties such as thickness, filling, hardness, etc.

The CSM cell gave accurate and repeatable performance, and is very satisfactory for making in situ modulus measurements.

3.4 Goodman Jack Tests

The Goodman Jack is a borehole device for measuring in situ modulus. Designed to operate in a 76-mm (3.0-inch)-diameter borehole, the instrument

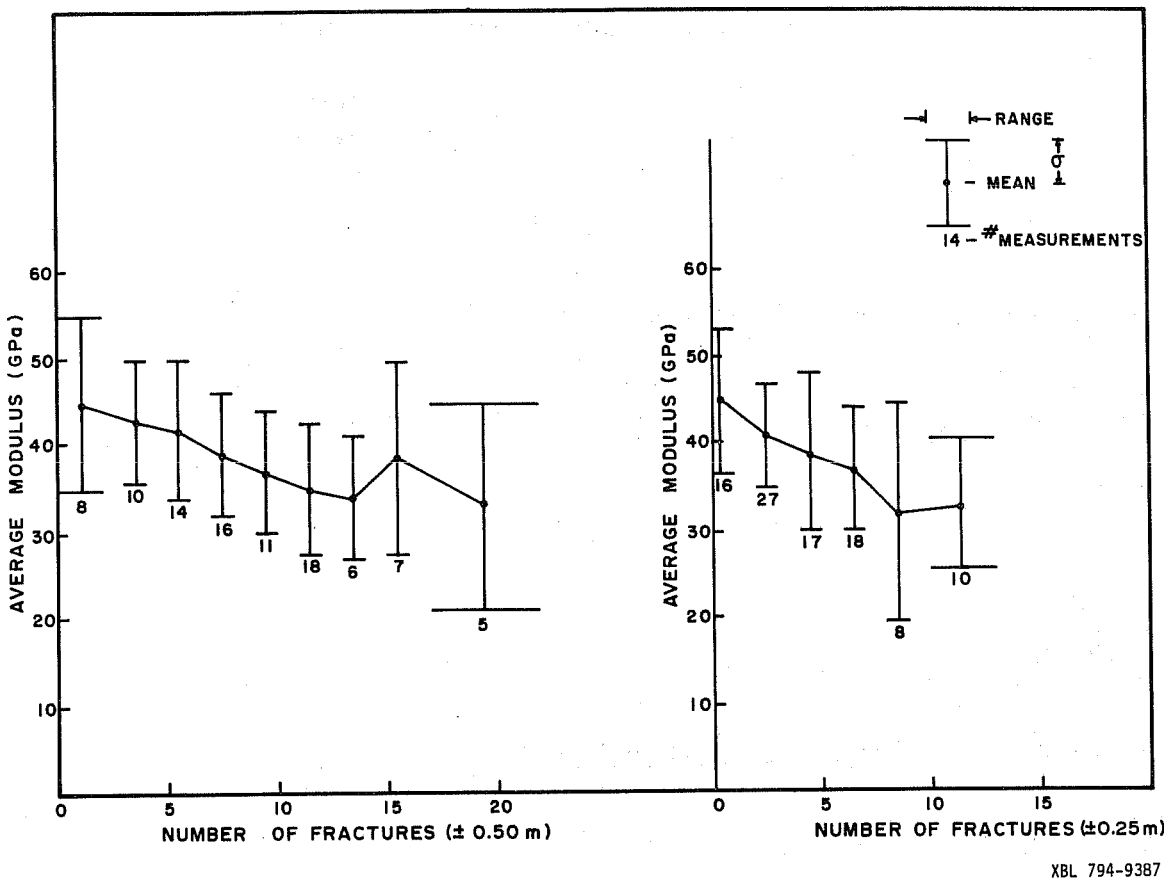

Fig. 3.6 In situ Young's modulus determinations versus fracture density from visual inspection of core.

consists of a hydraulic jack fitted with two opposing platens. The platens are curved to match the borehole diameter and fitted with two linear variable-displacement transducers (LVDT) to measure platen movement when opening and closing the jack. Jack pressure is monitored by a standard pressure gage with a range of 0 to 5000 psi. A small hand pump, fitted with two pressure lines and a valve, enables the jack to be opened or closed. LVDT output is fed into a scaling amplifier with an optical readout.

The Goodman Jack is inserted in the hole to the test depth and pressurized by steps to 3000 psi. Platen displacements are then recorded. The evaluation of the corresponding jack pressure - platen displacement

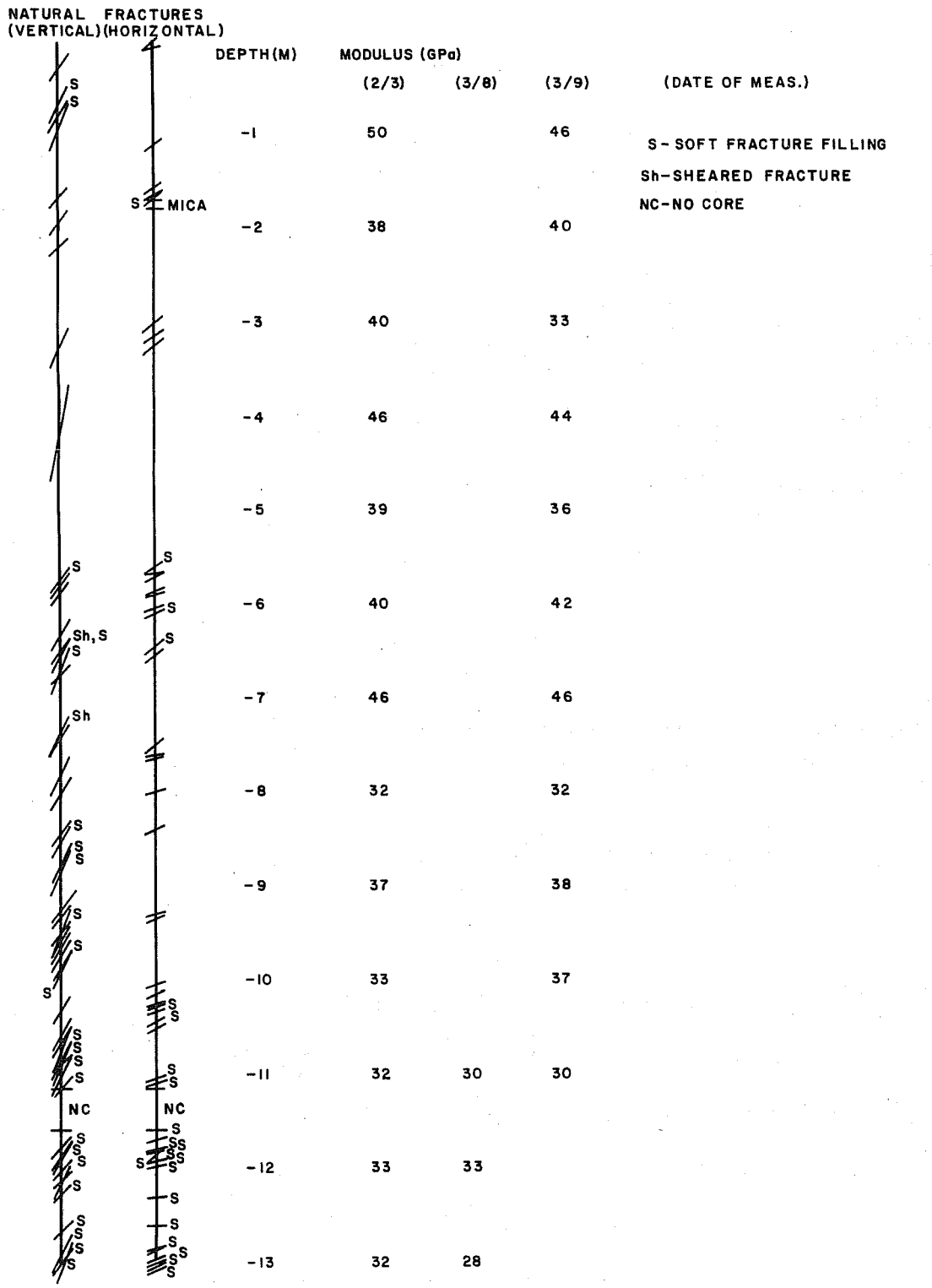

Fig. 3.7 CSM-cell determinations of Young's modulus and fractures observed in core from borehole T6.

curve on the basis of effective platen loading pressure and contact area is only approximate, because the effective platen contact area is not exact, but rather estimated for each measurement.

3.4.1 Calibration

A single calibration of the Goodman Jack LVDT transducers suffices for all measurements. First, the jack is opened inside a reference cylinder and the LVDTs are zeroed. A second sized cylinder can be used to adjust scaled output. The jack is then placed on its side and pumped open very gradually. Large calipers are used to measure platen displacement (diameter) as a function of voltage output.

3.4.2 Downhole Testing

Downhole testing was carried out at regular intervals, from 13 m upwards to 2 m. Installing rods were marked so that orientation of the jack platens was known. Testing was conducted in both east-west and north-south orientation. Furthermore, repeat measurements were made both consecutively and after the tool was removed from the hole, to determine the repeatability of the measurements.

During testing, the jack is lowered downhole by drill rod sections which enclose the two hydraulic leads and a third electrical lead. Two men were able to move the jack up and down the hole to 13 m--for greater depths, additional help probably would be needed. The jack is positioned at the proper depth and orientation, opened until it contacts the borehole, and the initial LVDT readings are recorded. The jack is then loaded to various pressures (250, 500, 750, 1000, 1500, 2000, 2500, and 3000 psi), and displacement readings are taken at each step. Sample data from a loading curve are shown in Fig. 3.8.

The Goodman Jack is not suitable for quantitative measurements on a

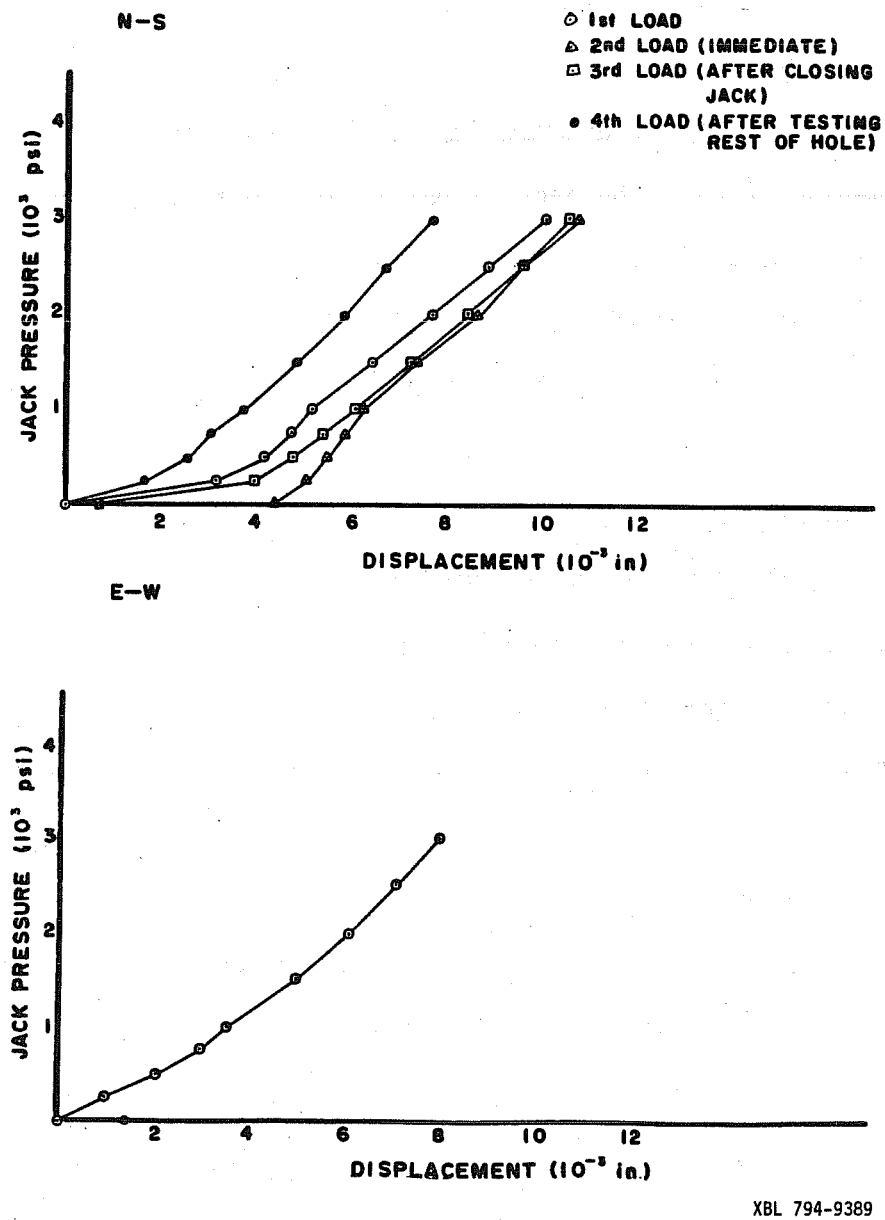

Fig. 3.8 Pressure-displacement data from the Goodman Jack.

hard rock such as the Stripa granite, because (1) the total measured displacement is extremely small, (2) the actual contact of the platens to the borehole is uncertain, and (3) the repeatability is poor.

4. ULTRASONIC PROPAGATION MEASUREMENTS

Ultrasonic wave propagation techniques are being applied at Stripa to examine the effect of fractures on wave propagation and also to monitor the change of ultrasonic wave characteristics during the heater experiment. The 56-mm-diameter "M" boreholes in the time-scale drift and around the H9 heater in the full-scale drift are kept open and accessible during the heater experiment for this purpose (see Table 1.1 and Figs. 1.2 and 1.3).

4.1 Equipment and Procedures

Two sets of equipment were evaluated before one was adopted for the cross-hole work. Both sets are experimental and operate in a stationary mode, with the transducer forced into firm contact against the borehole wall to ensure maximum transmission of energy into the rock. In this respect both sets of equipment differ from the continuous-logging tool discussed in Section 2 of this report, which requires a water-filled borehole to transmit the acoustic energy into the rock.

The first set of equipment, provided by Professor M. S. King of the University of Saskatchawan, uses hydraulically activated arms to force the transducer housing against the borewall. The transmitter consists of a vertically polarized shear-wave crystal, operated at a 20-kHz frequency and a repetition rate of 10 to 50 Hz. Both an in-hole receiver spaced 30 cm from the transmitter, and a separate receiver for cross-hole work were made available. This system appeared to perform reliably, but due to its lower operating voltage, the cross-hole signals lacked the reproducibility obtained with the second system.

The second set of equipment, designed by Mr. R. Lingle of Terra Tek, provides separate compressional- and shear-wave piezoelectric crystals packaged in an aluminum housing which is expanded by a worm screw arrangement

to force the transducer housing against the borewall. Figure 4.1 shows a block diagram of the borehole probes and the associated surface electronic and recording equipment. The high-voltage pulse generator supplies the electrical pulse to excite the transmitter; it also generates a synchronization pulse coincident with the onset of the high-voltage pulse to trigger the oscilloscope. Depending on the load impedance, the output pulse can exceed 20,000 V.

The received signal is amplified 40 to 60 dB as required, and applied to the oscilloscope, which uses a 100-MHz internal clock to provide accurate time differences between pairs of events selected on the oscilloscope face with an adjustable bright spot. Compressional (first arrival)- and shear-wave arrivals are picked and timed during the measurement sequence, and the times recorded on data sheets. In addition, the waveform is photographed using a Polaroid camera mounted on the oscilloscope face. Time delays due to the instrumentation are accounted for by clamping the receiver and

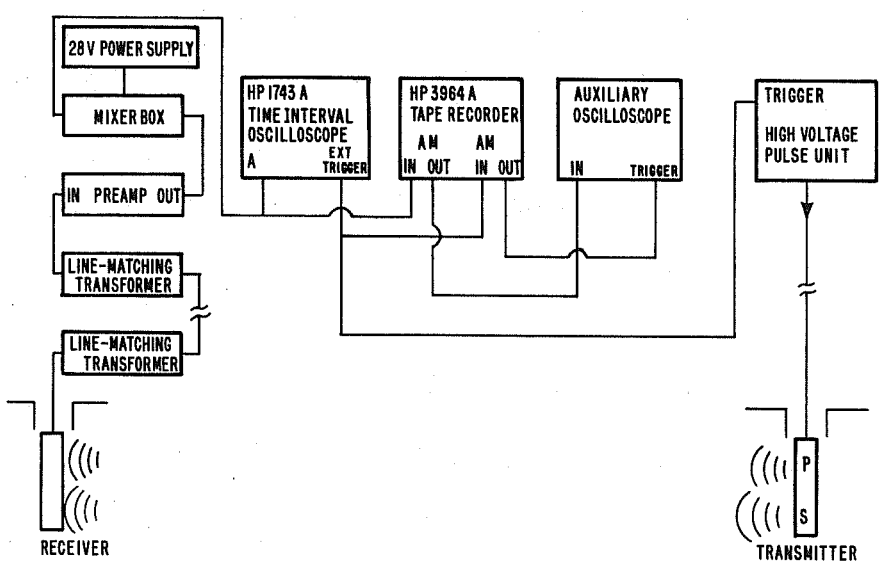

XBL 792-7380

Fig. 4.1 Block diagram of cross-hole ultrasonic equipment.

transmitter units together to measure the instrument travel time, which is about 6 μsec and 11 μsec for the compressional and shear waves, respectively.

As indicated in Fig. 4.1, the signals are also directly recorded on a HP3960A magnetic instrumentation tape recorder, using a 100-Hz to 60-kHz band width. Hence, both frequency and amplitude information are available for later processing and analysis.

Two operational problems were encountered and solved with the prototype cross-hole equipment. To decrease signal loss the piezoelectric crystals are glued to the housing. The original one-component glue was too rigid, breaking after several measurement runs due to the small flexure of the housing as it expanded against the wall. A more flexible glue solved this problem. The high-pulse voltage applied in the transmitter resulted in arcing between the transducer and the housing whenever small amounts of moisture got into the housing. This second problem was solved by potting the transducers in "RTV" compound, and taking care to dry the holes before commencing measurements.

The ultrasonic equipment is used for repeatability checks (discussed below), and for three surveys in the underground boreholes. First, before the heater tests, in-hole surveys were conducted in all six of the "M" boreholes, and eight cross-hole profiles were obtained. Second, the cross-hole equipment is used to monitor weekly any changes in cross-hole transit time induced by the heating of the rock around H9. This is done with four transducers at the level of the heater mid plane in boreholes M6, M7, M8, and M9. Four cross-hole paths are covered between these four boreholes. Two of these paths intersect areas close to the heater, the first parallel to the major fracture discontinuities, and the second perpendicular to the

discontinuities. The other two paths are farther from the heater (see Fig. 1.2). Two of these transducers are kept in position so that changes due to resetting the transducers can be eliminated. The other two transducers are used periodically to survey an entire profile between boreholes M7 and M9. Third, the cross-hole equipment is used at longer (six-month) intervals to repeat several profiles at a higher sampling density.

4.2 Repeatability

The greatest source of error in repeating a measurement appears to be re-establishing the contact between the transducer and the borewall. Errors in repositioning compound this problem. The present technique uses a tape attached to the center of the transducer so that the depth is read directly as the transducer is lowered into the hole. This method is reliable to about ±1 cm. A better method is desirable.

One particular pair of measurement positions, free of fractures and close to the surface, is used as a reference line to establish repeatability and check for system malfunctions and drift during the course of the experiment. Figure 4.2 shows photographs of repeat measurements taken on consecutive days, when the transducers were removed from the measurement positions and put back again before the second measurement. Table 4.1 shows the transit times measured over this same interval during a time period of less than a month. The range of both the compressional and shear measurements lies within a spread of about 0.5 percent, excluding the checks with different pairs of transducers on September 13.

4.3 Preliminary Results

Tabulated in Table 4.2 are the time-interval measurements, the computed distances between the measurement points computed from survey data, and the computed velocities. The measurement points lie on horizontal planes

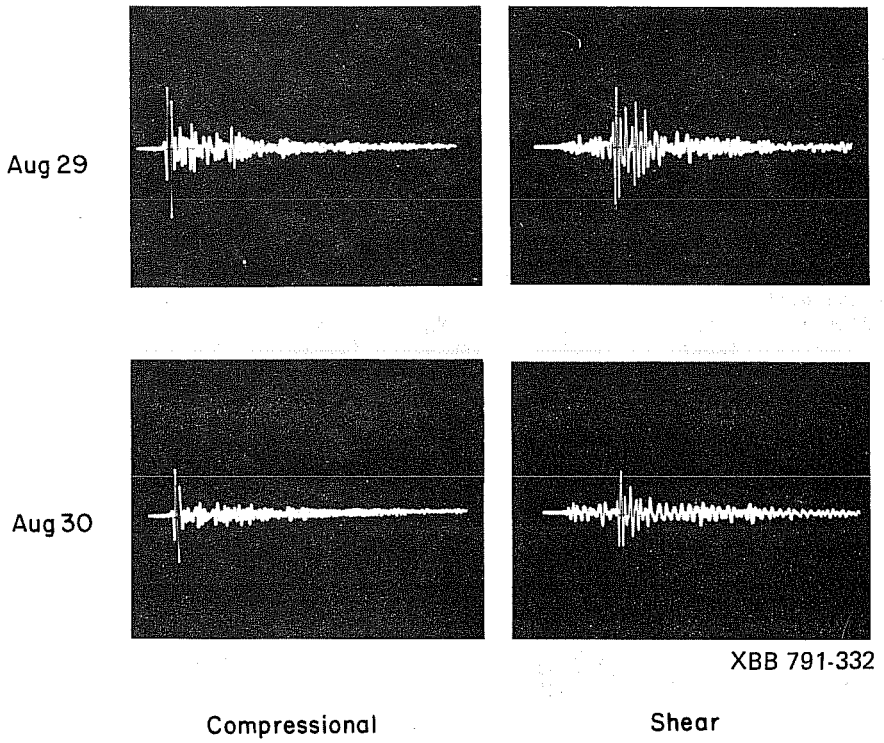

Fig. 4.2 Waveforms taken along the reference line using the compressional transducers (left) and shear transducers (right). The transducers have been removed and then replaced between Aug 29 and 30 to illustrate the repeatability. Horizontal scale is 200 μsec per division.

Table 4.1 Repeatability checks at reference positions in boreholes M6 and M9.

Date	Compressional transit time (m sec)	Shear transit time (m sec)	
August 23	0.4770	0.8071	
August 24	0.4766	0.8069	
August 29	0.4769	0.8070	
August 30	0.4766	0.8064	
September 7	0.4769	0.8099	transducer problems
September 8	0.4783	0.8061	transducer reglued
September 12	0.4764	0.8065	transducer reglued
September 13	0.4750	0.8098	four combin-
September 13	0.4752	0.8043	ations of
September 13	0.4768	0.8110	different
September 13	0.4753	0.8097	transducers

Table 4.2. Measured transit times (columns 3 and 4) between stations in boreholes M6 and M8.

Elevation (m)	Horizontal distance (m)	t_p (msec)	t_s (msec)	V_p (km/s)	V_s (km/s)	ν	G (GPa)	E (GPa)	K (GPa)
339.0	4.185	0.7120	1.2297	5.878	3.403	0.248	30.1	76.0	50.2
339.5	4.186	0.7069	1.2442	5.922	3.364	0.262	29.7	75.1	52.5
340.0	4.185	0.7050	1.1987	5.936	3.491	0.236	32.0	79.2	49.9
340.5	4.184	0.7116	1.2250	5.880	3.416	0.245	30.6	76.4	50.0
341.0	4.184	0.7112	1.2953	5.883	3.230	0.284	27.4	70.4	54.4
341.5	4.182	0.7194	1.2432	5.813	3.364	0.248	29.7	74.3	49.1
342.0	4.181	0.7236	1.2638	5.778	3.308	0.256	28.7	72.3	49.4
342.5	4.182	0.7159	1.3148 1.2815	5.842	3.181 3.263	0.289 0.273	26.6 28.0	68.6 71.3	54.2 52.4
343.0	4.181	0.7103	1.3141	5.886	3.182	0.294	26.6	68.8	55.6
343.5	4.181	0.7091	1.2425	5.896	3.365	0.258	29.7	74.9	51.7
344.0	4.181	0.7110	1.2446	5.880	3.359	0.258	29.6	74.6	51.3
344.5	4.180	0.7106	1.2237	5.882	3.416	0.246	30.6	76.4	50.0
345.0	4.180	0.7123	1.2016	5.868	3.479	0.229	31.8	78.2	48.1
345.5	4.179	0.7049	1.2629	5.929	3.309	0.274	28.7	73.3	54.0
346.0	4.178	0.7052	1.2115	5.925	3.449	0.244	31.2	77.8	50.6
346.5	4.176	0.7056	1.2781	5.918	3.267	0.281	28.0	71.9	54.6
347.0	4.176	0.7029	1.2125	5.941	3.444	0.247	31.1	77.7	51.2
347.5	4.175	0.7079	1.2856	5.898	3.248	0.282	27.7	71.1	54.4
348.0	4.174	0.7087	1.2081	5.890	3.455	0.238	31.3	77.7	49.3
348.5	4.173	0.7013	1.2010	5.950	3.475	0.241	31.7	78.8	50.7

Note: Computed velocities include the instrument times of 6.2 μsec (p-p) and 11.3 μsec (s-s), and a distance correction of 56 mm. Moduli are computed from the equations in the text, using a bulk density of 2.63 g/cm^3. The 343.0-m elevation is the heater mid-plane; 339.0 m is just below the floor of the drift.

at the given elevations in boreholes M6 and M8. Also given are the dynamic moduli computed from the following formulae:

for Young's modulus

$$E = 3\rho\, V_s^2 \; \frac{V_p^2 - 4/3\, V_s^2}{V_p^2 - V_s^2} \qquad \text{(GPa)}$$

the bulk modulus is $K = (V_p^2 - 4/3\, V_s^2)$(GPa)

the shear modulus is $G = \rho\, V_s^2$ (GPa)

and Poisson's ratio is

$$\nu = \frac{V_p^2 - 2V_s^2}{2(V_p^2 - V_s^2)}$$

where V_s is the shear wave velocity (km/sec), V_p the compressional wave velocity (km/sec), and ρ the bulk density (Mg/m^3).

We can compare the cross-hole velocity data with the laboratory measurements on Stripa core given in Appendix G. The lithostatic load at the 340-m level at Stripa is in the 10- to 20-MPa range (Carlsson 1978). The average cross-hole velocities of Table 4.2 are 5889 and 3356 m/sec for the compressional- and shear-wave velocities, respectively. These values are only a few percent lower than the averages of the laboratory velocities at 10 MPa confining pressure, which are 5906 and 3450 m/sec. Other velocity measurements on Stripa granite by Swan (1978) and Pratt et al. (1977) were done at atmospheric pressure, and hence the values are lower than the averages given above.

The computed Young's moduli given in Table 4.2 have an average value of 74.5 GPa for the twenty-one measurements in the M6-M8 profile. Table 4.3 lists some other determinations of Young's modulus done at comparable confining pressures on the Stripa granite. The two acoustic determinations

agree closely and also agree quite well with the static laboratory values. Such agreement is not typical, as dynamic determinations are usually greater than static determinations (Jaeger and Cook 1969).

As mentioned above, cross-hole monitor measurements are performed weekly at the elevation of the center of the heater H9. The arrival times between boreholes M7 and M9 over the forty-five day period following the turn-on of H9 are shown in Fig. 4.3. Decreases in the transit times shown correspond to increases in compressional and shear velocities of about +3 percent and +4 percent. During this time period, the volume surrounding the heater undergoes compressional stress. Continued monitoring and examination of the data in conjunction with the extensometer and stress measurements around the heater will be required to sort out the influences of fracture and micro-crack closure on the ultrasonic velocity changes.

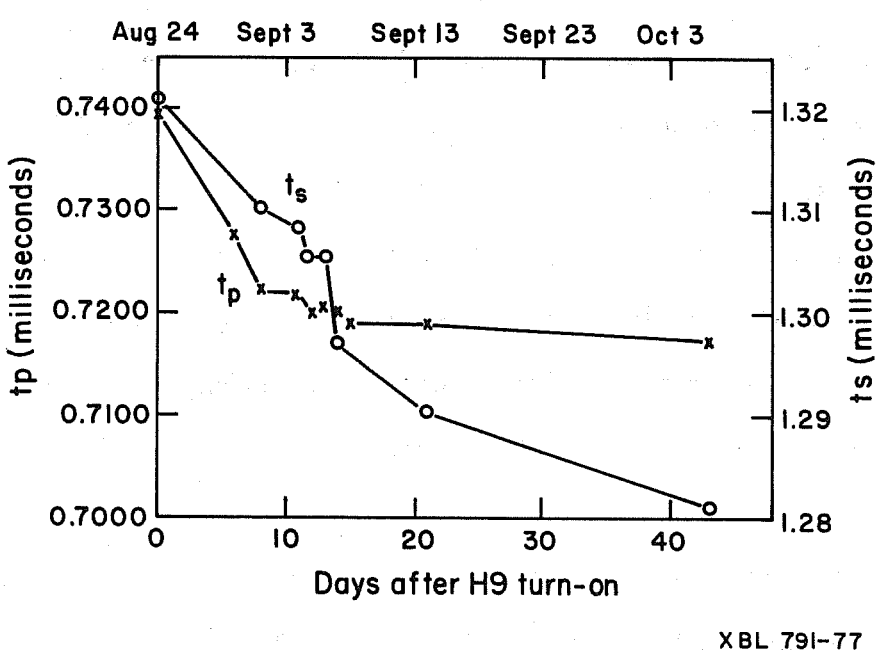

Fig. 4.3 Transit times t_p and t_s for the compressional and shear waves between M7 and M9 at the heater midplane.

Table 4.3 Sampling of Young's modulus (GPa) determinations in the laboratory and in situ on Stripa granite.

	Mechanical		Acoustic	
Laboratory	61	CSM-sect. 3 biaxial confinement, 10.3 MPa	78	King-Appendix G axial confinement, 10 MPa, N = 9
	77	Swan triaxial, 10 MPa N = 4		
In situ	37±9	CSM-sect. 3 N = 269	74	cross-hole acoustic- sect. 4, N = 21

5. GEOPHYSICAL LOGS WITH THE SGU LOGGING SYSTEM

On behalf of the Swedish authority for nuclear fuel safety (KBS), the Geological Survey of Sweden (SGU) has carried out an electrical well-logging program in order to determine the applicability of different geoelectrical techniques in delineating and characterizing the fracture systems in crystalline rocks. The tools and measuring instruments used in the geophysical survey were specially designed for the aforementioned purpose by the SGU Geophysical Laboratory in Malå, Sweden. The following logs were recorded.

- Resistivity logs, lateral and normal arrays
- Single-point resistance and differential resistance
- Gamma-ray log

All the geophysical logs were recorded at a vertical scale of 100 mm to 1 mm. Logs have been run in vertical boreholes in the full-scale and time-scale drifts as indicated in Table 1.1 and Figs. 1.2 and 1.3. The core logging was carried out by LBL.

5.1 Resistivity Measurements

Rock and soil testing in sedimentary formations with electrical methods has been developed over the years and refined to a satisfactory status. However, the application of electrical methods in crystalline rock is not satisfactory. The reasons for this discrepancy are both instrumental and physical. Most of the available commercial instruments are designed to measure relatively low resistivities, less than 1000 Ω m. In crystalline rocks resistivity values as high as 100,000 Ω m are very common.

The electrical properties of crystalline rocks are governed by the pore space and fracture characteristics. Over a long period of time geologic stresses have fractured most rocks into a pattern of intersecting fractures. Some of the fractures are open, some closed, and the remainder filled with

clay alteration and other secondary minerals. The different fracture patterns and the conducting fissure minerals raise problems for the correct interpretation of the electrical logs.

The resistivity logs were recorded in about thirty-five shallow holes situated in the time-scale and full-scale drifts. The depth of the holes varies between 6 m and 15 m. The following electrode spacings were used:

Lateral 1.65 m

Lateral 0.85 m

Normal 0.80 m

Normal 1.60 m

The potential electrode spacing for the lateral configuration was 0.1 m. The logs were recorded at a vertical scale of 100 mm to 1 mm.

A constant current generator with current adjustable over the range 0.1 mA to 100 mA was used at a frequency of 0.25 Hz. Station measurements with the tool stopped in the hole were made at intervals of 0.5 m.

Different electrode spacing and array types were used to define fractures better. A detailed account of the logging methods is given by Magnusson and Duran (1978).

Because the distribution of the current varies over wide limits due to the complicated geometry of discontinuities as well as the water quality, the results were used in a qualitative sense for identification of fracturing or discontinuities. An individual assessment for thin discontinuities is not possible because of the limitation of the tool.

Bedrock with high resistivity gives rise to induction effects in the electrode array. This problem has been overcome by using a very low frequency of 0.25 Hz.

If we write for the lateral array:

$$R_A = \frac{j}{j_o} R_{MN}$$

where R_A is the apparent resistivity, j is the current density in the hole, and j_o is the current density in a homogeneous and isotropic medium, and R_{MN} is the true resistivity of the medium where the potential electrodes are situated. For the normal array, the relationship between the apparent resistivity and the true resistivity is more complicated:

$$R_A = \left(\frac{j}{j_o} R_\infty\right)_{medium.}$$

R_∞ are the values of the rock resistivities from point M (potential electrode) to an infinitely removed point. It is very important to remark that in crystalline rocks the variation of the resistivity of the rocks and the current propagation near the measuring electrodes can give rise to large differences in the measured apparent resistivities. This is due to the irregular distribution of the current.

Because the holes are shallow and because of the electrode spacing, the interpretable part of the curve was limited to the middle part of the hole. Near the limits of the hole (at the bottom and at the water level), the emitted current from electrode A is controlled by the end effects, either reducing or increasing the current density between the potential electrodes, and thereby altering the measured apparent resistivity. The propagation effect at the bottom of the holes for the normal array can be explained in similar way.

Because of the high resistivity of crystalline rock, the current penetration in the rock is poor, and much of the current flows along the borehole, both

upward and downward away from a current electrode A to a second current electrode, B, placed at the surface. The resistivity in the direction of the potential electrodes in high-resistivity rocks depends on the product 1R. (The 1 represents the length of the section between the current electrode A and the first conductive zone below the current electrode; R is the resistance of the borehole liquid.) The distribution of the current is proportional to the resistance of the section, thereby explaining the asymmetrical shape of the lateral curve. The maximum amplitude of the curve decreases (increases) when the measuring electrodes first enter the conductive (resistive) zone. The lower units of the resistive/conductive zones are also more clearly indicated than the upper limits. In logging underground at Stripa, neither the current nor the potential electrode was far enough removed from the borehole, and errors were thereby introduced which were not included in the geometric factor. In addition, the close distance to the "remote" electrodes enhanced any perturbations due to local resistivity inhomogeneities.

The shape and amplitude of the normal curves are a function of the position of the potential electrodes. If the potential electrodes are at infinite distance from each other, the curves are symmetric with respect to the middle point of the conductive zone. If one of the potential electrodes is not at "infinite" distance the curve becomes asymmetrical about the midpoint of the anomalous zone. Other factors which influence the amplitude of the curves are the ratio of fluid resistivity in the holes to the granite resistivity, the ratio of the discontinuity thickness to the electrode spacing, and the borehole diameter.

5.2 Differential Resistance

The tool used in the investigation consists of two electrodes which

function both as current and potential electrodes (Fig. 5.1). The electrodes are separated by a 12-mm-thick insulator. The negative electrode (140-mm long) is situated above the shorter (10-mm) positive electrode, and therefore has less variable contact resistance; i.e., the lower electrode is more sensitive to variations in the surrounding resistance.

Because the resistivity of the borehole liquid (20 to 300 Ω m) is lower than that of the crystalline rocks (1000 to 100,000 Ω m), the current tends to flow in the liquid. Therefore it is necessary to have an insulator between the electrodes, with a diameter very close to the borehole diameter. The insulator works as a guard which forces the current towards the borehole wall and the discontinuities. In most of the measurements in the full-scale drift, an extra insulating guard was applied to the tool. The diameter

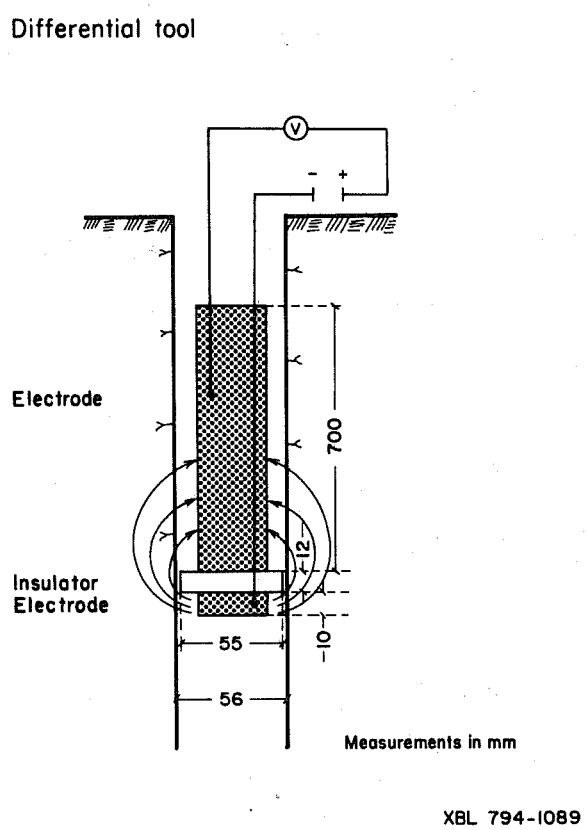

Fig. 5.1 Schematic of SGU differential resistance probe with 12-mm-thick insulator between the upper and lower electrodes.

of the guard is a few tenths of a millimeter thinner than the borehole. This increased the sensitivity of the tool, as demonstrated in Fig. 5.2.

From Fig. 5.2 it is evident that the reproducibility of the measurements is excellent. The background level of the resistance from ten boreholes was logged with and without the extra guard. Without the extra guard, logged values were about 200 to 300 Ω lower. The tool without the extra guard was tested in the laboratory, where several kinds of fissures were simulated in an insulating tube (Fig. 5.3). Three different water salinities were used in the test: fresh water, 0.25 g/liter, and 0.55 g/liter NaCl dissolved in water. High salinity lowered the signal amplitude (Fig. 5.4), due to the change of current density around the tool.

Two scales were used in the measurements: the 1- to 100,000-Ω scale compresses the signals, and is therefore less sensitive than the 1- to 10,000-Ω scale.

5.3 Results

Figures 5.5 and 5.6 present the resistance and resistivity logs obtained in boreholes E6 and E7 in the full-scale room. These two examples are fairly typical of the data obtained in the full-scale drift. The logs from the time-scale room are less useful, because the extra guard was not used on the differential resistance probe.

A preliminary qualitative interpretation of the logs resulted in three designated categories: low fracturing (LF), moderate fracturing (MF), and high fracturing (HF). The interpretation was based mainly on the inflections and peaks in the lateral curves and the separation between the two lateral curves. These interpreted categories are indicated in the resistivity column on Figs. 5.5 and 5.6. Note the rough correspondence with the core-log data. The next steps in the examination of the data will

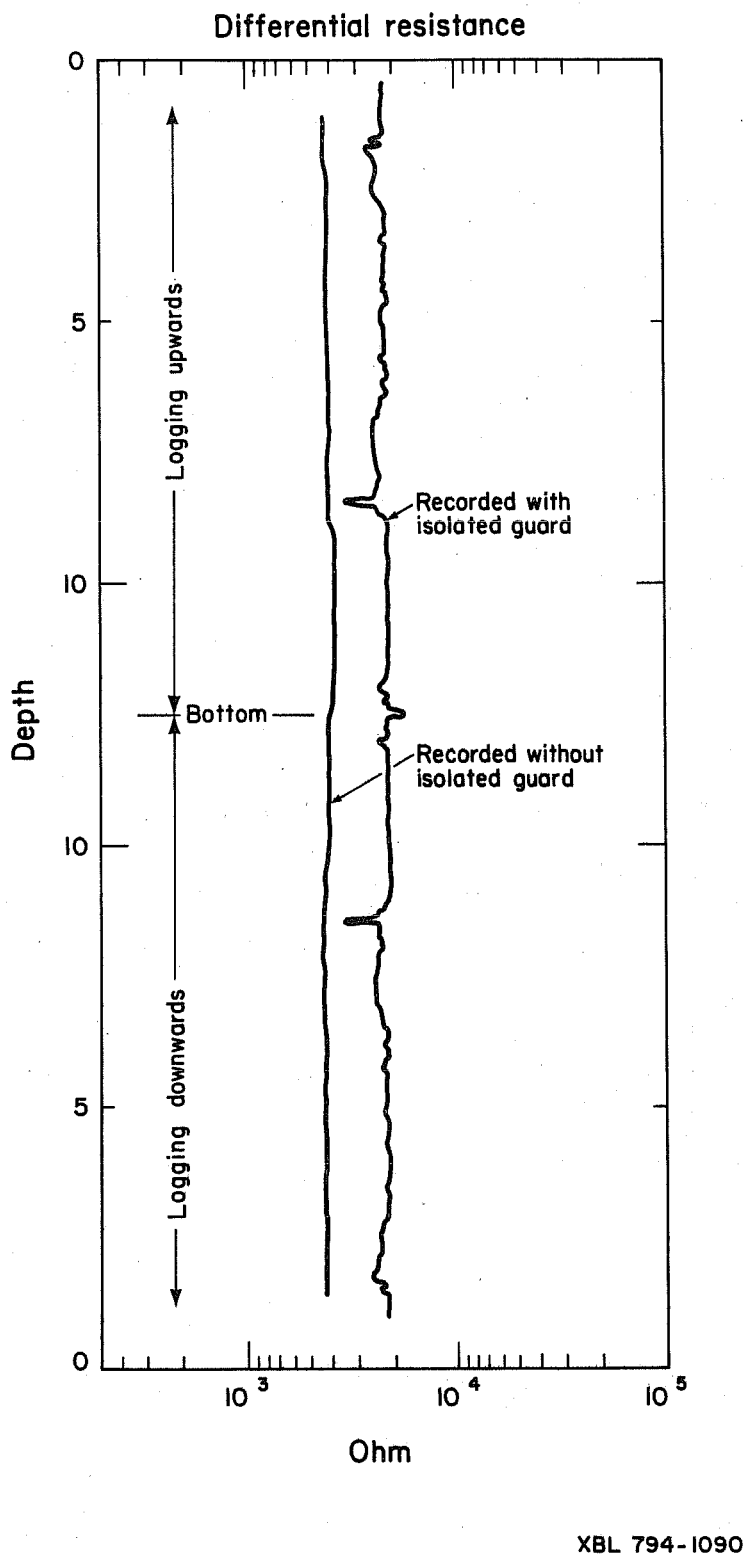

Fig. 5.2 Differential resistance log in borehole E7.

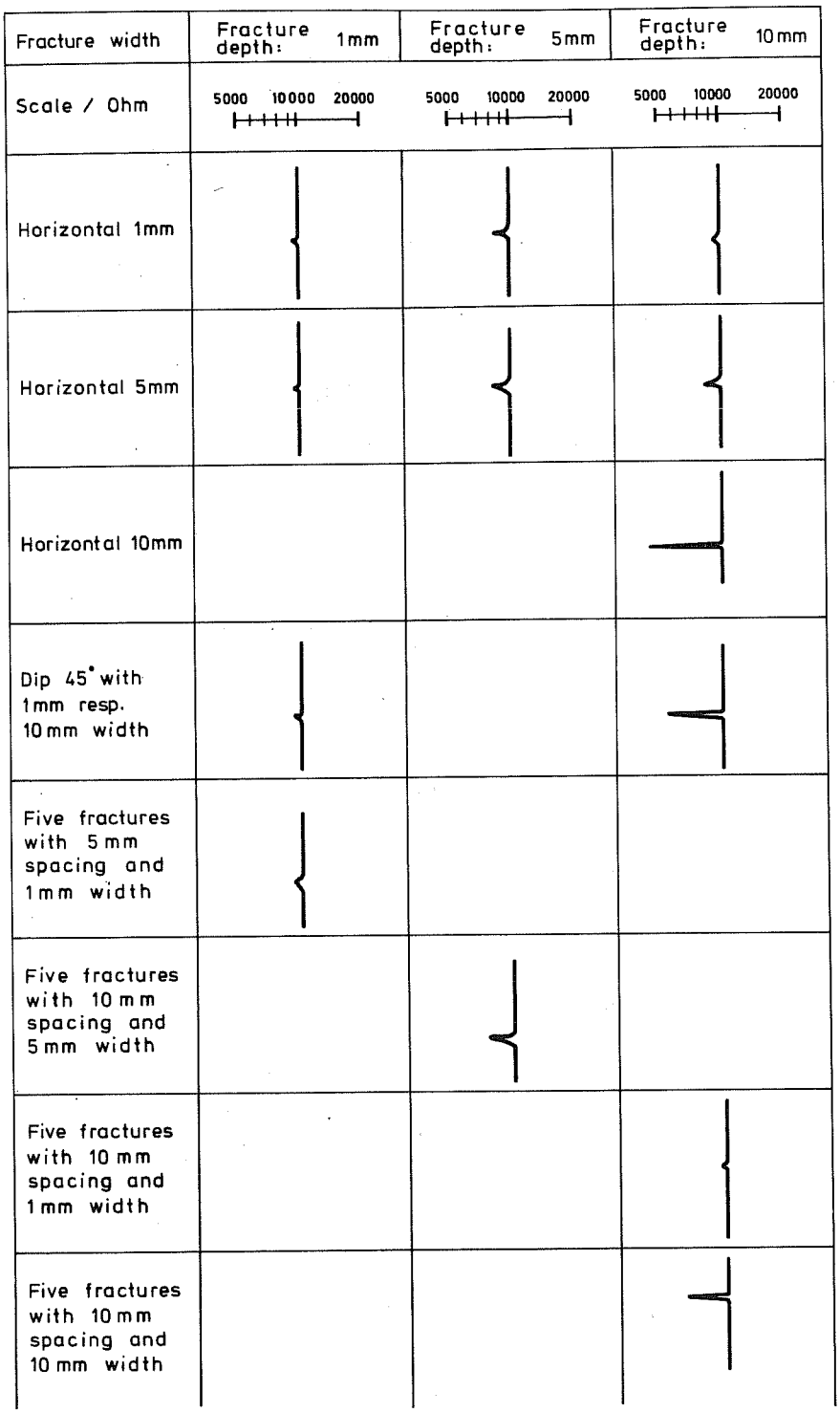

XBL 794-9390

Fig. 5.3 Laboratory tests of the differential resistance tool in an insulating medium with simulated fissures.

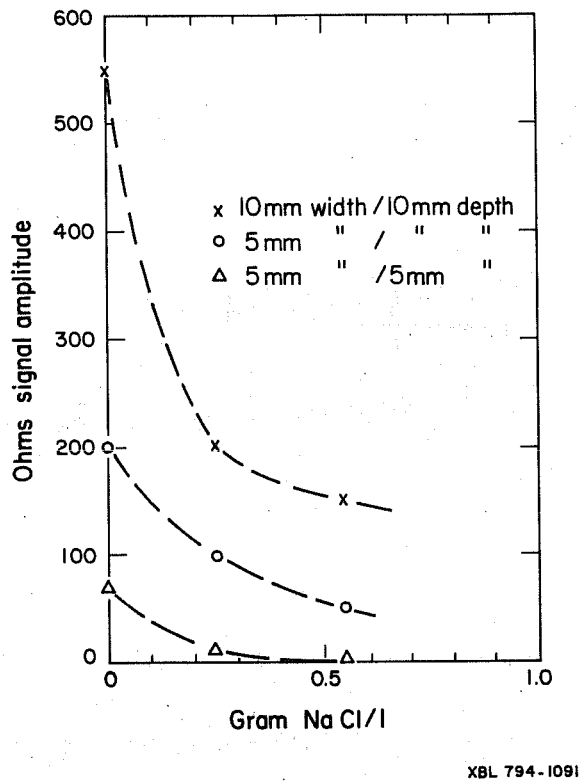

Fig. 5.4 Differential resistance signal amplitude against water salinity and width of discontinuities.

involve a hole-to-hole correlation of the interpreted zones and a more thorough comparison between the interpreted zones and the fractures. Some discrepancies in the correlation of the resistivity-log information and the core logging could be due to the fact that the core logging includes closed and filled discontinuities. These results are a preliminary evaluation of the available resistivity logs for fracture detection. A computer treatment and calibration of the tools are some of the objectives of the logging research program at SGU.

Because of its sensitivity to small features, the differential resistance log is of special interest. Hence the differential resistance logs obtained along the profile down the center of the full-scale drift have already

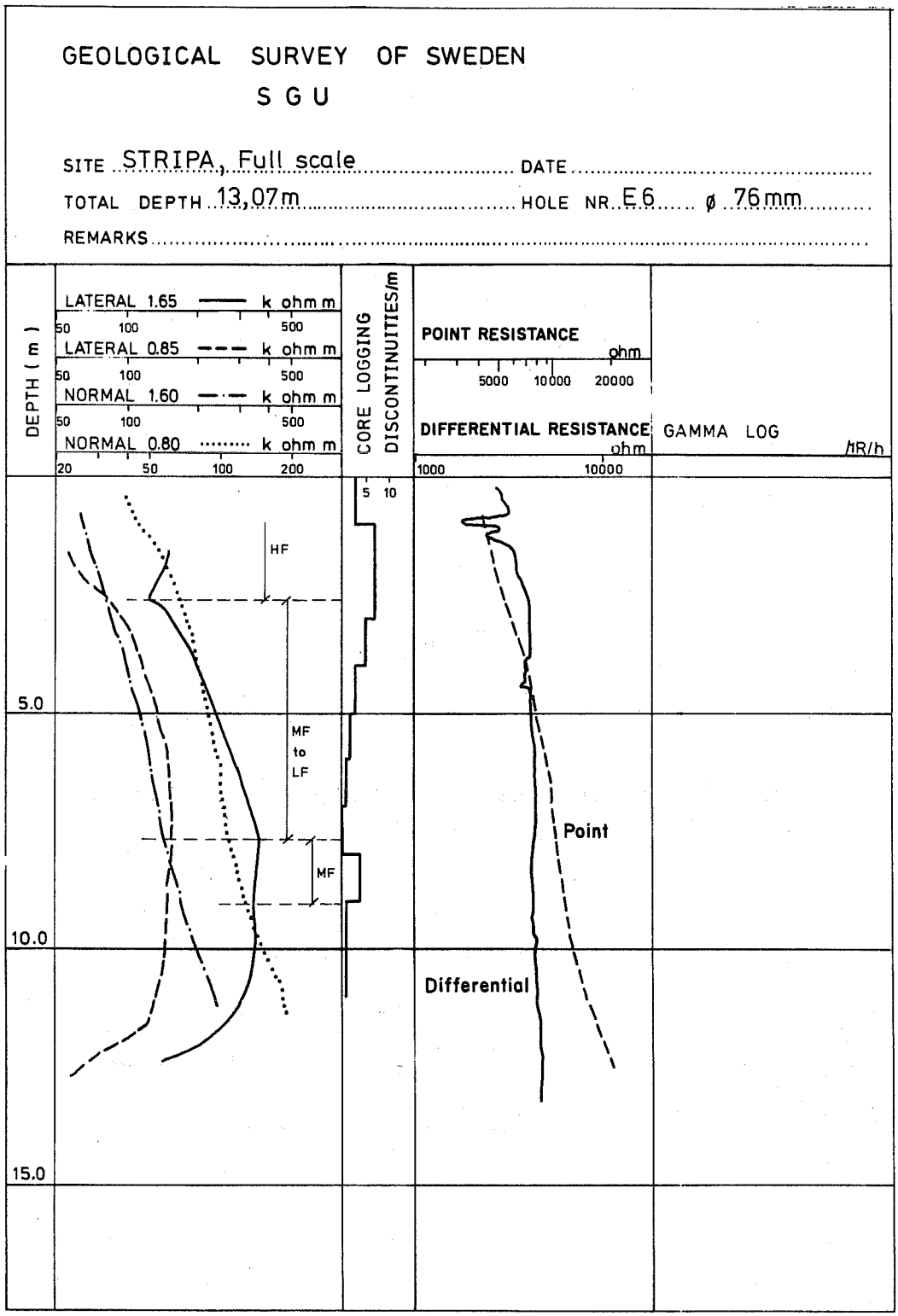

Fig. 5.5 Resistivity and resistance logs from borehole E6 in full-scale room.

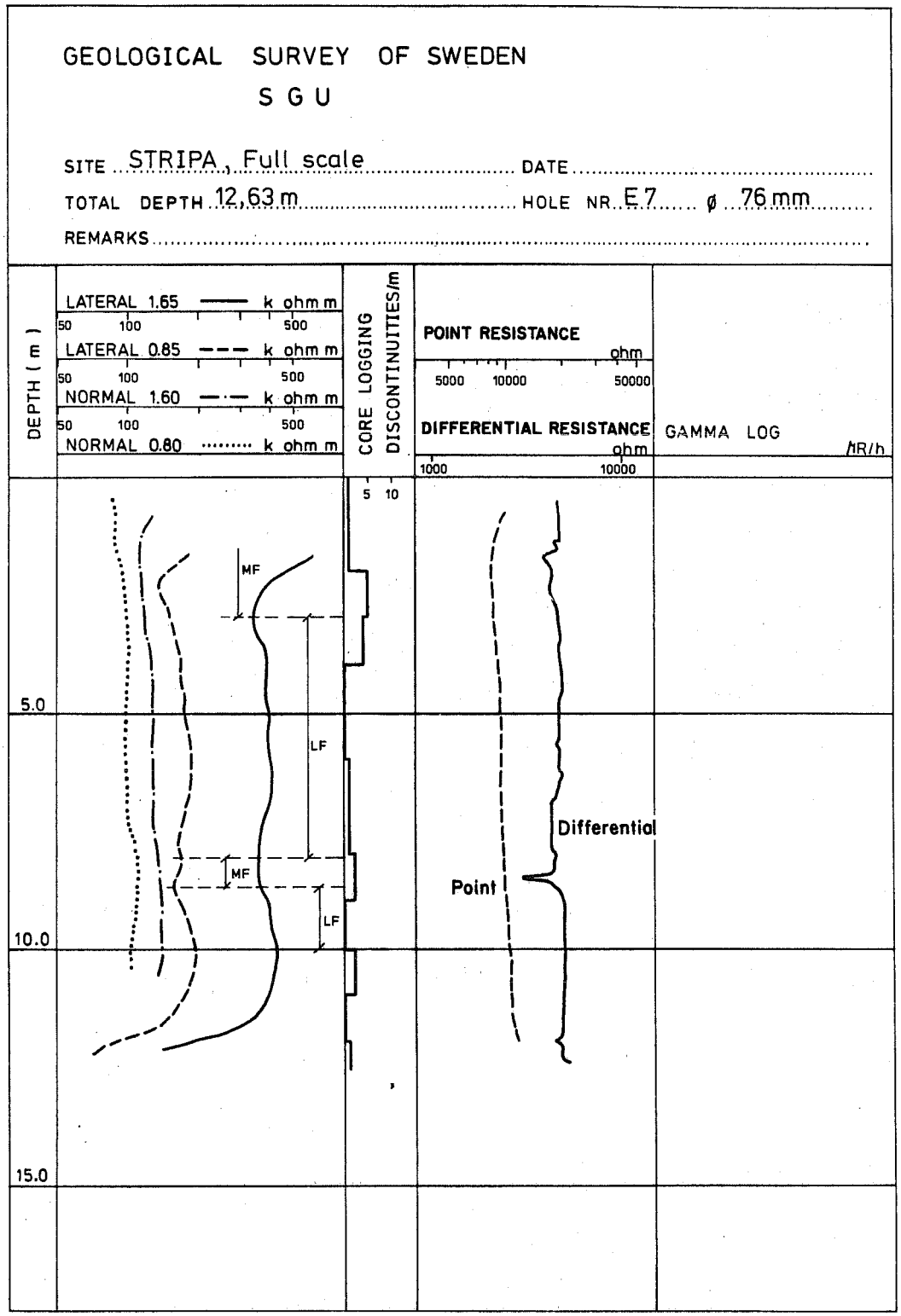

Fig. 5.6 Resistivity and resistance logs from borehole E7 in full-scale room.

been presented in Fig. 2.7 of this report and discussed briefly there. Also, the differential resistance log from E6 has been included in Fig. 2.8 for comparison with the other types of logs.

Fracture detection with resistivity logs is relative, and limited to special geological and tool conditions. A complete procedure for identifying fractured rocks needs to be based on the comparison of resistivity-log fracture interpretation with acoustic and nuclear methods.

This preliminary research on fracture detection with resistivity logs indicates that:

- It is important to choose a favorable electrode spacing. A proper combination of different electrode spacings and arrays is helpful in the determination of the limits of different conductive zones. In the underground logging we found the differential resistance and the short-spaced lateral to be the most useful. The longer-spaced lateral usually duplicated the short-spaced array. Least useful in this application were the two normal arrays.
- There is good correlation between the core logging and interpretation of the lateral resistivity logs. A correlation between the resistivity values and the degree of fracturing for a quantitative assessment is difficult and relative.
- Tools must be carefully calibrated, taking account of the characteristics of crystalline rocks.
- For the assessment of rock quality, the resistivity logs are generally satisfactory. They provide qualitative data rapidly and at a reasonable cost. More sophisticated equipment and methods give results that frequently permit quantitative or semi-quantitative evaluations.

6. SUMMARY

1. A suite of logs in the surface hole SBH-1 was used to interpret the existence of eleven zones where the permeability is expected to be greater than in most of the 380 m of the hole. About half of these eleven features are considered likely to be more permeable than the others, and hence deserve higher priority in a hydrological testing program. Below 330-m slant depth (230-m true depth) indications of fracturing decrease considerably and the rock appears homogeneous and intact. The planned injection testing of SBH-1 will test the utility of the log interpretation.

2. The interpretation of the logs in SBH-1 demonstrates the high desirability of running a full suite of logs in an exploratory open hole. A critical feature, such as fracture or a dike, is more readily diagnosed if more than one log responds to that feature. Similarly, an anomalous response on one log due to an unusual or unexpected cause can very easily be misinterpreted unless contradictory evidence is available to check the interpretation. Of the logs run, the acoustic waveform recording was the most sensitive to fracturing.

3. In the underground experimental areas at 340 m, the borehole logs document the physical properties and their variations in two volumes of rock of dimensions 5 m x 8 m x 12 m (deep) in the full-scale room, and a third volume of 6 m x 21 m x 14 m (deep) in the time-scale room. The following observations indicate that these three volumes are generally homogeneous and mechanically intact, at least with the resolution of the respective probes:

a. The borehole walls are generally smooth to a fraction of a millimeter, as determined by the mechanical caliper. The differential resistance probe, which in some ways can be regarded as an electrical

caliper, also produced few anomalies and those usually correspond with the mechanically determined enlargements.

b) Disruptions in the sonic wave train which indicate open fractures are few in number, typically three to five per hole, and are subtle in appearance, indicating that the discontinuities are generally closed or sealed, much more so than in hole SBH-1.

c) With the exception of the few anomalous zones in the time-scale room, the neutron log indicates that total water content does not vary by more than 1 volume percent, that is, ± 0.5 percent. From core analysis, the total water content in the Stripa granite is 2.4 ± 0.5 volume percent.

d) The electrical resistivity shows few variations, indicating rock of uniform and low porosity. Small fluctuations in the lateral resistivity curves were used to categorize the degree of fracturing, with some success.

e) The gamma-gamma (density) log is generally monotonous but, unfortunately, its resolution is not yet known.

4. In contrast to the above, three sets of data show interesting variations in the underground test volumes:

a) The mechanical modulus drops from 45 GPa to 33 GPa as fracturing increases. The standard deviation of the measurement is typically 10 GPa.

b) The gamma-ray log is monotonously single-valued in the full-scale room, except at the pegmatite dike intercepts. In the time-scale room, local anomalies are attributed to uranium and thorium increases in small zones of chlorite mineralization. Dramatic increases in the gamma-ray log in a few holes are associated with higher rates of water

inflow carrying radon decay products into the holes.

c) The ultrasonic cross-hole measurements appear to correlate with increased fracturing observed in core, but this conclusion is tentative.

5. In the detection of fracture discontinuities, the sonic waveform, the mechanical caliper, and the differential resistance probes have all provided useful data and merit further development:

a) The sonic waveform record provided the most useful data of all the logs run in SBH-1. The pronounced sonic-waveform anomalies are usually associated with open fractures; subtle anomalies are associated with open fractures or with closed fractures with calcite fillings. However, only a small fraction of the fracture features logged in core or with television produce anomalous sonic-waveform events. Further study of the waveform behavior and correlation with fracture character is underway.

b) The mechanical caliper resolution is better than 0.5 mm of diametral change in a 76-mm borehole. Both diametral and vertical resolution can be improved with modification of the probe.

c) The differential resistance probe appears to be sensitive to small features, but its sensitivity is highly dependent on probe geometry and the annulus between the insulating segment and the borewall. Improvements in understanding and design of the probe are warranted.

6. A neutron-thermal neutron probe has been calibrated for the measurement of water in low porosity ($\lesssim$3 percent) felsic rock, with sensitivity of -80 cps per 1 percent volume increase in water content in a 76-mm, water-filled borehole. Its radius of investigation is about 0.4 m in low porosity rock. An attempt to use the probe to monitor changes in water content

during the heater test has been thwarted by temperature sensitivity of the tool.

7. An ultrasonic (~30 kHz) propagation system is operating successfully, measuring compressional- and shear-wave arrival times over 4- to 5-m intervals between pairs of boreholes. The observed velocities appear to be lower across zones of higher fracture density. The system is also operated periodically as the heater tests progress, with small increases in velocities observed. Both results are on the order of a few percent, and further analysis of a large amount of complex data is required for substantiation.

8. Determinations of Young's modulus in situ with the CSM cell are roughly one-half the values obtained in laboratory triaxial tests. Estimates of modulus using both in situ and laboratory acoustic propagation methods are quite comparable with the laboratory triaxial results (Table 4.3). The CSM modulus determinations show a modest decrease with increasing fracture density.

7. ACKNOWLEDGMENTS

A number of people contributed to the operation of the LBL logger. C. Riveros, M. Roach, and J. Oriva aided significantly in its modifications and maintenance. The TVA sonic tool was made available through the cooperation of H. Harrell and was operated by D. Scott. A. Smith provided helpful comments during the calibration of the radiation tools, besides contributing the spectral analysis data. C. Weaver provided software development and support for the data file and retrieval system at LBL.

The ultrasonic propagation measurements would not have been successful without the equipment and advice provided by R. Lingle of Terra Tek and M. King of the University of Saskatchawan.

Finally, we wish to acknowledge the assistance provided by the LBL Site Managers at Stripa, P. Kurfurst and H. Carlsson.

8. REFERENCES

Beers, Y. 1962. Introduction to the Theory of Error. Reading, Massachusetts: Addison-Wesley Publishing Co.

Carlsson, Hans. 1978. Stress Measurements in the Stripa Granite. Lawrence Berkeley Laboratory report LBL-7078, SAC-04. Berkeley, California.

Clark, Jr., S. P., ed. 1966. Handbook of Physical Constants. Geological Society of America Memoir 97. New York, N.Y.

Fritz, P., J. F. Barker, and J. E. Gale. In press. Geochemistry and Isotope Hydrology of Groundwaters in the Stripa Granite: Results. Lawrence Berkeley Laboratory report LBL-8285, SAC-12. Berkeley, California.

Hustrulid, W. A., and W. B. Hustrulid. 1972. Development of a Borehole Device to Determine the Modulus of Rigidity of Coal to Measure Rocks. Report to the U.S. Bureau of Mines. Colorado School of Mines. Golden, Colorado.

International Atomic Energy Agency. 1970. Neutron Moisture Gauges, A Guidebook on Theory and Practice. Technical Reports Series No. 112. Vienna.

_____ 1976. Radiometric Reporting Methods and Calibration in Uranium Exploration. Technical Reports Series No. 147. Vienna.

Jaeger, J. C., and N. G. W. Cook. 1969. Fundamentals of Rock Mechanics. London: Halsted Press.

Keys, W. S., and L. M. McCary. 1971. Application of borehole geophysics to water-resource investigations. In Techniques of Water Resource Investigations, Book 2, Ch. E1. Washington, D. C.: United States Geological Survey.

Kurfurst, P. J., T. Hugo-Persson, and G. Rudolph. 1978. Borehole Drilling and Related Activities at the Stripa Mine. Lawrence Berkeley Laboratory report LBL-7080, SAC-05. Berkeley, California.

Magnusson, K., and O. Duran. 1978. Permeabilitetsbestamningar and Geofysik Borrholsmatning. KBS (Karn-Bransle-Sakerhet). Teknisk rapport 61. Stockholm.

Pratt, H., T. Schrauf, L. Bills, and W. Hustrulid. 1977. Thermal and mechanical properties of granite, Stripa, Sweden. Terra Tek Report TR77-92. Salt Lake City, Utah.

Swan, Graham. 1978. The Mechanical Properties of the Stripa Granite. Lawrence Berkeley Laboratory report LBL-7074, SAC-03. Berkeley, California.

Thorpe, R. 1979. In press. Characterization of the Fracture System for the Time-Scaled Experiment at Stripa. Lawrence Berkeley Laboratory report LBL-7083. Berkeley, California.

Van Schalkwyk, A. 1976. Rock engineering testing in exploratory boreholes. In Proc. of the Symposium on Exploration for Rock Engineering, ed. Z. T. Bieniawski. Rotterdam: A. A. Balkema.

West, F. G., and A. W. Laughlin. 1976. Spectral gamma logging in crystalline basement rocks. Geology 4: 617-618.

Witherspoon, P. A., and O. Degerman. 1978. Swedish-American Cooperative Program on Radioactive Waste Storage in Mined Caverns. Lawrence Berkeley Laboratory report LBL-7049, SAC-01. Berkeley, California.

9. APPENDICES

Page

A. Potassium, Uranium, and Thorium Content by Spectral Gamma-Ray Analysis. 127

B. Calibration of the Neutron-Thermal Neutron Borehole Probe. . . . 131

C. Description of Thin Sections from Borehole N1 in Time-Scale Room 143

D. Laboratory Determinations of Porosity and Density of Stripa Granite 149

E. Laboratory Determinations of Structural Water, Density, and Porosity. 151

F. Tabulation of CSM Cell Determinations of Modulus 153

G. Laboratory Measurements of Density and Ultrasonic Velocity . . . 163

Appendix References. 165

APPENDIX A. POTASSIUM, URANIUM, AND THORIUM CONTENT OF STRIPA GRANITE BY SPECTRAL GAMMA-RAY ANALYSIS

The following data were obtained on whole core samples of Stripa granite from borehole N1 in the time-scale drift. Samples were trimmed to 4-inch lengths and analyzed in the low background counting facility by A. Smith of the Health Physics Division at LBL. He reports:

In the following analyses, errors in background values and calibration constants are much smaller than errors in counting data from sample runs. Thus the listed errors on (U,Th,K) quantities are only those which arise from counting statistics on sample data.

The uranium and thorium standard samples are mixtures based on NBL-assayed ore materials, which are quoted as known to ±1.0 percent absolute accuracy. The uranium standard does not contain a measurable amount of thorium. The amount of uranium in the thorium standard is about 0.035 of the total. The potassium standard consists of chemically pure KCl, and is known to better than ±1.0 percent absolute accuracy.

Thus when uranium and thorium values are listed as having errors smaller than 1.0 percent this precision is meaningful only in terms of reproducibility and internal-consistency testing. Potassium values are not similarly limited in absolute accuracy, as noted above.

In all cases, our gamma-spectrometric method assumes there is radioactive equilibrium in the uranium and thorium series. This is generally expected in the fresh, unaltered materials for both series, and in almost all natural materials for the thorium series. However, the uranium series may present problems when sample materials have been subjected to deep weathering or recent hydrothermal alteration. In these cases, additional analyses may be required to determine whether the given uranium values represent uranium or only radium-226.

Sample (depth)	Uranium (ppm)	Thorium (ppm)	Potassium (%)
0.43-0.55 m	39.9 ± 1.6	27.1 ± 3.0	4.06 ± 0.25
0.74-0.85 m	40.9 ± 1.6	31.7 ± 3.2	4.16 ± 0.2
0.85-1.02 m	38.0 ± 1.3	33.5 ± 2.7	4.23 ± 0.2
1.08-1.19 m	42.9 ± 1.7	37.8 ± 3.5	4.19 ± 0.2
1.44-1.53 m	42.8 ± 1.8	28.6 ± 3.5	4.46 ± 0.2
1.72-1.82 m	44.6 ± 1.8	33.9 ± 3.5	4.60 ± 0.2
2.14-2.23 m	44.3 ± 1.9	35.4 ± 3.8	3.93 ± 0.2
2.43-2.53 m	46.0 ± 1.9	35.2 ± 3.8	4.80 ± 0.3
2.73-2.80 m	41.9 ± 1.9	25.2 ± 3.6	5.16 ± 0.3
3.10-3.19 m	43.9 ± 1.8	26.6 ± 3.3	4.16 ± 0.2
3.41-3.49 m	45.4 ± 2.1	27.5 ± 3.9	4.05 ± 0.3
3.86-3.96 m	41.9 ± 1.8	36.8 ± 3.8	4.69 ± 0.2
4.01-4.09 m	45.3 ± 2.0	31.7 ± 3.9	4.36 ± 0.3
4.15-4.26 m	35.3 ± 1.5	28.8 ± 3.1	4.27 ± 0.2
4.27-4.35 m	41.7 ± 2.1	25.1 ± 4.0	4.78 ± 0.3
4.36-4.43 m	46.3 ± 2.0	22.9 ± 3.5	3.69 ± 0.3
4.44-4.47 m	35.8 ± 2.6	30.7 ± 5.7	4.58 ± 0.4
4.48-4.49 m	143.4 ± 3.3	84.8 ± 5.9	4.02 ± 0.4
4.50-4.59 m	115.1 ± 2.7	77.5 ± 5.0	3.67 ± 0.3
4.60-4.71 m	53.7 ± 1.8	35.4 ± 3.4	3.74 ± 0.2
4.75-4.82 m	52.8 ± 2.3	32.2 ± 4.4	4.14 ± 0.3
4.90-5.02 m	40.5 ± 1.6	30.6 ± 3.2	4.15 ± 0.2
5.30-5.39 m	40.8 ± 1.9	29.9 ± 3.9	4.02 ± 0.3
5.59-5.68 m	39.3 ± 1.6	30.6 ± 3.3	3.82 ± 0.26
5.89-6.02 m	38.1 ± 1.4	31.2 ± 2.8	4.03 ± 0.22
6.30-6.40 m	39.3 ± 1.9	29.5 ± 3.8	3.77 ± 0.30
6.65-6.75 m	47.1 ± 1.9	22.7 ± 3.3	4.51 ± 0.30
6.92-7.00 m	43.6 ± 1.9	24.3 ± 3.5	3.58 ± 0.29
7.01-7.12 m	40.8 ± 1.8	27.0 ± 3.5	3.50 ± 0.28
7.13-7.26 m	29.1 ± 1.3	14.4 ± 2.3	3.77 ± 0.22
7.27-7.39 m	36.3 ± 1.5	24.9 ± 2.9	3.58 ± 0.23
7.49-7.59 m	48.6 ± 1.8	37.2 ± 3.6	3.19 ± 0.27
7.61-7.72 m	30.8 ± 1.5	27.2 ± 3.1	3.63 ± 0.24

Sample (depth)	Uranium (ppm)	Thorium (ppm)	Potassium (%)
7.81-7.90 m	26.9 ± 1.5	11.0 ± 2.7	3.88 ± 0.26
7.91-7.99 m	28.1 ± 1.5	22.2 ± 3.1	4.07 ± 0.26
8.10-8.19 m	34.9 ± 1.7	29.4 ± 3.5	4.25 ± 0.28
8.31-8.40 m	35.6 ± 1.7	26.2 ± 3.4	4.15 ± 0.28
8.60-8.70 m	33.4 ± 1.5	24.2 ± 3.0	4.11 ± 0.25
8.88-8.99 m	32.4 ± 1.3	24.7 ± 2.7	4.19 ± 0.22
9.01-9.11 m	67.8 ± 2.1	37.2 ± 3.8	4.40 ± 0.32
9.12-9.21 m	26.0 ± 1.4	26.2 ± 3.2	4.31 ± 0.25
9.30-9.40 m	37.4 ± 1.6	29.8 ± 3.3	3.78 ± 0.26
9.52-9.63 m	40.6 ± 1.6	27.9 ± 3.1	3.63 ± 0.25
9.65-9.72 m	37.5 ± 1.9	40.7 ± 4.2	3.62 ± 0.30
9.72-9.77 m	163.8 ± 4.2	98.8 ± 7.6	3.83 ± 0.58
9.78-9.85 m	29.7 ± 1.8	19.7 ± 3.6	3.10 ± 0.29
9.93-10.06 m	34.4 ± 1.3	22.7 ± 2.4	3.32 ± 0.20
10.33-10.43 m	35.5 ± 1.6	19.6 ± 2.9	4.39 ± 0.26
10.54-10.60 m	29.8 ± 1.7	17.0 ± 3.3	4.20 ± 0.29
10.78-10.88 m	23.9 ± 1.4	19.2 ± 2.9	4.30 ± 0.25
10.89-10.99 m	59.7 ± 2.0	37.5 ± 3.8	3.43 ± 0.30
11.00-11.08 m	46.6 ± 2.0	32.2 ± 3.8	3.90 ± 0.30
11.20-11.30 m	40.3 ± 1.7	27.7 ± 3.8	4.03 ± 0.27
11.51-11.61 m	34.5 ± 1.6	21.5 ± 3.0	3.76 ± 0.25
11.78-11.85 m	30.1 ± 1.7	9.7 ± 2.9	3.77 ± 0.28
12.08-12.20 m	23.6 ± 1.2	17.3 ± 2.4	3.82 ± 0.21
12.45-12.55 m	23.5 ± 1.3	10.0 ± 2.3	3.83 ± 0.23
12.67-12.80 m	20.9 ± 1.1	11.8 ± 2.0	3.68 ± 0.19

APPENDIX B. CALIBRATION OF THE NEUTRON-THERMAL NEUTRON BOREHOLE PROBE

Introduction

Before the neutron probe can be used to determine water content it must be calibrated with measurements in the medium of interest with known moisture content. Such calibrations must be done experimentally in a laboratory simulator because of the number and complex interaction of the parameters affecting the measurement:

- density and chemical composition of the medium
- density and composition of the borehole fluid
- borehole diameter
- probe geometry
- position of the probe in the borehole.

Other simulators for specific applications have been described in the literature, for example, by Allen, Caldwell, and Mills (1965) and Hearst (1975). The simulators used here were a sand tank and a granite block. The granite block is directly applicable to the immediate problem of measuring small amounts of water in igneous rock. In retrospect, the sand tank results demonstrate the difficulty of using calibration materials different from the material of interest. The tool calibrated was purchased from Comprobe, Inc. It is 32-mm o.d. and has a 1.4 Ci Am-Be source and a He^3 detector.

Sand-Tank Calibration

The neutron tool was first calibrated in a steel tank of 99.3-cm (39.1-inch) i.d. The borehole liner was an aluminum tube with a 76-mm (3.0-inch) o.d., 1.6-mm (1/16-inch) wall thickness, and a bottom plate to prevent water entry or loss. The annulus between the liner and the outer steel wall was filled with a fine high silica sand called "Portage Silica Sand"

from Martin Marietta Aggregates. Water content of the dry sand was checked by laboratory analysis and found to be negligible. The sand-water mixture filled the tank to a level of 60.9 cm (24 inches) with a volume of 378.1 liters (13.36 ft^3). Checks showed that the tool was best operated with the source resting on the bottom. In all measurements the tool was decentralized with a piece of spring steel so that the tool was always firmly positioned against the borehole wall. The moisture content was changed by adding measured volumes of water to the tank in six sequential steps, in each step adding a measured volume of sand and water, and mixing thoroughly by hand.

During the test sequence the tool was placed in a water-filled 55-gallon drum to check the stability of the count rate. The count rate in the water drum was 152 ± 2 cps indicating a measurement error of ±1.3 percent due to instrument drift and/or chart resolution. It should be mentioned that in air the tool gave 6.5 cps and 0.5 cps with and without the source attached, respectively.

Figure B-1 gives the calibration results for the water-sand mixture. The water-filled borehole gives both a higher total count and a reduced sensitivity to change in water content, both features attributed to the higher thermal neutron population produced by the water column. Note that the water-filled borehole response is linear while the air-filled borehole response is slightly concave upward. It has been pointed out (International Atomic Energy Agency 1970) that the curve shape is strongly influenced by the tool and borehole geometry.

The more likely errors in the sand-tank calibration procedure are:

1) Loss of water due to evaporation during mixing. After each run the top few centimeters of sand dried out before the next run was begun.

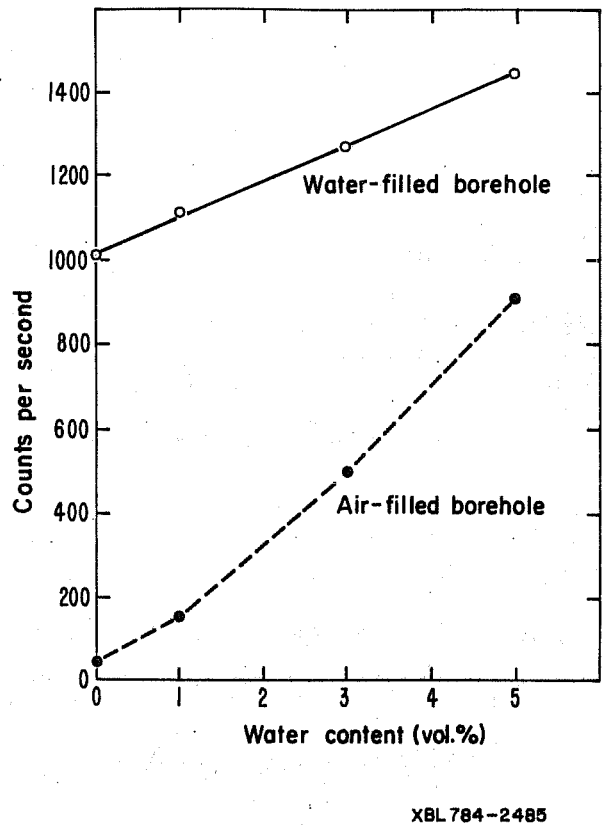

Fig. B-1 Neutron-tool count rate in sand tank. Borehole liner is aluminum of 76-mm (3.0-inch) outside diameter and 1.6-mm (1/16-inch) wall thickness.

This effect is probably small due to the volume handled and would tend to shift the measured curve to the right of the "true" curve.

2) Insufficient tank size permitting neutron loss. This possibility was not checked experimentally. Escape would steal proportionately more neutrons from the low water content than the high, hence the "true" slopes would be less than the measured slopes.

3) Density changes. The mechanical properties of sand change dramatically with the addition of small amounts of water. One effect is "fluffing," causing a density decrease as water is added. Our attempt to measure the sand density was neither timely nor sufficiently precise, but the dry sand

density was around 1.6 gm/cc and the added moisture appeared to decrease this figure by 0.1 to 0.2 gm/cc. A density decrease would tend to reduce the back-scattered neutrons and there would be fewer heavy elements per unit volume. Hence the "true" curve produced by a rigid sand matrix would be higher in absolute counts and have a greater slope than our test curves.

Granite Block Calibration

A 1-m cubic block of "sierra white" granite (actually a quartz monzonite) from the quarry at Raymond, California was core drilled with a center hole of 76-mm (3.0-inch) diameter. Additional holes surrounding the center hole produce an approximate 3 percent volume porosity. These additional holes occur in four rings, with both the spacing between the rings and the diameter of the holes progressively increasing from the inner to the outer ring. The holes within a given ring are spaced at equal 45° azimuths, but adjacent rings are offset so that no radial lines of holes occur at any given azimuth. Table B-1 lists the hole specifications averaged for each ring. Figure B-2 shows the block.

The induced porosity ϕ_3 occurs when all holes are water-filled, ϕ_1 when the holes are filled with the core rods and water, and ϕ_2 when half the holes in each ring are as in ϕ_1 and half as in ϕ_3. Because the fourth ring of holes affected the neutron-tool response much less than the inner three, only the first three are used to compute the average porosity in the bottom line of Table B-1.

All tests were run with the neutron tool decentralized in the 76-mm center hole. A check for vertical homogeneity dictated a tool position with the source 9 inches above the bottom of the block. Azimuthal variation in this position was about ±15 cps out of 1860 or ±0.8 percent. All measure-

Table B-1. Geometric specifications of the granite calibration block.

	Core o.d. (cm)	Hole i.d. (cm)	Di-1 (cm)	Di (cm)	ϕ_1 (%)	ϕ_2 (%)	ϕ_3 (%)
1 (inner)	1.08	1.385	7.62	22.10	1.40	2.48	3.57
2	1.63	2.00	22.10	38.15	1.11	2.21	3.31
3	2.82	3.40	38.15	64.36	1.07	2.26	3.44
4 (outer) a	2.82	3.40	64.36	99.06	0.94	2.19	3.44
b	5.71	6.57	99.06				
c	4.32	5.40					
d	6.77	7.78					
e	3.44	3.94					
Avg. of Rings 1,2,3					1.19	2.32	3.44

Note: Item 4a refers to 4 holes, items 4b-4e are individual holes of various sizes also in the 4th (outer) ring.

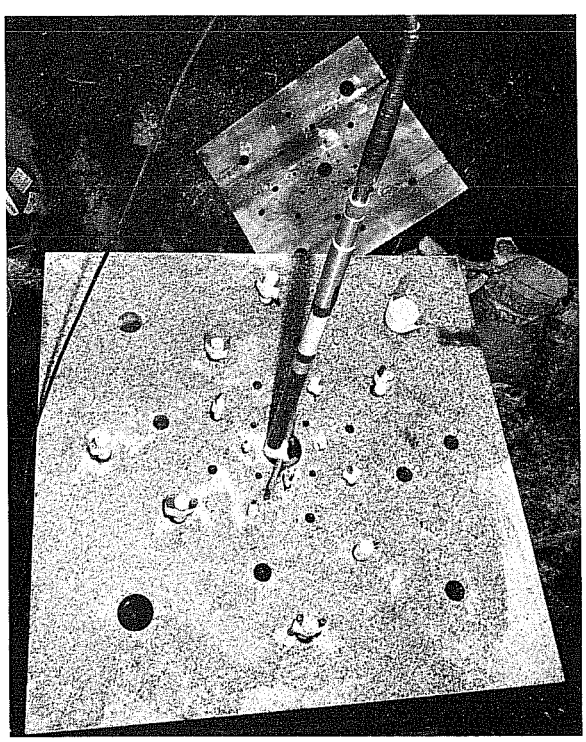

BBC 770-12561

Fig. B-2 Neutron probe in center borehole of quartz monzonite calibration block. Half of the boreholes are water-filled, the other half are filled with core supported by sticks and tape.

ments were recorded with the chart recorder using 4-sec continuous integration on dual scales of 500 cps per cm (absolute) and 100 cps per cm (relative).

Figure B-3 displays the calibration results from the granite block with the center borehole either air filled or water filled. The abscissa is labeled "induced porosity" because the neutron count responds to total water; hence at zero volume percent induced porosity, the total is responding to the bound water and free water in the pore spaces of the block. As determined by laboratory analysis of one sample taken from the center hole of the block (see Appendix E), the natural pore volume is 0.68 percent

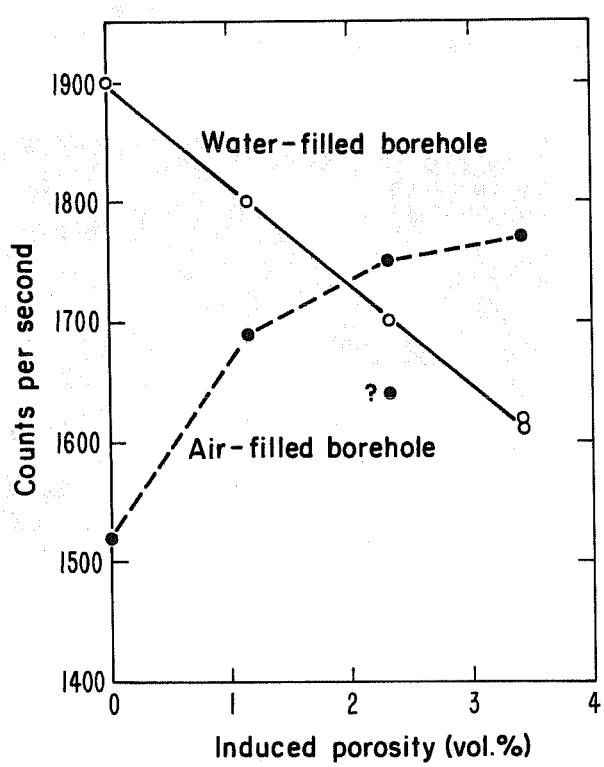

XBL 784-2486

Fig. B-3 Neutron tool count rate obtained with various combinations of water and core filling the boreholes in granite test block.

and the structural water is 1.72 volume percent, for a combined natural moisture content of 2.40 volume percent.

The granite-block calibration differs from the sand-tank calibration in two ways. Firstly, the total count rate is higher, attributed to both the higher density and the non-zero background water content of the granite. Secondly, the slope for the water-filled borehole in granite shows a decrease of counts for an increase in water content, whereas in the sand the counts increase as the water content increases. Since the two tests differ mainly in the density and chemical composition of the matrix, the prime candidates for these differences are (1) higher backscatter of thermalized neutrons in rock due to the higher density of heavy nuclei, and (2) a higher concentration of strongly absorbing nuclei in the rock which would confine the thermal neutron population to a smaller volume. For the moment, we conjecture that the increased backscatter accounts for the higher count rate in rock, and a higher concentration of absorbing nuclei accounts for the negative slope in rock.

Figure B-4 further emphasizes the difference between air- and water-filled boreholes with the additional complication of the presence and absence of iron casing. Borehole N1 is 46-mm diameter, the casing is 44-mm o.d. and 37-mm i.d., and the tool diameter is 32 mm. In this test the hole was logged "open," that is, without casing, first with water (OW) and then with air (OA) after blowing out the water with an air hose. Then the casing was installed and again logs were run with the casing air-filled (CA) and water-filled (CW). Note that curve OW has the highest count rate, as would be expected from Fig. B-3 for pore volumes of 1 percent or less (the numerical discrepancy between Figs. B-3 and B-4 is presumed due to hole diameter differences). Note also that the OA and OW anomalies tend to be reversed,

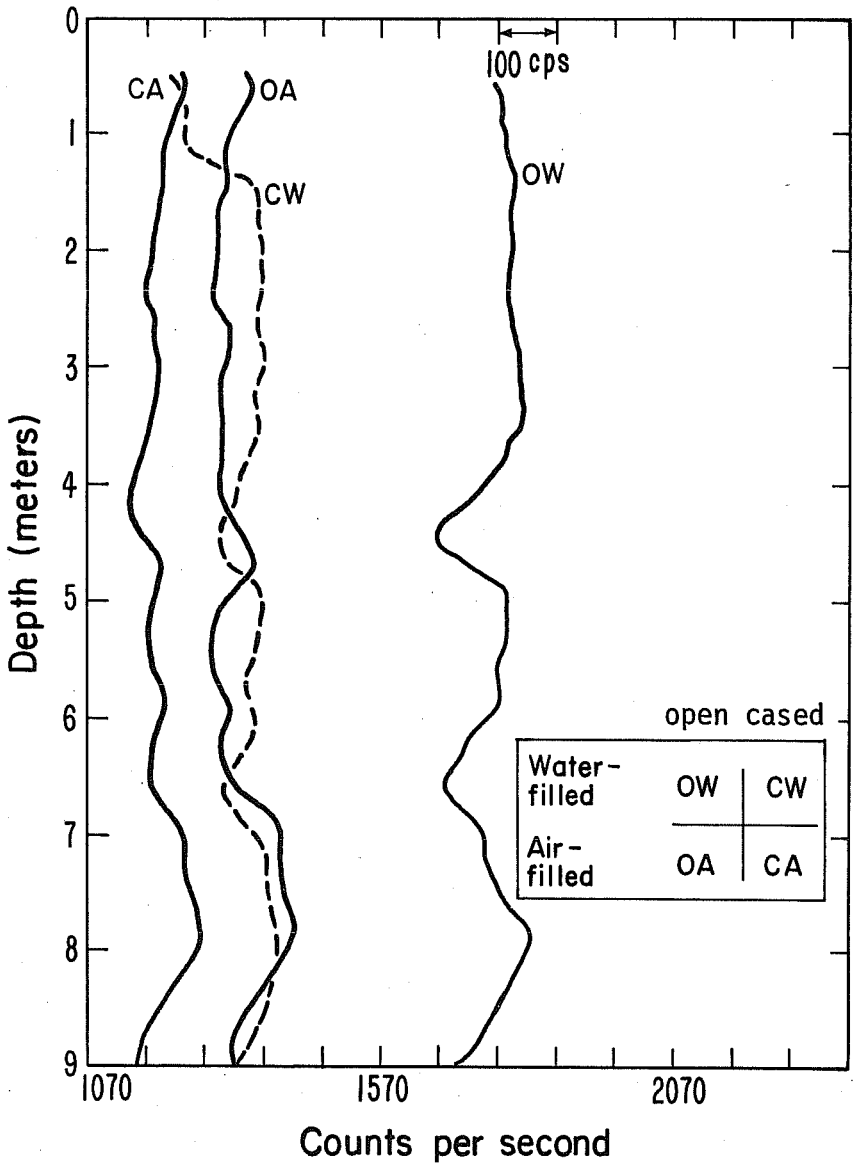

Fig. B-4 Neutron logs in borehole N1, with four combinations of fluid and casing.

also in accordance with the curves in Fig. B-3, which show opposite slopes for air- and water-filled boreholes. When the tool is run in casing the observations are the same, but reduced in total counts due to the casing which both reduces the amount of water around the tool and absorbs thermalized neutrons. The observed result is a reduced sensitivity to water variations as well as the reduced total count.

Hole Size Effect

Obviously the count rate must depend strongly upon the hole diameter if the hole is water-filled, since the volume of water in the vicinity of the source changes with hole diameter. The data in Fig. B-5 show this effect for water-filled boreholes. The Stripa data are averaged from logs in the underground holes, excluding anomalies. It appeared that the average non-anomalous water content in rock does not vary much over the 100-m space

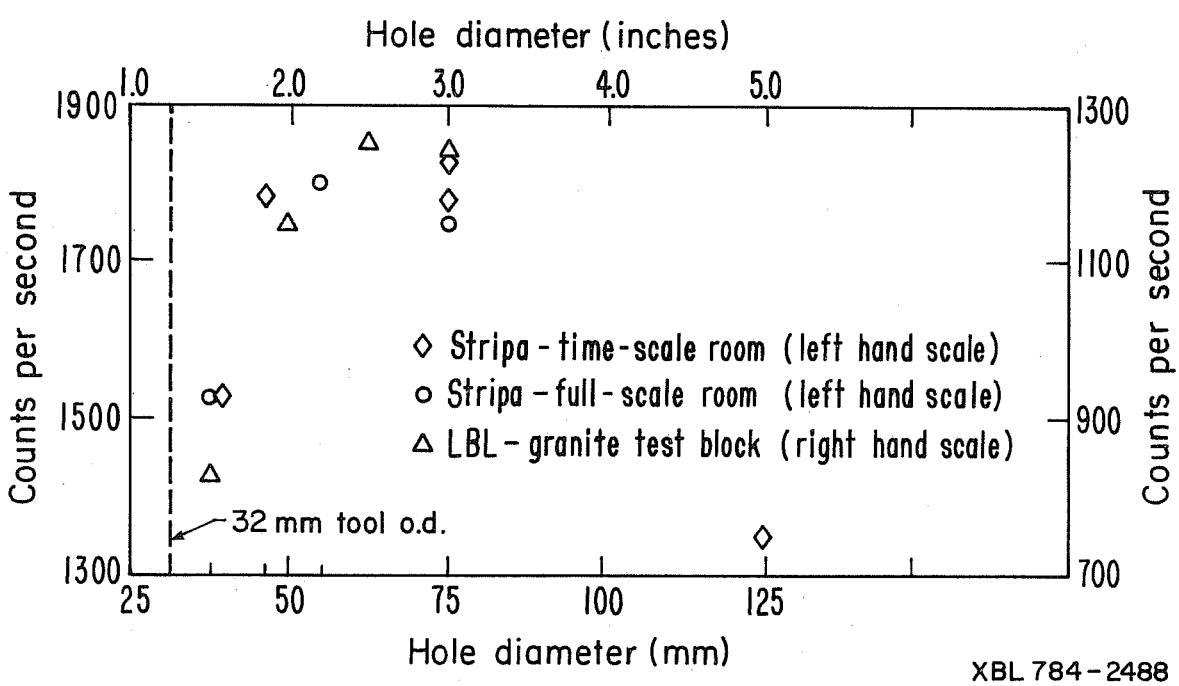

Fig. B-5 Effect of hole size on count rate for decentralized neutron tool in water-filled boreholes.

where the boreholes are situated. The granite block data are single-point measurements from four boreholes of different sizes situated near the corner of the block. Because of neutron leakage from the edges of the block, the count rate is reduced and the data points are adjusted to coincide with the Stripa data points.

From Fig. B-5 there appears to be a range of optimum hole sizes which contain enough water around the tool to thermalize neutrons, but not so much that a large fraction is thermalized and captured before reaching the receiver, as appears to be the case for the 127-mm hole size.

Radius of Investigation

Another consideration in the design and use of neutron probes is the effective radius of investigation, not a simple parameter to define since it depends on both hole size and the water content of the rock. Figure B-6 shows two measurement sequences in the granite test block which indicate that the tool becomes ineffective around 40 cm in low porosity rock. In the first sequence, all holes were air-filled initially and then filled

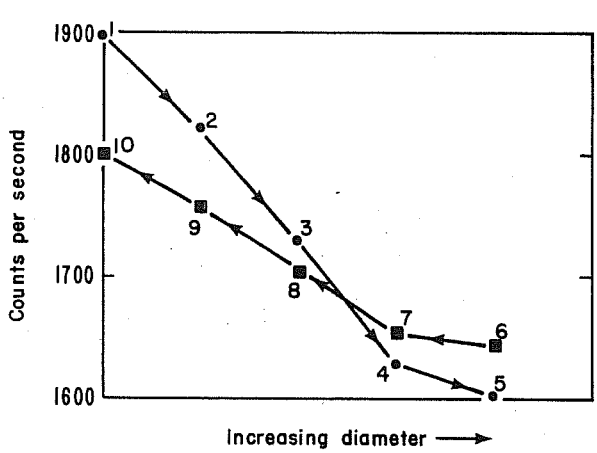

Step	Ring # 1 (inner)	2	3	4 (outer)
1	A	A	A	A
2	W	A	A	A
3	W	W	A	A
4	W	W	W	A
5	W	W	W	W
6	W	W	W	W
7	W	W	W	R
8	W	W	R	R
9	W	R	R	R
10	R	R	R	R

A = air-filled W = water R = rods and water

XBL 784-2489

Fig. B-6 Radius of investigation tests in granite block. Neutron tool in water-filled center (3-inch) borehole. Rings 1 through 4 are at radial distances of 7.9, 15.4, 25.9, and 40.3 cm, respectively, from the center of the block.

with water ring-by-ring until all holes were water-filled. The second sequence shows all holes initially water-filled and the core rods inserted ring-by-ring to decrease radially the induced porosity. Both tests show a slope change between the changes in the third and fourth rings.

Figure B-7 corroborates this estimate. The logs were acquired in four small-diameter holes all co-linear with the large-diameter (406-mm) heater

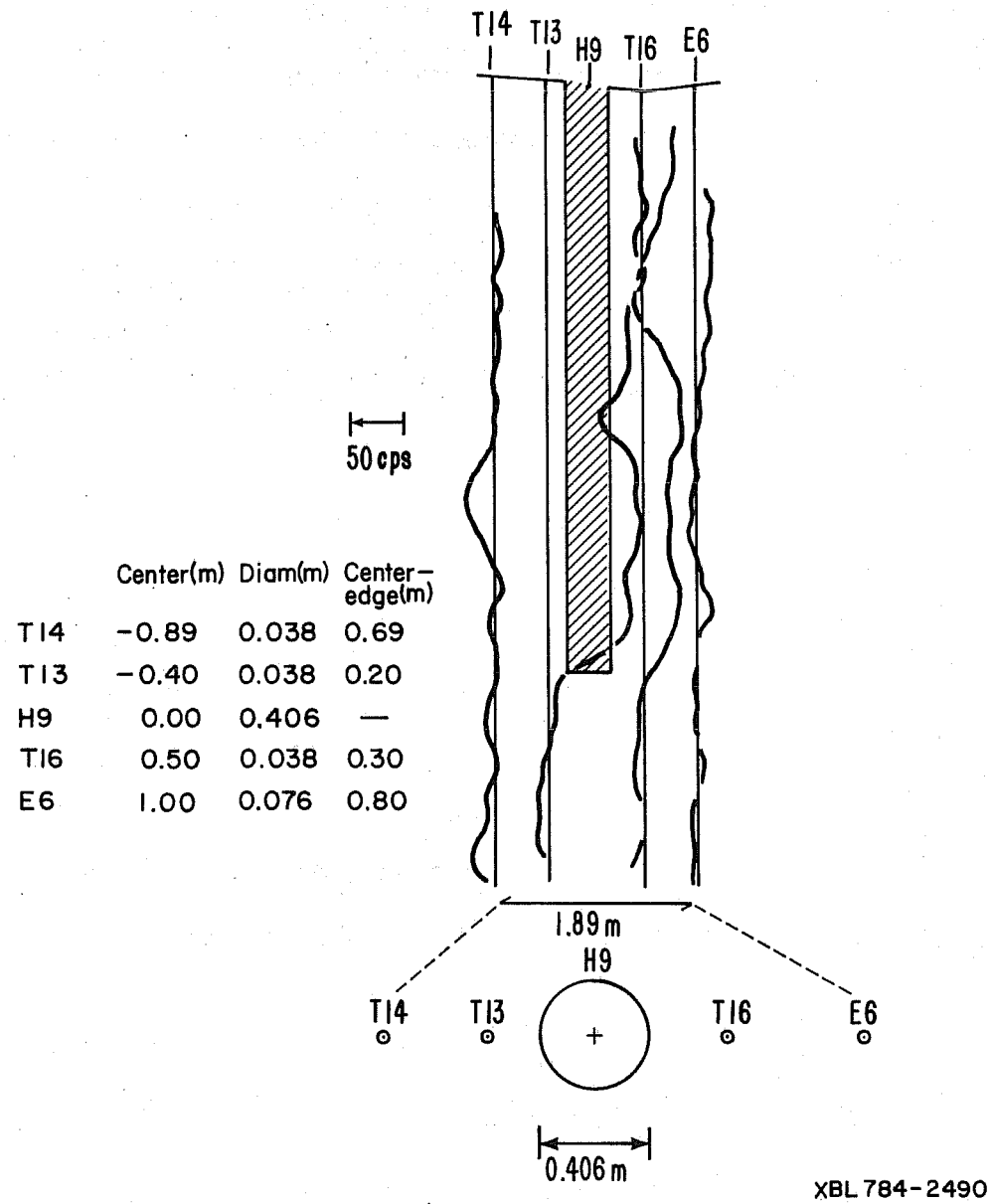

Fig. B-7 Neutron logs in holes adjacent to the 406-mm heater hole H9, which is full of water. Count rate increases to the left so water content increases to the right.

hole at Stripa. All holes were water filled during the measurements. As indicated in Fig. B-7, the bottom of the heater hole lies at about 5.5 m while the other holes extend another 2 m. The neutron logs in holes T13 and T16 clearly reflect the presence of the large volume of water nearby in the heater hole, while E6 and T14 are unaffected. Since holes T13 and T16 lie 20 cm and 30 cm from the nearest edge of the heater hole while T14 and E6 are 70 cm and 80 cm away, this result nicely brackets the 40- to 50-cm estimate for the effective radius found in the granite block.

For a continuous logging measurement system the parameters of count rate, standard deviation of the water estimate, logging rate, and vertical resolution all become somewhat interrelated. The moisture content, ϕ, expressed as a volume fraction will be estimated with some uncertainty due to statistical fluctuations in the count rate r. The standard deviation is

$$\sigma(\phi) = \frac{d\phi}{dr}\ \sigma(r) = \frac{d\phi}{dr}\ \sqrt{\frac{r}{t}}\ .$$

From Fig. B-3, we use r = 1800 cps and $d\phi/dr = 10^{-4}$. Hence:

$$\sigma(\phi) \simeq 0.004/\sqrt{t}\ .$$

Thus, if we were to make a stationary measurement for a fixed counting time, then a 16-sec integration would give a standard deviation of 0.1 volume percent. With the continuous integration, continuous pull mode, we have used a 4-sec time constant and a 2.5 m/min (4 cm/sec) pull rate. If we consider 40 cm as the effective radius of investigation of the tool, then 16 sec of record covers almost one-half that radius while integrating over four time constants. This appears to be adequate to determine water content changes to better than 1/2 volume percent.

APPENDIX C. DESCRIPTION OF THIN SECTIONS FROM BOREHOLE N1 IN TIME-SCALE ROOM

Introduction

Eight thin sections were cut from the N1 core, designated OV2-BHN1-01, -02,...-08, corresponding to depths of 12.55, 11.10, 8.20, 7.37, 4.60, 4.10, 1.54, and 0.34 m, respectively. These thin sections were examined by S. Flexser at LBL, and his petrographic description follows.

Primary Constituents

A mosaic of quartz, plagioclase, and K-feldspar predominates in the samples observed. Quartz is generally more abundant than plagioclase, while K-feldspar is significantly less abundant; together these minerals comprise ~90 to 95 percent by volume. They are complexly intergrown, and feldspar grains commonly enclose small rounded grains of quartz.

Plagioclase invariably has a dusty appearance, probably due to alteration to albite. It is also commonly altered to fine-grained sericite along fractures or in patches, and this sericite locally coarsens to coherent grains of muscovite. K-feldspar is in the form of microcline.

Besides quartz and feldspar, the only major primary mineral is muscovite, comprising 2 percent to perhaps 5 percent by volume. Muscovite also occurs as a secondary, fracture-filling material, in which case it is much finer-grained and is referred to as sericite (as above), or simply as fine-grained white mica.

Secondary Constituents and Fracture Fillings

Fine-grained white mica is ubiquitous in veins, and is also a common alteration product of plagioclase. The veins commonly originate (or terminate) in areas of muscovite of primary origin. The white mica is usually associated with highly pleochroic green chlorite, which is intergrown with white mica

and can be seen replacing it along cleavage planes.

This chlorite is the most common of the fracture-filling materials. Yellow or brown pleochroic haloes are extremely abundant in it, and these often enclose tiny equant grains (< 0.05 mm), which are either of high relief or opaque. To a lesser extent these same grains can also be found along grain boundaries, or within quartz or feldspar grains proper (with no associated haloes), with cracks radiating around them. Fission-track autoradiography shows that large concentrations of uranium are frequently, though not invariably, associated with these grains.

Commonly found with the chlorite is an opaque or nearly opaque material with either a cream-colored or a metallic look in reflected light, and sometimes associated with concentrations of uranium. Most probably this is pigmentary material with some clay, as it is present in most fractures, even locally within quartz of feldspar. It is possible that it is also composed in part of aggregates of extremely fine crystalline material, too fine to be resolved microscopically. Crystals of two different habits can be found within the chlorite and white mica: stubby, highly birefringent, high-relief prisms (particularly in samples 08 and 09, up to 0.2 mm) which locally grow at the expense of muscovite along cleavage planes and within chlorite proper; and fine, birefringent, high-relief needles (<0.05 mm) locally abundant in chlorite (particularly in sample 05). In either habit these crystals are yellow to dark brown, and are likely the same mineral, possibly in two generations of growth. It is possible also that they are the same mineral as the tiny equant grains mentioned above, although fission track evidence does not support this idea.

A rare secondary constituent of these rocks is fluorite, which is

isotropic, generally colorless, and of very low refractive index.* It occurs in late-stage veins along with quartz and fine-grained chlorite (particularly in samples 05 and 07), often with abundant calcite as well. Occasionally, lavender grains of fluorite occur, and this coloration has been observed elsewhere to correlate with inclusion of radioelements in fluorite. Such a correlation does not hold in this case, at least not with uranium.

Summary of Sequence of Alteration and Fracturing

1) Plagioclase is altered to albite, and quartz fills fractures in feldspars. The former, and possibly the latter as well, are related to the early cooling history of the granites.

2) Fine white mica and chlorite intrude along fractures, cutting earlier quartz veining. White mica (sericite) also is an alteration product of plagioclase; this is probably an earlier phenomenon related to the quartz veining. White mica and chlorite are generally closely intergrown, and may have been contemporaneous growths, but in some cases chlorite can be seen replacing white mica.

3) Opaque and crystalline materials develop in chlorite, in the form of fine needles and stubby prisms. Tiny equant, opaque, or high-relief grains also develop, commonly at the cores of pleochroic haloes in chlorite, but also along grain boundaries and in cracks in quartz and feldspar. These three materials--the opaque, the needles and stubby prisms, and the equant grains--may be contemporaneous growths or even similar mineralogically, but this is difficult to determine on microscopic evidence alone. Fission track autoradiography suggests that at least the equant grains are a different species.

---

*In some fine-grained occurrences this identification of fluorite is not certain, and sodalite or analcime are possible alternatives.

4) Veins of calcite, fluorite, fine-grained chlorite, fine-grained quartz, occur in various combinations. These are the latest stage of veining, as they cut all other features.

Occurrence of Uranium in Secondary and Fracture-Filling Materials

The fission-track radiographic method (Wollenberg 1972) was used to determine the location and abundance of uranium in an uncovered thin section. Uranium is most highly concentrated in the tiny high-relief or opaque grains. In most cases, only a lower limit can be set to these concentrations, as the fission tracks are too dense to allow individual counting. A reasonable lower limit is 10,000 ppm uranium and concentrations up to 15- to 25,000 ppm seem possible in the denser loci. These uranium-rich grains occur most frequently within the chlorite, but to a lesser extent they occur also in cracks in quartz or feldspar, and along grain boundaries together with opaque materials.

The second most abundant locus of uranium concentration is in opaque material which occurs, again, along grain boundaries and in cracks within grains (Fig. C-1). Concentrations up to 4000 to 6000 ppm are common. These occurrences are similar to those above except that they do not contain the equant grains, and their uranium concentrations are lower and less densely localized. For these reasons it seems possible that the uranium-rich grains have crystallized from the opaque, largely pigmentary material, further concentrating uranium in the process.

Finally, uranium is occasionally found associated with aggregates of the stubby prismatic grains. In one such aggregate a concentration of 500 ppm was noted, but this appears exceptional and may be due more to opaque material between grains than to the grains themselves.

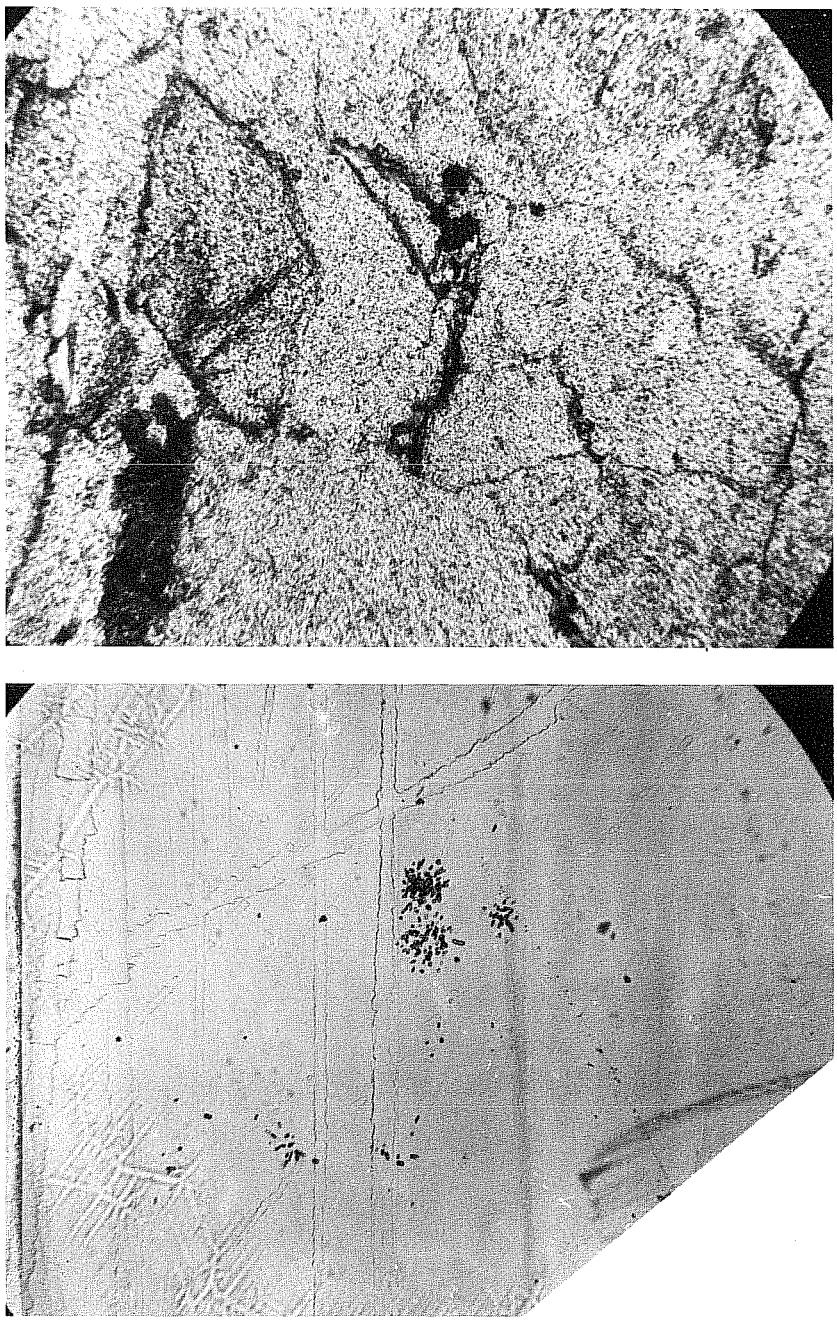

XBB 792-2908

Fig. C-1 Fission tracks (a) associated with uranium concentrated between an altered grain of quartz and surrounding plagioclase (b). Some uranium is more lightly disseminated in a chloritic zone in the lower left portion of the field. Magnification X125.

Uranium concentration in unfractured quartz or feldspar is essentially zero, and the late-stage calcite and fluorite veins also contain negligible uranium.

APPENDIX D. LABORATORY DETERMINATIONS OF POROSITY AND DENSITY OF STRIPA GRANITE

Six core samples from borehole N1 in the time-scale drift were sent to Core Laboratories in Dallas, Texas for analysis. From their report:

The plugs were trimmed with a diamond saw and their dry weights were obtained. The bulk volume of each plug was then measured using a mercury pump as a pyncometer, and bulk densities were calculated. Porosity and grain density measurements were then determined on each sample with an extended-range helium porosimeter. The results of these determinations are reported in the following table:

Porosity and Density

Sample number	Identification	Porosity, %	Bulk density gm/cc	Grain density gm/cc
1	OV2 BHN1 0.64	0.3	2.62	2.63
2	OV2 BHN1 2.51	0.3	2.62	2.63
3	OV2 BHN1 9.30	0.2	2.62	2.63
4	OV2 BHN1 5.40	0.3	2.64	2.65
5	OV2 BHN1 7.49	0.3	2.64	2.65
6	OV2 BHN1 12.08	0.4	2.62	2.63

APPENDIX E. LABORATORY DETERMINATIONS OF STRUCTURAL WATER DENSITY AND POROSITY

Ten samples from borehole N1 and one sample from the LBL neutron probe calibration block (sierra white) were analyzed for bulk density, grain density, and structural water by Hazen Research (Golden, CO), under the direction of S. Cone of Cone Geochemical (Lakewood, CO). The core samples were split, dried for three days, and both halves used to determine the bulk density, one half with a plastic coating and one without. Only the uncoated results are given here. The uncoated half was then ground, dried, and used to determine grain density. The structural water was determined gravimetrically. The finely ground sample was first dried for a number of hours at 105°C to drive off the absorbed water, then heated at approximately 1200°C for fifteen minutes in an induction furnace to remove the structural water. The water driven off is entrained in a nitrogen stream and absorbed by magnesium perchlorate which is then re-weighed to determine the structural water. In the right-hand column, an equivalent volume percent of structural water was obtained by multiplying the weight percent water by the bulk density.

Sample	Depth	Bulk density (g/cc)	Gram density (g/cc)	Porosity (%)	Structural water (wgt. %)	Structural water (vol. %)
1	0.34	2.638	2.665	1.01	0.98	2.59
2	1.54	2.636	2.623	-0.50	0.46	1.21
3	4.10	2.623	2.610	-0.50	0.48	1.26
4	4.50	2.701	2.732	1.14	1.77	4.78
5	6.85	2.637	2.627	-0.38	0.84	2.22
6	7.27	2.628	2.650	0.83	0.51	1.34
7	8.10	2.632	2.653	0.79	0.62	1.63
8	9.75	2.632	2.634	-0.08	0.53	1.39
9	11.00	2.645	2.669	0.90	0.82	2.17
10	12.45	2.618	2.653	1.32	0.38	0.99
Sierra White		2.640	2.658	0.68	0.65	1.72

APPENDIX F. TABULATION OF CSM CELL DETERMINATIONS OF MODULUS

In the following table, N indicates that the loading shows strong nonlinearity.

Hole number	Depth (m)	E modulus (GPa)		
		Date of measurement		
		(1-23)	(1-24)	(1-25)
T-3	12.35	20	19	
	11.0		35	
	10.0		32	
	9.0		35	32
	8.0			32
	7.0			37
	6.0			34
	5.0			26
	4.0			39
	3.0			34
	2.0			42
	1.0			62
		(1-25)	(1-27)	
T-4	12.72	37		
	12.0	40		
	11.0	33		
	10.0	43		
	9.0	37		
	8.0	37		
	7.0	38		
	6.0	48		
	5.0	54	35	
	4.0		41	
	3.0		40	
	2.0		28	
	1.0		39	
		(2-3)	(3-7)	(3-8)
T-6				
	13.0	32	28	
	12.0	33	33	
	11.0	32	30	30
	10.0	33		37

Hole number	Depth (m)	E modulus (GPa)		
		Date of measurement		
		(2-3)	(3-7)	(3-8)
	9.0	37		38
	8.0	32		32
	7.0	46		46
	6.0	40		42
	5.0	39		36
	4.0	46		44
	3.0	40		33
	2.0	38		40
	1.0	50		46
		(1-30)		
T-7	12.63	17		
	12.0	35		
	11.0	34		
	10.0	40		
	9.0	38		
	8.0	23		
	7.0	30		
	6.0	29		
	5.0	32		
	4.0	19		
	3.0	34		
	2.0	28		
	1.0	44		
		(1-31)		
T-8	12.55	16		
	12.0	48		
	11.0	34		
	10.0	28		
	9.0	24		
	8.0	22		
	7.0	31		
	6.0	24		

Hole number	Depth (m)	E modulus (GPa)	
		Date of measurement	
		(1-31)	
	5.0	27	
	4.0	32	
	3.0	37	
	2.0	38	
	1.0	32	
		(2-2)	(2-3)
T-9	13.0		
	12.0	46	
	11.0	46	
	10.0	43	
	9.0	38	
	8.0	39	
	7.0	43	
	6.0	37	
	5.0	27	
	4.0	28	
	3.0		46
	2.0		57
	1.0		32
		(1-20)	
T-11	13.0	58	
	12.0	46	
	11.0	40	
	10.0	57	
	9.0	48	
	8.0	54	
	7.0	42	
	6.0	52	
	5.0	43	
	4.0	40	
	3.0	61	
	2.0	44	
	1.0	34	
		(2-1)	
T-12	12.77	22	
	12.0	57	
	11.0	48	
	10.0	44	
	9.0	43	

Hole number	Depth (m)	E modulus (GPa)		
		Date of measurement		
			(2-1)	
	8.0		39	
	7.0		45	
	6.0		38	
	5.0		31	
	4.0		41	
	3.0		39	
	2.0		49	
	1.0		47	
		(2-22)	(2-23)	(3-1)
T-13	7.40	36		
	7.0		36	34N
	6.73	48		
	6.0	35	34	38
	5.0	38	37	36
	4.0		32	41N
	3.0		23	31
	2.0		34N	37N
	1.0		34	
			(2-24)	
T-14	7.55		30	
	7.0		29N	
	6.0		48	
	5.0		36N	
	4.0		33	
	3.0		30	
	2.0		32N	
	1.0		32	
			(2-27)	
T-15	7.5		32	
	7.0		32	
	6.0		34	
	5.0		28N	
	4.0		26N	
	3.0		29N	
	2.0		30N	
	1.0		37	

Hole number	Depth (m)	E modulus (GPa)	
		Date of measurement	
		(2-23)	(2-24)
T-16	7.0	40	
	6.0	32	
	5.0	33	
	4.0	24	
	3.0	18[N]	
	2.0	23[N]	21[N]
	1.0		29
		(2-27)	(2-28)
T-17	7.50	26	
	7.0	28	
	6.0	31	
	5.0	32	
	4.0	28	
	3.0	29	37
	2.0		31[N]
	1.0		32
		(2-28)	
T-18	7.65	43	
	7.0	39	
	6.0	30	
	5.0	32	
	4.0	36[N]	
	3.0	34[N]	
	2.0	39	
	1.0	43	
		(2-17)	(2-20)
T-19	5.33	39	
	4.65	32	
	4.0	34	
	3.0	21	34
	2.0		36
	1.0		23

Hole number	Depth (m)	E modulus (GPa)		
		Date of measurement		
		(2-15)		
T-20	7.42	34		
	7.0	48		
	6.0	39		
	5.0	34		
	4.0	33		
	3.0	34		
	2.0	32		
	1.0	41		
T-21	7.50	26[N]		
	6.75	23		
	6.0	39		
	5.0	35		
	4.0	26		
	3.0	37		
	2.0	39		
	1.0	18[N]		
			(2-21)	
T-22	7.0		32	
	6.0		32	
	5.0		34	
	4.0		32	
	3.0		39	
	2.0		41	
	1.0		34	
		(2-21)		(2-22)
T-23	7.0	29		
	6.0	34		
	5.0	32		
	4.0	31		
	3.0	32		31
	2.0			31
	1.0			36

Hole number	Depth (m)	E modulus (GPa)	
		Date of measurement	
		(2-15)	(2-17)
T-24	7.0	37	
	6.0	42	
	5.0	31	29
	4.0		37
	3.0		39
	2.0		25
	1.0		21
		(2-6)	
H-11	6.33	45	
	5.60	39	
	5.0	41	
	4.0	38	
	3.0	39	
	2.0	44	
	1.0	44	
		(2-7)	
H-12	6.40	37	
	6.0	37	
	5.0	34	
	4.0	25	
	3.0	35	
	2.0	38	
	1.0	38	
		(2-7)	
H-13	6.2	19	
	5.0	33	
	4.0	37	
	3.0	33	
	2.0	36	
	1.0	39	

Hole number	Depth (m)	E modulus (GPa)		
		Date of measurement		
		(2-10)		
H-14	6.28	33		
	6.0	31		
	5.0	35		
	4.0	38		
	3.0	46		
	2.0	43		
	1.0	39		
		(2-13)		
H-15	6.0	39		
	5.0	32		
	4.0	35		
	3.0	43		
	2.0	33		
	1.0	41		
			(2-13)	
H-16	6.0		29N	
	5.0		47	
	4.0		49	
	3.0		46	
	2.0		42	
	1.0		40	
		(2-13)		(2-14)
H-17	6.15	42		
	5.0	58		
	4.0	41		43
	3.0			46
	2.0			41
	1.0			33
		(2-14)		(2-15)
H-18	6.0	66		
	5.0	53		
	4.0	59		
	3.0	47		
	2.0	42		39
	1.0			43

Hole number	Depth (m)	E modulus (GPa)
		Date of measurement
		(3-2)
U-1	3.50	29.7[N]
U-2	5.03	37.2[N]
U-3	3.54	60.0
U-4	3.32	46.9
U-5	4.99	34.5[N]
		(3-3)
U-6	4.96	32
U-7	4.90	39[N]
U-8	4.90	43[N]
U-9	3.41	42
U-10	3.42	32[N]
C-1	3.42	21
		(3-6)
C-2	4.93	28.3[N]
U-11	3.20	36.6
U-12	4.71	31.7
U-13	4.71	37.2
U-15	4.73	49.7
U-16	3.26	40.7
U-17	4.89	49.7
U-18	3.31	35.9
U-19	3.29	28.3

Hole number	Depth (m)	E modulus (GPa)
		Date of measurement
		(3-7)
U-14	4.87	33.1
U-20	4.80	34.5
C-3	4.85	53.1
C-4	3.47	49.7
C-5	3.10	42.8

APPENDIX G. LABORATORY MEASUREMENTS OF DENSITY AND ULTRASONIC VELOCITY

The following measurements were done at the University of Saskatchewan by M. S. King in May 1978, on core samples from the full-scale room:

			Velocities (m/sec)							
			Compressional				Shear			
			Axial stress (MPa)							
Sample number	Location	Density (kg/m^3)	4	10	20	40	4	10	20	40
9	M8, 1.91-2.00	2635	5710	5908	5935	5961	3403	3430	3448	3510
10	M8, 5.25-5.35	2627	5843	5887	5955	5996	3391	3421	3475	3504
11	M8, 7.82-7.93	2624	5817	5909	6004	6004	3486	3525	3576	3611
12	M8, 9.31-9.42	2629	5883	5945	5970	5990	3501	3545	3553	3568
3	M6, 7.86-7.96	2631	5631	5695	5829	5874	3367	3390	3413	3452
21	E20, 9.53-9.63	2633	5881	5989	6033	6074	3403	3417	3424	3439
19	E20, 10.72-10.81	2631	5974	6046	6046	6071	3410	3442	3458	3474
16	E19, 8.60-8.73	2627	5736	5846	5922	5957	3397	3404	3442	3474
18	E18, 6.97-7.07	2623	5838	5977	6019	6062	3449	3470	3498	3526

Four ultrasonic velocity measurements were made on a single sample of Stripa granite from an unknown location, as reported by Pratt et al. (1977). The first column gives the velocity measured along the axial direction of the sample, which is cut in the shape of a right hexagonal cylinder. The last three columns are transverse velocities made across the sample between opposing pairs of faces.

	Axial	Transverse		
V_p	5.84	5.61	5.39	5.54 km/sec
V_s	3.50	3.47	3.37	3.41 km/sec

Appendix References

Allen, L. S., R. L. Caldwell, and W. R. Mills. 1965. Borehole models for nuclear logging. Soc. Pet. Eng. J. 5: 109-112.

Hearst, J. R. 1975. Neutron logging in partially saturated media. In Sixteenth Annual Logging Symposium Transactions. Soc. Prof. Well Log. Analysts. Houston, Texas.

International Atomic Energy Agency. 1970. Neutron Moisture Gauges, A Guide-Book on Theory and Practice. Technical Reports Series No. 112. Vienna.

Pratt, H., T. Schrauf, L. Bills, and W. Hustrulid. 1977. Thermal and mechanical properties of granite, Stripa, Sweden. Terra Tek Report TR 77-92. Salt Lake City, Utah.

Wollenberg, H. A. 1972. Fission-Track Radiography of Uranium and Thorium in Radioactive Minerals. In Geochemical Exploration, 1972. pp. 347-358. London: The Institute of Mining and Metallurgy.

This report is part of a cooperative Swedish-American project supported by the U.S. Department of Energy and/or the Swedish Nuclear Fuel Supply Company. Any conclusions or opinions expressed in this report represent solely those of the author(s) and not necessarily those of The Regents of the University of California, the Lawrence Berkeley Laboratory, the Department of Energy, or the Swedish Nuclear Fuel Supply Company.

Reference to a company or product name does not imply approval or recommendation of the product by the University of California or the U.S. Department of Energy to the exclusion of others that may be suitable.

TECHNICAL INFORMATION DEPARTMENT
LAWRENCE BERKELEY LABORATORY
UNIVERSITY OF CALIFORNIA
BERKELEY, CALIFORNIA 94720